AD-A135 455 EFFECTS OF LONG-TERM LOW-LEVEL RADIOFREQUENCY RADIATION EXPOSURE ON RATS..(U) WASHINGTON UNIV SEATTLE BIOELECTROMAGNETICS RESEARCH LAB A W GUY ET AL. SEP 83 1/2

UNCLASSIFIED SR-19 SAM-TR-83-18 F33615-80-C-0612 F/G 6/18 NL

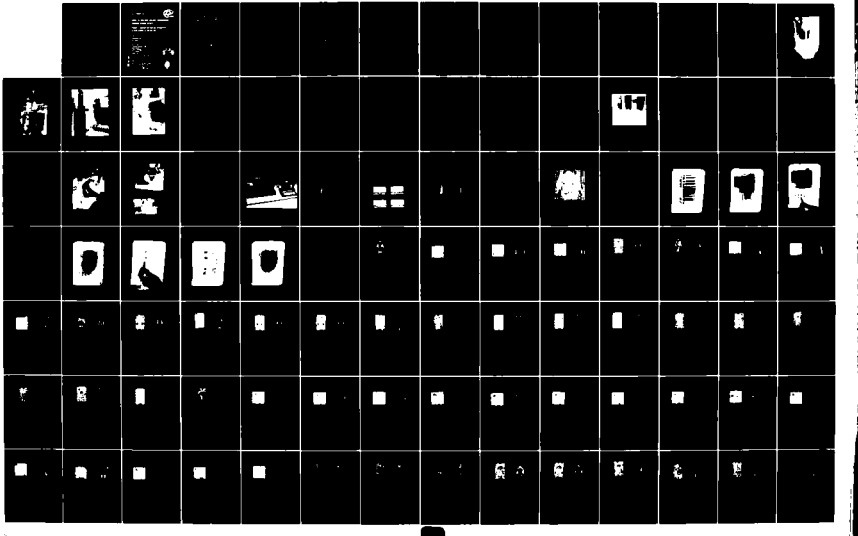

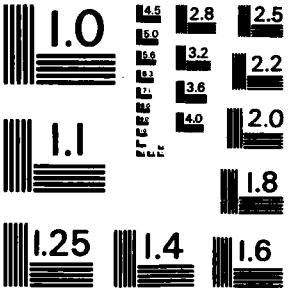

MICROCOPY RESOLUTION TEST CHART
NATIONAL BUREAU OF STANDARDS - 1963 - A

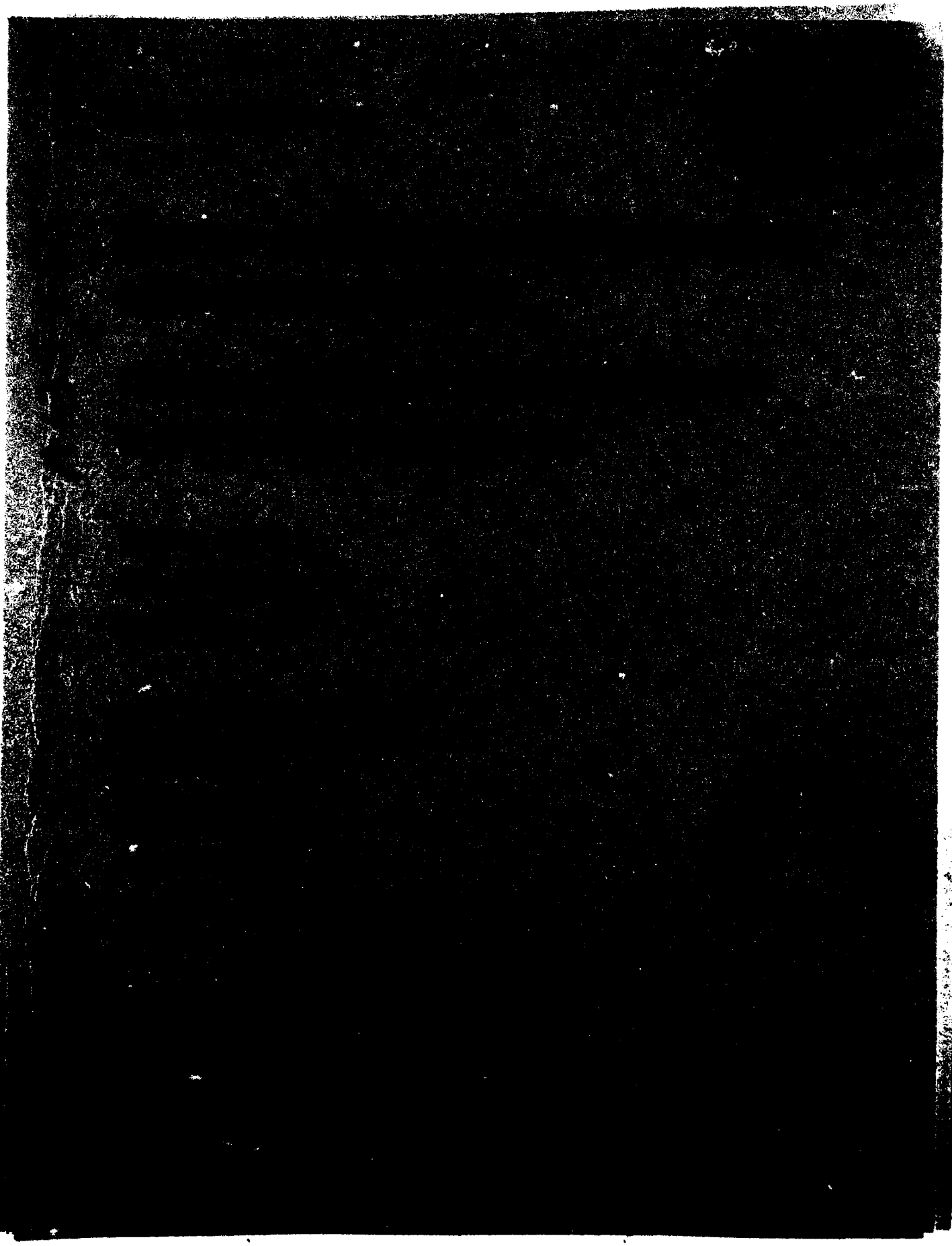

UNCLASSIFIED

SECURITY CLASSIFICATION OF THIS PAGE *(When Data Entered)*

REPORT DOCUMENTATION PAGE	READ INSTRUCTIONS BEFORE COMPLETING FORM
1. REPORT NUMBER: USAFSAM-TR-83-18	2. GOVT ACCESSION NO.: A135455
3. RECIPIENT'S CATALOG NUMBER:	
4. TITLE *(and Subtitle)*: EFFECTS OF LONG-TERM LOW-LEVEL RADIOFREQUENCY RADIATION EXPOSURE ON RATS VOL. 2. AVERAGE SAR AND SAR DISTRIBUTION IN MAN EXPOSED TO 450-MHz RFR	5. TYPE OF REPORT & PERIOD COVERED: Final Report June 1980-December 1982
	6. PERFORMING ORG. REPORT NUMBER: S.R. #19
7. AUTHOR(s): Arthur W. Guy, Ph.D.; Chung-Kwang Chou, Ph.D.; Barry Neuhaus, B.S.	8. CONTRACT OR GRANT NUMBER(s): F33615-80-C-0612
9. PERFORMING ORGANIZATION NAME AND ADDRESS: Bioelectromagnetics Research Laboratory, Department of Rehabilitation Medicine, School of Medicine, University of Washington, Seattle, Washington 98195	10. PROGRAM ELEMENT, PROJECT, TASK AREA & WORK UNIT NUMBERS: 62202F 7757-01-71
11. CONTROLLING OFFICE NAME AND ADDRESS: USAF School of Aerospace Medicine (RZP), Aerospace Medical Division (AFSC), Brooks AFB, Texas 78235	12. REPORT DATE: September 1983
	13. NUMBER OF PAGES: 107
14. MONITORING AGENCY NAME & ADDRESS *(if different from Controlling Office)*	15. SECURITY CLASS. *(of this report)*: Unclassified
	15a. DECLASSIFICATION/DOWNGRADING SCHEDULE

16. DISTRIBUTION STATEMENT *(of this Report)*

Approved for public release, distribution unlimited.

17. DISTRIBUTION STATEMENT *(of the abstract entered in Block 20, if different from Report)*

18. SUPPLEMENTARY NOTES

19. KEY WORDS *(Continue on reverse side if necessary and identify by block number)*

RFR
Dosimetry
450 MHz
2450 MHz
Exposure models
Thermography
Computer
SAR

Accession For
NTIS GRA&I [X]
DTIC TAB [ ]
Unannounced [ ]
Justification
By
Distribution/
Availability Codes
Dist | Avail and/or Special
A/1

20. ABSTRACT *(Continue on reverse side if necessary and identify by block number)*

This volume presents the methodology for and results of estimating values for the average SAR and the SAR distribution in man exposed to 1-mW/cm² 450-MHz radiofrequency radiation for various polarizations and body positions. The results were obtained by calorimetry and thermography from 1/5 scaled models of man and were analyzed by an interactive computer system. The mean SAR as averaged over the body remained relatively constant at 0.050 W/kg, with a standard deviation of ± .007 W/kg for all exposure polarization conditions and body postures. Peak SAR values were as high as 0.650 W/kg, occurring typically in the wrist.

DD FORM 1 JAN 73 1473 EDITION OF 1 NOV 65 IS OBSOLETE

UNCLASSIFIED

SECURITY CLASSIFICATION OF THIS PAGE *(When Data Entered)*

BLANK PAGE

TABLE OF CONTENTS

List of Illustrations

List of Tables

EFFECTS OF LONG-TERM LOW-LEVEL RADIOFREQUENCY RADIATION EXPOSURE ON RATS

VOLUME 2. AVERAGE SAR AND SAR DISTRIBUTIONS IN MAN EXPOSED TO 450-MHZ RADIOFREQUENCY RADIATION

INTRODUCTION

This report is the second of nine reports on monitoring the health of laboratory rats exposed under conditions simulating those of human exposure in order to assess the effects of long-term low-level 450-MHz radiofrequency radiation (RFR) on man. The rationale and description of the experiment are covered in Volume 1: Design, Facilities, and Procedures. The present report covers the measurement of the average specific absorption rate (SAR) of energy and the SAR distribution in man under various conditions of exposure.

A third report covers the dosimetry for simulating the exposure of humans to 450-MHz RFR by exposure of laboratory rats to a proportionately higher frequency, 2450 MHz. This frequency is required in order to produce an SAR distribution in the test animals similar to that produced in humans by 450 MHz; thus, there would be the highest probability of duplicating in the rats any biological or health effects that can occur in humans.

Basically the same techniques were used in these studies as had been previously reported (Guy et al., 1978): Approximately 1/4- to 1/10-scaled models of man composed of synthetic muscle tissue were exposed to frequencies from 4 to 10 times higher than the exposure frequency for a full-sized man. In the scaled models, SAR was measured by a calorimetric system and SAR distribution by a thermographic system; then the values for a full-sized man were obtained by extrapolation. The entire system was modernized, however, to enable the use of digital data-collecting

techniques. Software was also developed for greater efficiency and accuracy in processing and printing of the thermogram images.

The study consisted of the following four major tasks:

(1) Determination by calorimetry of the values for the average SAR in man for different body postures and sizes under conditions simulating free-space exposure to 450 MHz.

(2) Development of an interactive computer system for analysis and processing of thermograph images of exposed phantom scale-models of man to reflect actual SAR distribution patterns (previous thermographs displayed temperature patterns only) and formulation of a computer program for rapid retrieval of SAR values from a large data base.

(3) Determination of SAR distributions in man for different body postures and sizes under exposure conditions simulating free-space exposure to 450 MHz.

(4) From the data in this volume and in Volume 3, establishment of the exposure parameters required for simulation, with rats, of those in humans exposed to 450-MHz RFR.

The details and results of each of the above tasks are discussed in the following sections.

EXPERIMENTAL METHODOLOGY

Exposure Facilities

For biological effects observed in rats exposed to RFR in the waveguide system to relate to safe or unsafe exposure levels for man, the dosimetry information for the rats exposed in the waveguides (discussed in Volume 3) must be correlated to that obtained for humans exposed to free-field 450-MHz 1-mW/cm^2 radiation. Using the facilities of the large anechoic chamber previously discussed by Guy et al. (1978), we obtained the dosimetry information for full-scale man from approximately 1/5-scale models of man fabricated from synthetic tissue (with the same dielectric properties as human tissue), with proper modifications for the scaling

factor. With a scaling factor (sf) of 5.44 (inverse of the reduction factor from the full-scale man to the scale-model man), we used 2450-MHz radiation in the anechoic chamber for these models to simulate 450-MHz RFR exposure for the full-scale man.

Previous work of this type had been conducted in the chamber, but exposure levels had been limited to 350 mW/cm^2 because the maximum output of the power source was 2.5 kW. The thermographic technique requires relatively short exposure times to maintain maximum accuracy of results (to reduce effect from diffusion of thermal energy from hot to cooler areas). Therefore, at the outset we decided to reduce exposure times by enlarging the power source by a factor of 4; we thus replaced the existing 750- to 1000-MHz, 10-kW klystron with an 1800- to 2450-MHz, 10-kW klystron. Installed on a portable cart, the klystron (Fig. 1) could be easily wheeled into the klystron amplifier-chamber and interfaced with the existing power supply and cooling system (Fig. 2). The output of the klystron was connected by waveguide to the standard gain horn in the anechoic chamber (Fig. 3). Associated instrumentation for monitoring input power to the horn is shown in Fig. 4. Incident power density in the anechoic chamber was measured with the NBS (model EDM-1C) energy density meter and the Narda (model 8635) power density meter. The NBS meter measurement was in consonance with that prescribed in theory, but the Narda meter measurement was 13% less. Since the guaranteed calibration accuracy of the meters was no better than $\pm$ 1 dB, according to the Bureau of Radiological Health, we decided that using the theoretical gain of the horn (corrected for near-zone field) of 13.9 dB and a carefully calibrated coaxial directional coupler would provide a more reliable prediction of the power density than the meters. All data reported in the following sections are based on the theoretical input power as measured by the calibrated Microlab/FXR CB-68LN coaxial directional coupler attached to a coax-to-waveguide adaptor connected to the standard gain horn.

Figure 1. Klystron tube mounted on cart for easy installation.

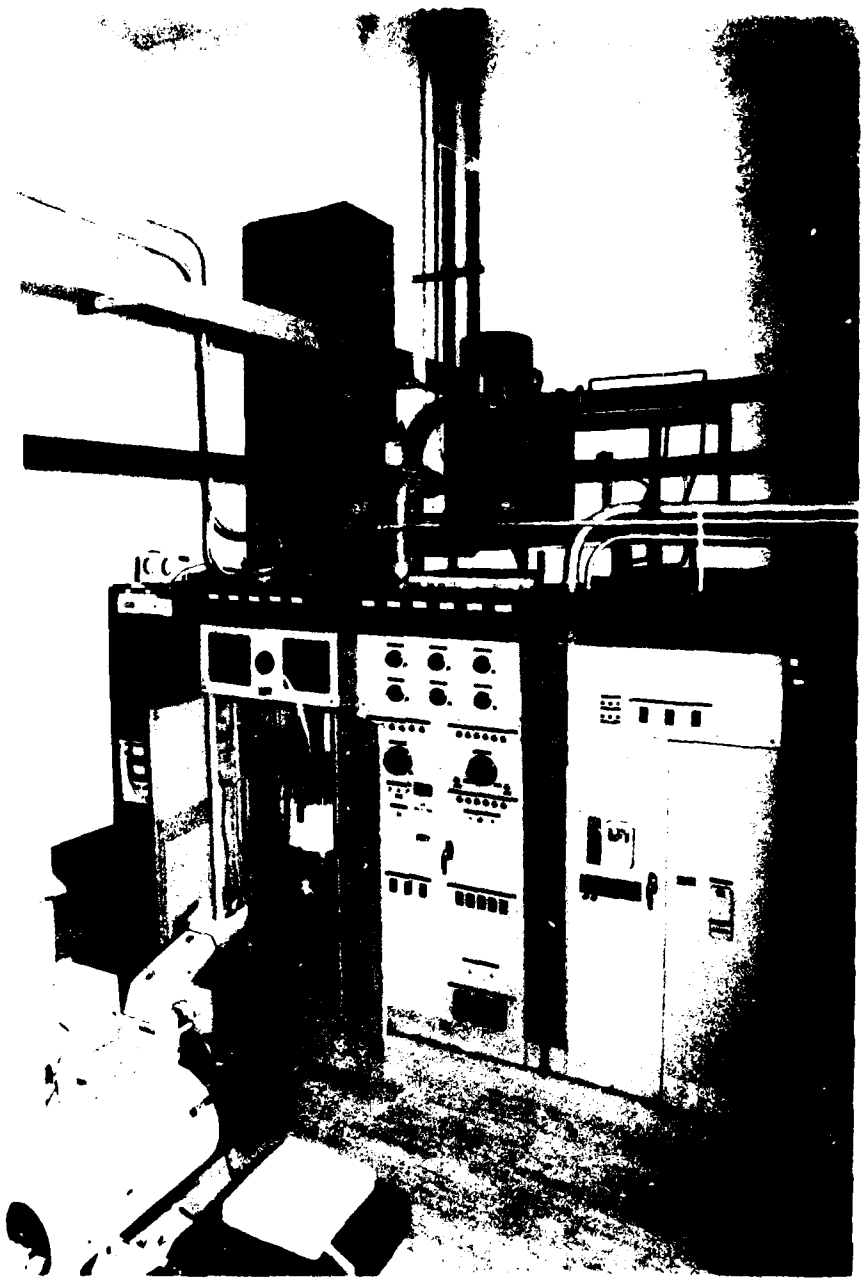

Figure 2. Klystron tube completely interfaced to amplifier system.

Figure 3. Interior of anechoic chamber: standard gain horn and a half-section of a scale model man in exposure position.

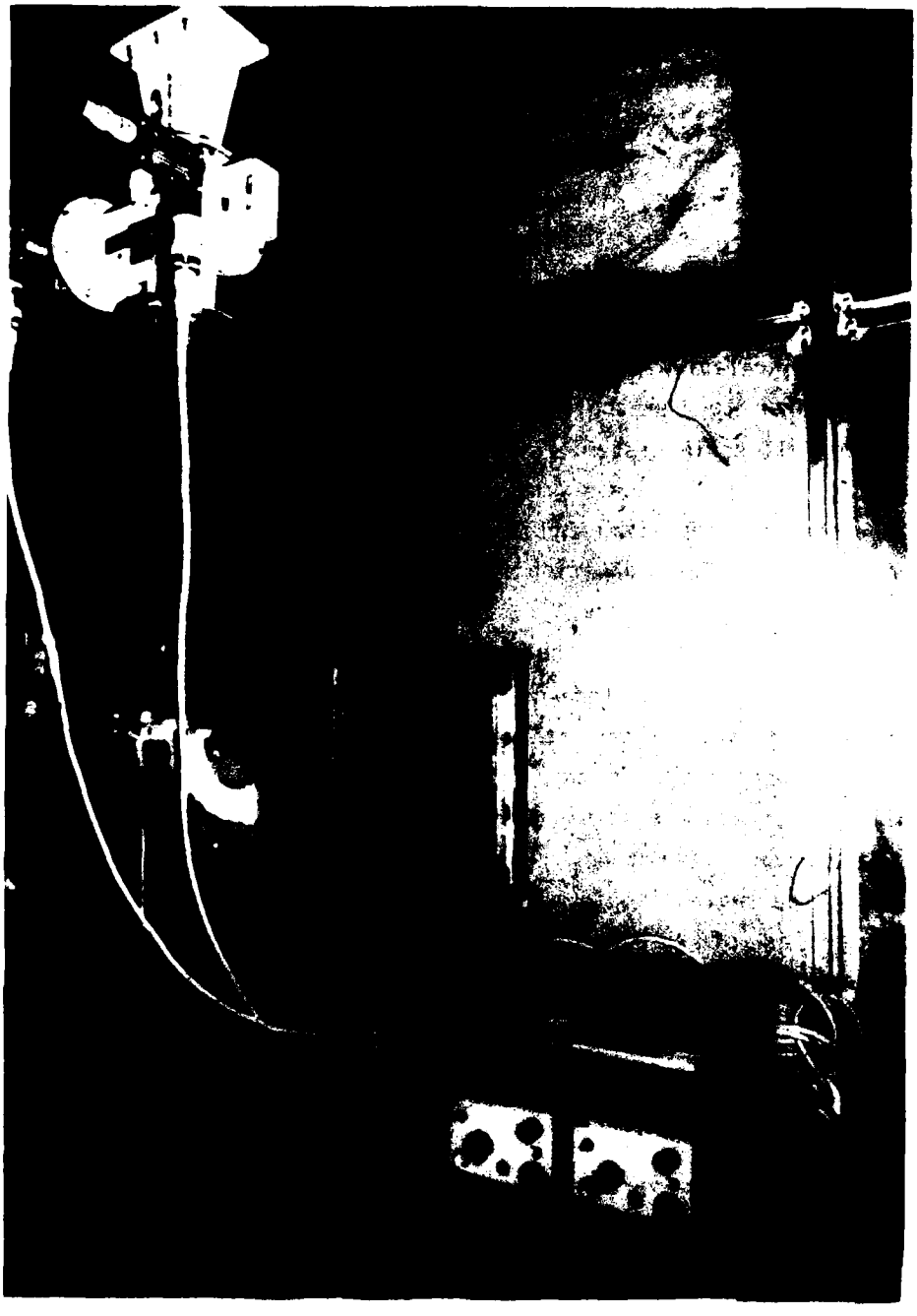

Figure 4. Waveguide and associated instrumentation for monitoring input power to standard gain horn.

Synthetic Tissues for Scale Models

To simulate the exposure of a full-scale man to 450 MHz, we needed a suitable synthetic tissue with proper dielectric constant to match the scaling criteria. The scaling conditions (Stratton, 1941) pertinent to developing phantom muscle mixtures are

$$\varepsilon' = \varepsilon \tag{1}$$

and

$$\tan \delta' = \tan \delta \tag{2}$$

where ε is the relative permittivity, $\tan \delta$ is the loss tangent, the prime quantities refer to the scale-model system, and the unprimed quantities specify the full-scale system.

Since $$\tan \delta = \sigma / \omega\varepsilon \tag{3}$$

where σ = conductivity (S/m) and ω = radian frequency ($2\pi f$, where f is the frequency), the scaling condition for conductivity may be derived as

$$\sigma' = sf \times \sigma \tag{4}$$

The dielectric properties of the full-scale and scaled models are shown in Table 1. The only difference between them is that the electrical conductivity of the latter is increased by the scaling factor. The dielectric properties for the scale-model tissues were measured under controlled temperature conditions of 20°C. The properties were obtained by the transmission-line methods described by Guy et al. (1976, 1978). In addition to the scaled liquid muscle, a scaled liquid tissue was used, with the properties of a homogeneous mixture of muscle, fat, and bone representative of the human body with an electrical conductivity of 2/3 that of muscle as described in the Radiation Handbook, second edition (Durney et al., 1978).

Average SARs in Spherical Models

To test the validity of the dielectric property measurements and the calibration of the anechoic chamber, we determined the SAR in a number of spherical models with radii measuring between 2 and 6 cm. The average SAR in watts per kilogram can be calculated from the increase in temperature,

TABLE 1. CHARACTERISTICS OF SCALE MODELS* (SYNTHETIC TISSUES) FOR SIMULATING 450-MHz EXPOSURE AT 2450-MHz RFR

Full-Scale Dielectric Constant ($T=37^{o}C$)	Scale Synthetic Tissue	Composition % Total Weight						Scale Dielectric Constant ($T=20^{o}C$)	Specific Heat (kcal/kg $.^{o}C$)	Density (g/cm^3)
		H_2O	Ethylene Glycol	NH_4Cl	NaCl	PEP	TX150			
$\varepsilon'=53$ $\sigma = 1.18$	Muscle (gel)	82			4.2	5.8	8.0	$\varepsilon'=53.3$ $\sigma = 6.4$	.86	1.000
$\varepsilon'=53$ $\sigma = 1.18$	Muscle (liquid)	53.9	40.6	5.5				$\varepsilon'=50.2$ $\sigma = 6.4$	.87	1.074
$\varepsilon'=33$ $\sigma = 0.88$	Mixture (liquid: 2/3 muscle; 1/3 fat)	29	65.2	5.8				$\varepsilon'=33.1$ $\sigma = 4.8$	.71	1.099

*Scale factor = 5.44

ε = relative permittivity

σ = conductivity (S/m)

in the manner described by Guy et al. (1978), by the following equation:

$$SAR_{avg} = 4.184 \times 10^{3} \; c\Delta T / \Delta t \qquad (5)$$

where c is the specific heat in kcal/kg·°C, ΔT is the temperature increase due to exposure in °C, and Δt is the exposure time in s. In Table 2 are given the measured dielectric properties at 25°C for 3.0 and 2.45 GHz and at 20°C for 2.45 GHz, together with values reported by von Hippel (1954). The measured values for average SAR for the phantom models filled with distilled water are shown in Fig. 5; for those consisting of ethylene glycol, in Fig. 6; and for spheres filled with liquid synthetic muscle and exposed to 2450-MHz planewave, in Fig. 7. The calculated values are in consonance with the theoretical values obtained by evaluation of the Mie-theory equations developed by Ho and Guy (1975) on a digital computer.

TABLE 2. MEASURED DIELECTRIC PROPERTIES OF VARIOUS LIQUIDS USED FOR SPHERICAL PHANTOMS

Liquid	von Hippel	Slotted Line Measurements			Density	Specific Heat
	@25°C	@25°C	@ 25°C	@ 20°C	(g/cm^3)	(kcal/kg.°C)
	3 GHz	3 GHz	2.45 GHz	2.45 GHz		
Distilled	76.70*	79.31	72.27	79.29		
water	2.01	2.55	2.08	2.18	1.0	1.0
Ethylene	12.00	13.69	15.94	14.54		
glycol	2.00	2.14	2.08	1.97	1.113	0.571
Butyl	3.70	4.84	4.21	4.58		
alcohol	0.41	0.33	0.30	0.37	0.810	0.563
Propyl	3.50	3.76	3.60	3.22		
alcohol	0.28	0.25	0.28	0.23	0.804	0.586

*Upper number = dielectric constant; lower number = conductivity in S/m

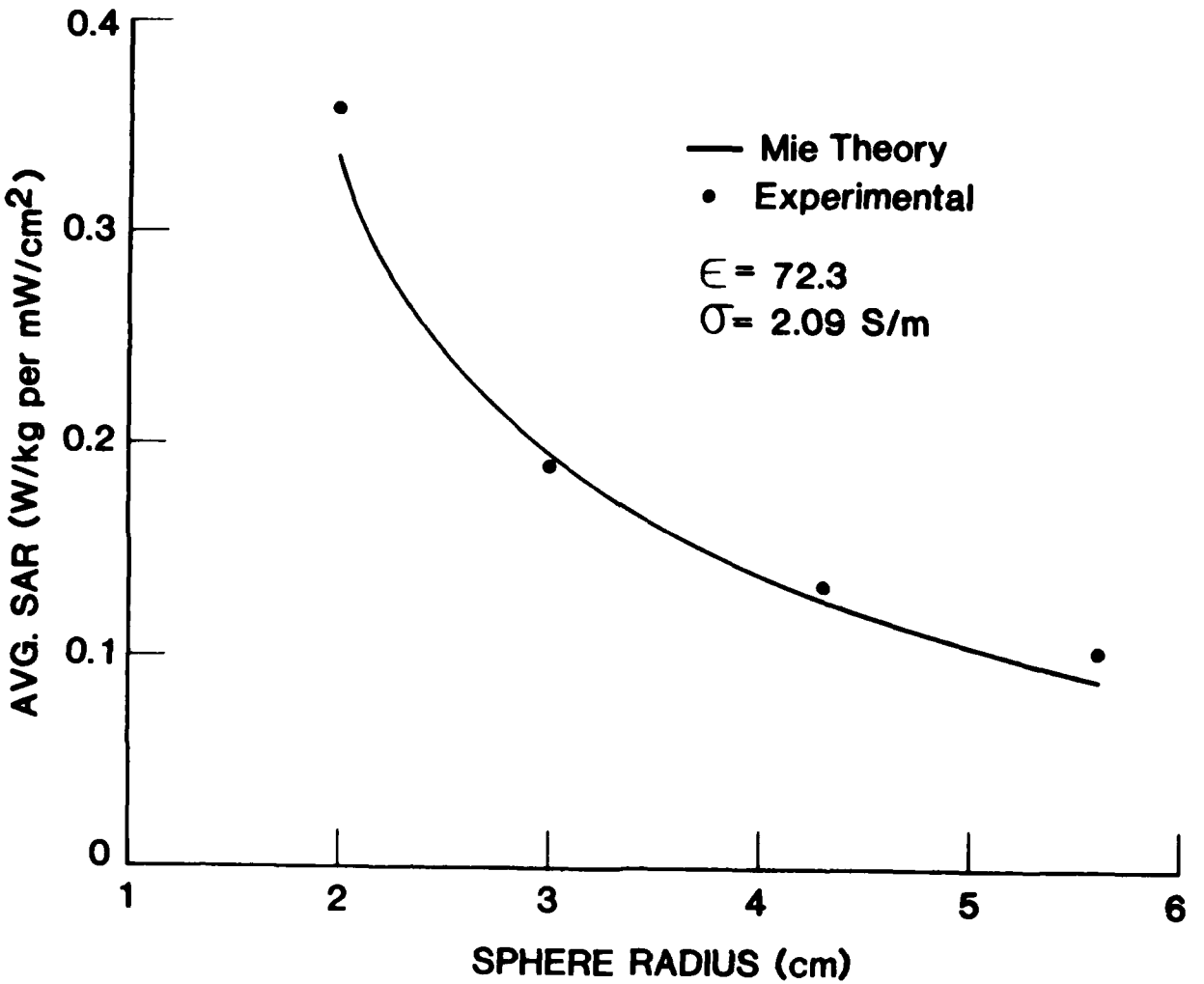

Figure 5. Average SARs for spherical models consisting of distilled water and exposed to 2450-MHz planewave radiation.

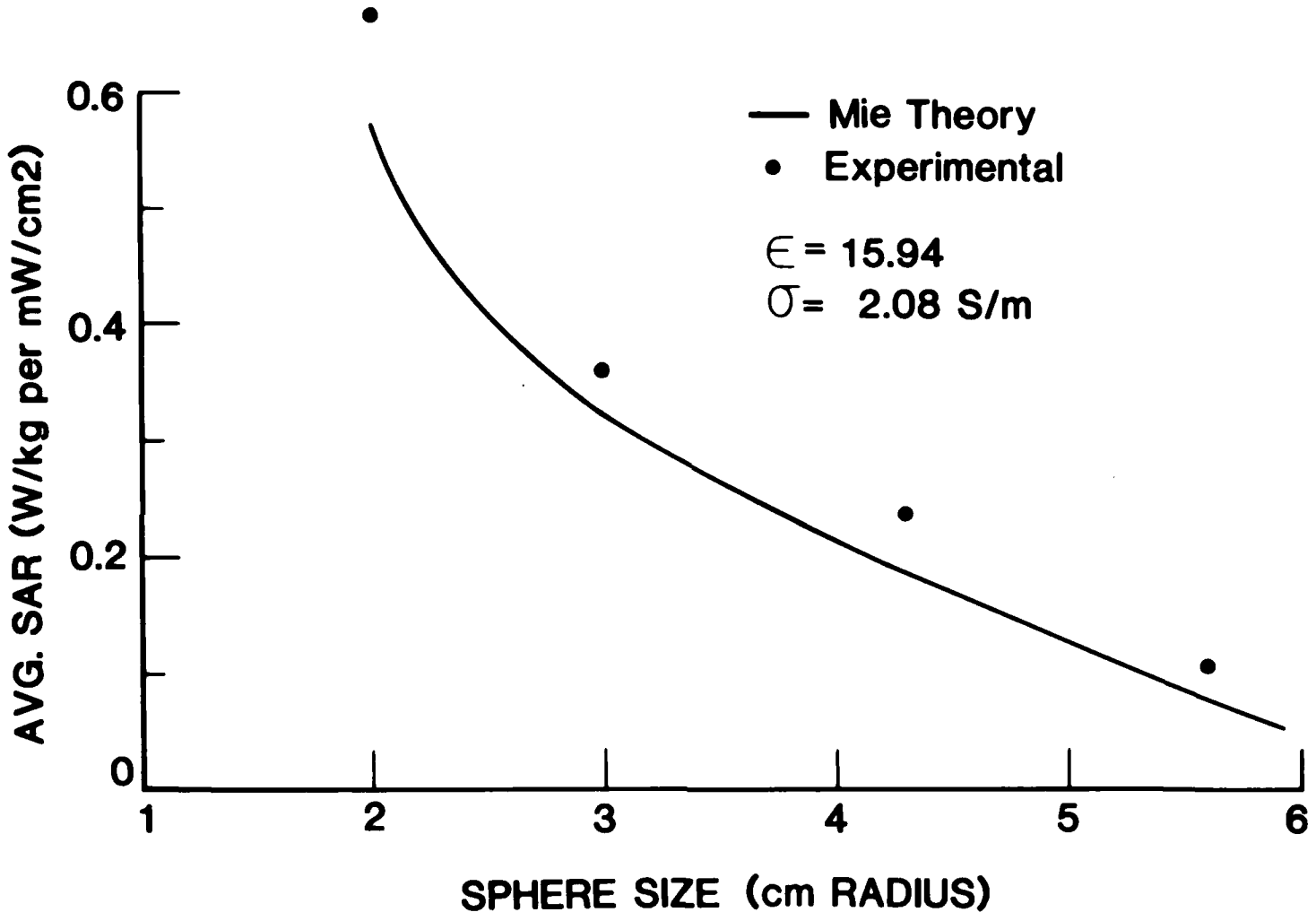

Figure 6. Average SARs for spherical models consisting of ethylene glycol and exposed to 2450-MHz planewave radiation.

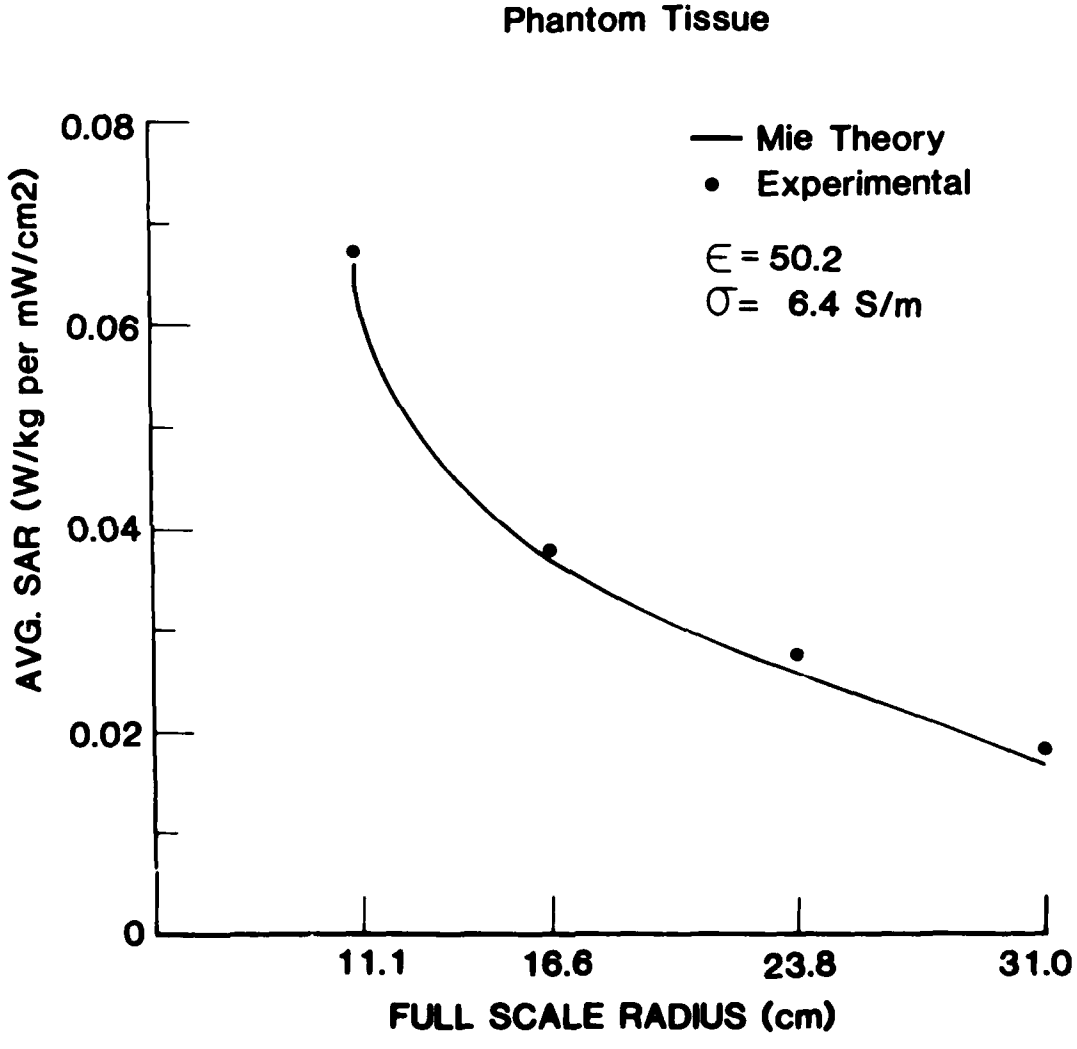

Figure 7. Average SARs for spherical models consisting of liquid synthetic muscle and exposed to 2450-MHz planewave radiation.

MEASUREMENT OF AVERAGE SAR IN MAN MODELS

Hollow Styrofoam molds were used to hold liquid synthetic tissue for the determination of average SAR in man models. The mold halves, before being glued together, are illustrated in Fig. 8. The halves were joined with a liquid-tight seal, and liquid synthetic tissue was poured in. The forms consisted of 5.44-scaled models of erect adult man (full-scale height = 171 cm) and child (full-scale height = 86 cm), with arms down. We used the full-scale figure to reflect a worst-case situation involving exposure of a small man or a woman (size is inversely proportional to SAR at 450-MHz exposure). Each model was exposed in the anechoic chamber to 2450-MHz radiation fields of 750-mW/cm^2 incident power density (140 cm from a standard gain horn) for about 20 to 60 s. After exposure the average rise in temperature in the model was measured with a thermocouple; the heat loss during the several minutes needed for the measurements was negligible. The SAR for a full-scale man was obtained by multiplication of the SAR calculated for the model by the scaling factor (sf) of 5.44.

SAR distributions were measured for 12 primary orientations of the model man with respect to the incident field. We may designate these primary polarizations, using the nomenclature of the Radiation Handbook (Durney et al., 1978), by considering a coordinate system oriented with respect to the model man, with the x-axis parallel to the long axis of the body, the y-axis parallel to the frontal plane, and the z-axis perpendicular to the frontal plane. Then we can define the polarization by which the field vectors $\underline{E}$, $\underline{H}$, and $\underline{k}$ are parallel to the x, y, and z axes. Thus, EHK polarization is the orientation in which $\underline{E}$ lies along x, $\underline{H}$ lies along y, and $\underline{k}$ lies along z. Since man is asymmetrical from front to back, we must consider the six polarizations specified for the ellipsoidal model in the Radiation Handbook plus six others. If we assume the EHK and HEK polarizations to correspond to exposures of the man facing the source, we then designate -EHK and -HEK as exposures of the man with his back to the source. Likewise, if EKH and HKE represent exposures with the left side to source, -EKH and -HKE will correspond to exposures with the right side to the source. Finally, KEH and KHE will correspond to exposures with the head toward the source, and -KEH and -KHE will correspond to exposures with the feet toward the source.

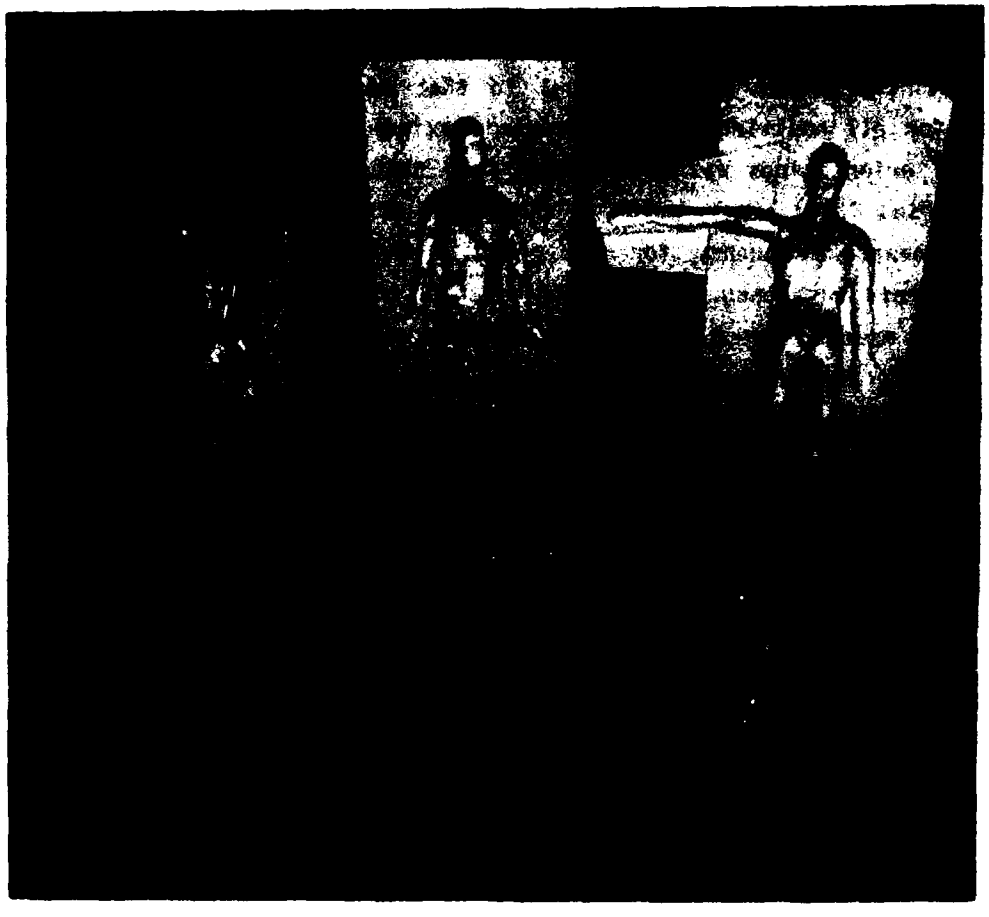

Figure 8. Scale models of man used for average SAR and SAR distribution measurements.

The results of the first series of measurements are listed in Table 3; each datum represents the average of several measurements, normalized to correspond to an exposure level of 1 mW/cm^2. The largest variation was less than 10%. The average SAR measured for the composite-tissue model consisting of fat and muscle (with two-thirds the conductivity of muscle) was slightly higher than or equal to that measured for the 100%-muscle model for all positions. The measured maximum average SAR for the child for all orientations was much higher than that for the adult (e.g., 0.187 W/kg versus 0.063 W/kg), which is expected since the frequency is closer to the resonance frequency for the child. Another series of scale-model measurements was conducted for determination of the average SAR values for man when exposed erect, with arms down, or both arms raised, or one arm extended to the right, and when exposed sitting. The results are shown in Table 4.

COMPUTERIZED THERMOGRAPHIC SYSTEM

We developed a computerized thermographic system to facilitate analysis of the large number of thermograms required to map the SAR distributions in man exposed to RFR under many possible conditions. Thermograms were taken of scale models of man similar to those used for the measurements of average SAR, shown in Fig. 8, but consisting of gelled synthetic muscle tissue with scaled conductivity. The technique was as described by Guy et al. (1976), and analysis was according to the method discussed in the same reference and a newly developed computer method discussed below.

A more modern interactive-computer approach to the thermographic-recording analysis was implemented for assessment of SAR distribution; the system is diagrammed in Fig. 9. The AGA thermovision 680 system was interfaced with an AGA-supplied Oscar digitizer-digital tape-recording system. The system was used to digitize and store thermographic images as well as to provide interfacing to a computer. Images could be recorded at will or recorded automatically over a selected sampling interval. The images could then either be played back and analyzed on the thermography system with its analog data-processing features or be transferred to digital tape (Fig. 10) and then to a computer (Fig. 11).

TABLE 3. MEASURED AVERAGE SAR IN SCALE MODELS OF MAN* UNDER DIFFERENT EXPOSURE ORIENTATIONS AND BODY POSTURES

Position	SAR (W/kg per 1 mW/cm^2)		
	Adult (1.71 m) Muscle Model	Child (0.86 m) Muscle Model	Adult Mixed Model
Standing			
Facing source (EHK)	0.050	0.164	0.059
Back to source (-EHK)	0.053	0.175	0.057
Left side to source (EKH)	0.041	0.187	0.046
Lying on Back			
Head to source (-KHE)	0.049	0.095	0.050
Feet to source (KHE)	0.050	0.095	0.048
Left side to source (HKE)	0.041	0.061	0.042
Lying on Left Side			
Facing source (HEK)	0.049	0.108	0.054
Head to source (-KEH)	0.053	0.158	0.054
Feet to source (KEH)	0.063	0.165	0.061

*Scaling Factor: 5.44
Operating frequency: 2450 MHz
Simulated frequency: 450 MHz

TABLE 4. AVERAGE SAR $(W/kg)_2$ VALUES FOR 1.71-m-TALL MAN (WITH HOMOGENEOUS-MUSCLE BODY) EXPOSED TO 1-mW/cm^2 450-MHz RFR UNDER DIFFERENT EXPOSURE POLARIZATIONS AND BODY POSTURES

Polarization	Orientation	Posture			
		Arms down	Arms up	R-Arm out	
HEK	Lying on left side--facing source	0.042	0.047	0.044	
-HEK	Lying on left side--back to source	0.040	0.046	0.045	
HKE	Lying on back--left side to source	0.049	0.046	0.052	
-HKE	Lying on back--right side to source			0.055	
KEH	Lying on left side--feet to source	0.061	0.070	0.055	
-KEH	Lying on left side--head to source	0.050	0.071	0.048	
KHE	Lying on back--feet to source	0.053	0.058	0.048	
-KHE	Lying on back--head to source	0.049	0.056	0.054	
		Standing			Sitting
EHK	Facing source	0.050	0.055	0.051	0.057
-EHK	Back to source	0.046	0.053	0.047	0.056
EKH	Left side to source	0.038	0.039	0.036	0.057
-EKH	Right side to source			0.040	0.060

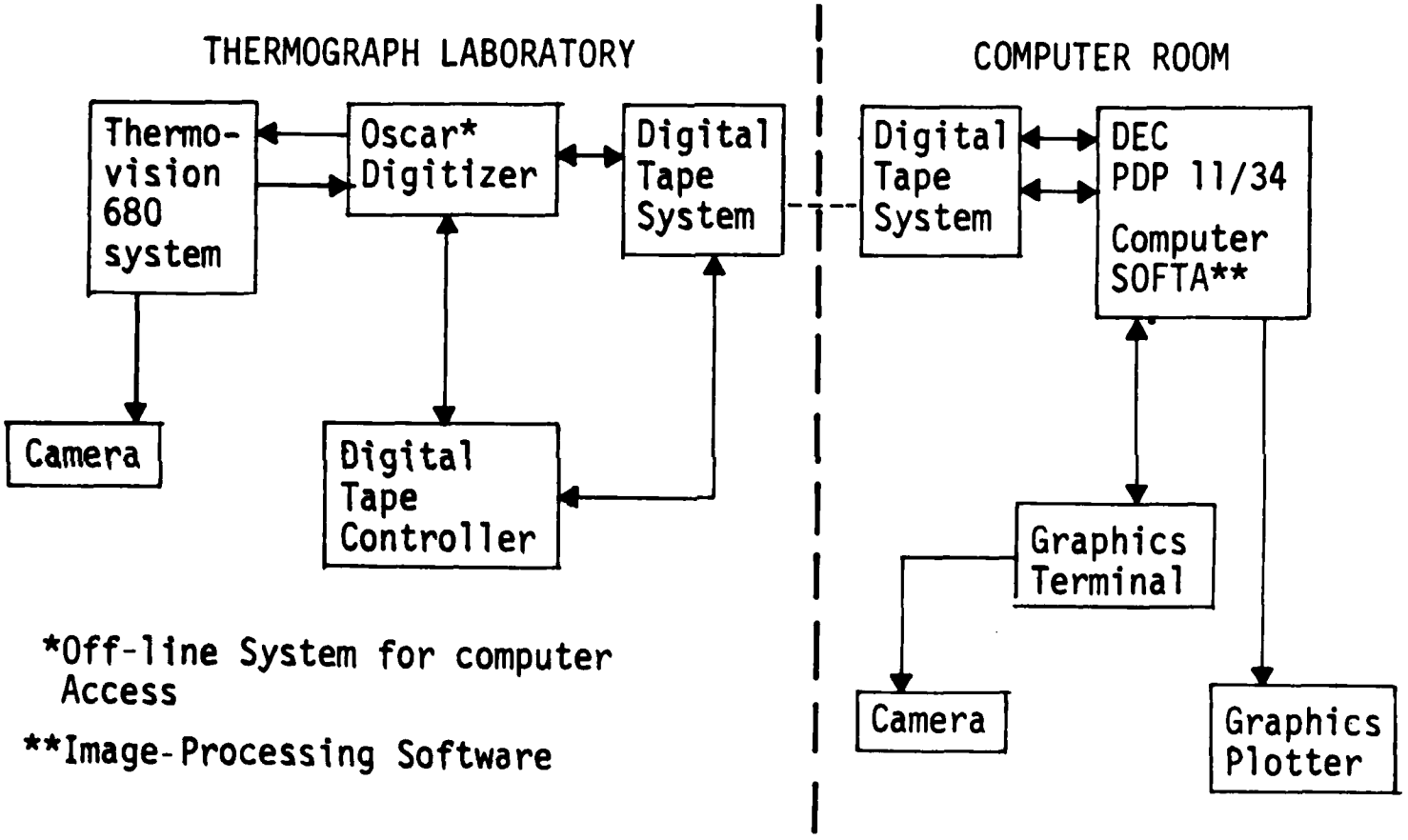

Figure 9. Diagram of digitized thermography system.

Figure 10. Digitized thermography system; data storage in magnetic tapes.

Figure 11. Transfer of data from magnetic tapes to DEC 11/34 computer system.

When the digital tape-recording system was interfaced with a PDP 11/34 computer, its graphics terminal and the graphics plotter (Fig. 12) could be used for analysis of the dosimetry thermograms. Magnetic tape was transported from the thermograph laboratory to the computer room for general image processing by software specially developed for detailed computer-image analysis. The analytical system is semi-interactive, enabling the operator to identify exactly which regions, in which images, are of interest. A 12-parameter intraregional statistical analysis can then be made of these regions; and in any selected region the following can be determined: highest and lowest SAR values, range, median, average, variance, and skewness of distribution; area of region; parameter, shape factor, geometric centroid, and percentage of total image observed. The software was arranged to enable tailoring to specific applications by selection and elimination of various subroutines. Algorithms were added to enable the computer to perform automatic interpretation and analysis. This system significantly accelerated the thermographic analysis of SAR distribution patterns and improved the reliability of data.

The graphics system employs the Hewlett/Packard 7220 flatbed plotter and the Qume Sprint-5 printer. Both serve as peripherals to the PDP 11/34 minicomputer. The HP-plotter output consists of four basic types of plot: gray-scale, contour, multiple-profile, and single-profile scans. The Qume-printer output consists of gray-scale printouts showing the different areas of heating as varying shades of gray.

An example of the contour plot is presented in Fig. 13; this plot corresponds to a midbody closeup plot of the thermogram shown in Fig. 14A, which was taken directly from the thermographic scope. Each curve in the contour plot is an iso-SAR line showing points of equal SAR in the thermographed object. Six contour levels appear in the example, but up to 20 different contour levels may be included in a plot. In addition, the contours are plotted in a sequence of four colors to simplify identification of isothermal lines; the colors are not visible in the example because of the photocopying process used for this report. This drawback is the primary consideration in not using this type of plot in this report. In Fig. 13, contours at equal intervals cover the range of SAR values from 0.05 to 0.39 W/kg per mW/cm^2.

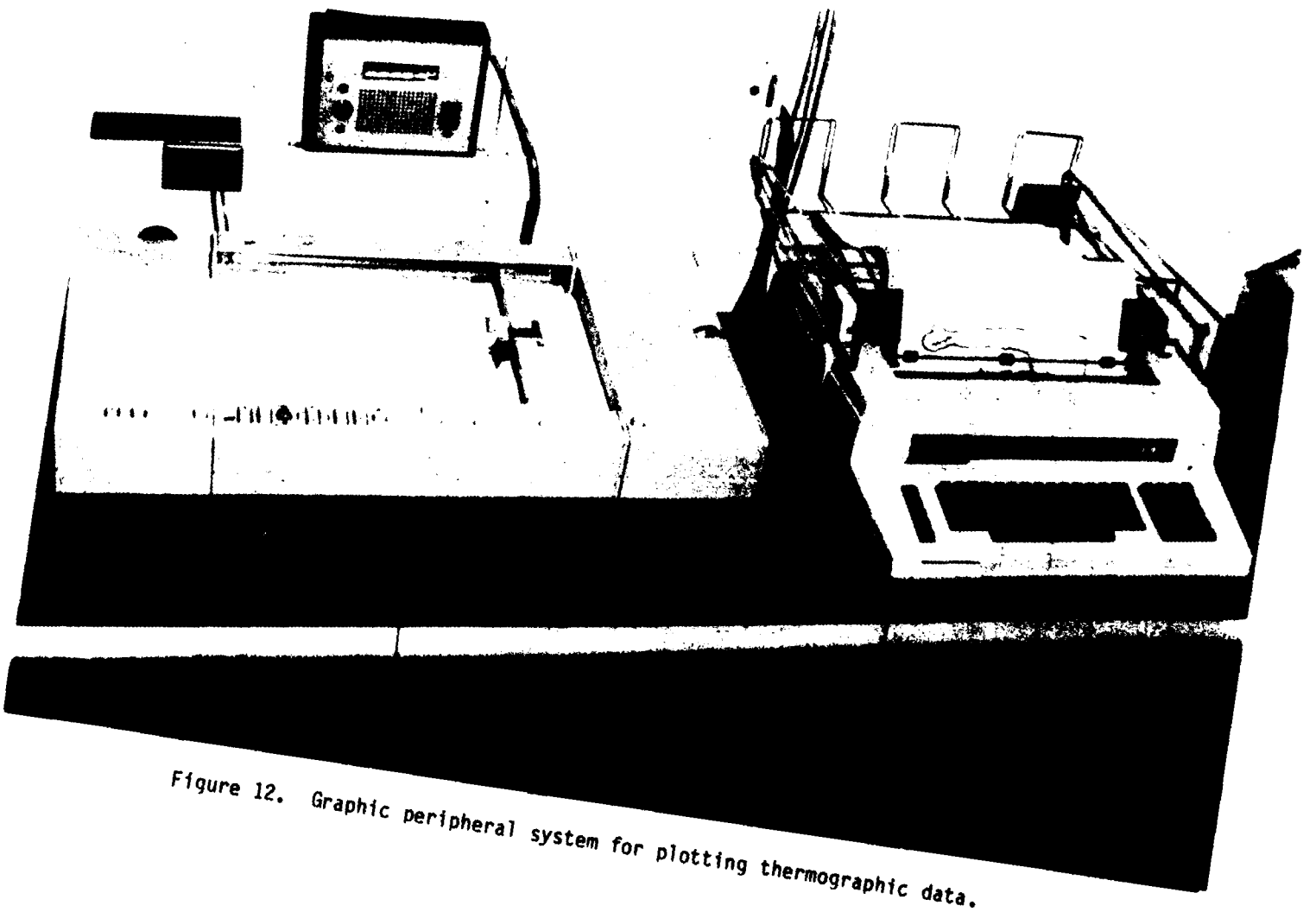

Figure 12. Graphic peripheral system for plotting thermographic data.

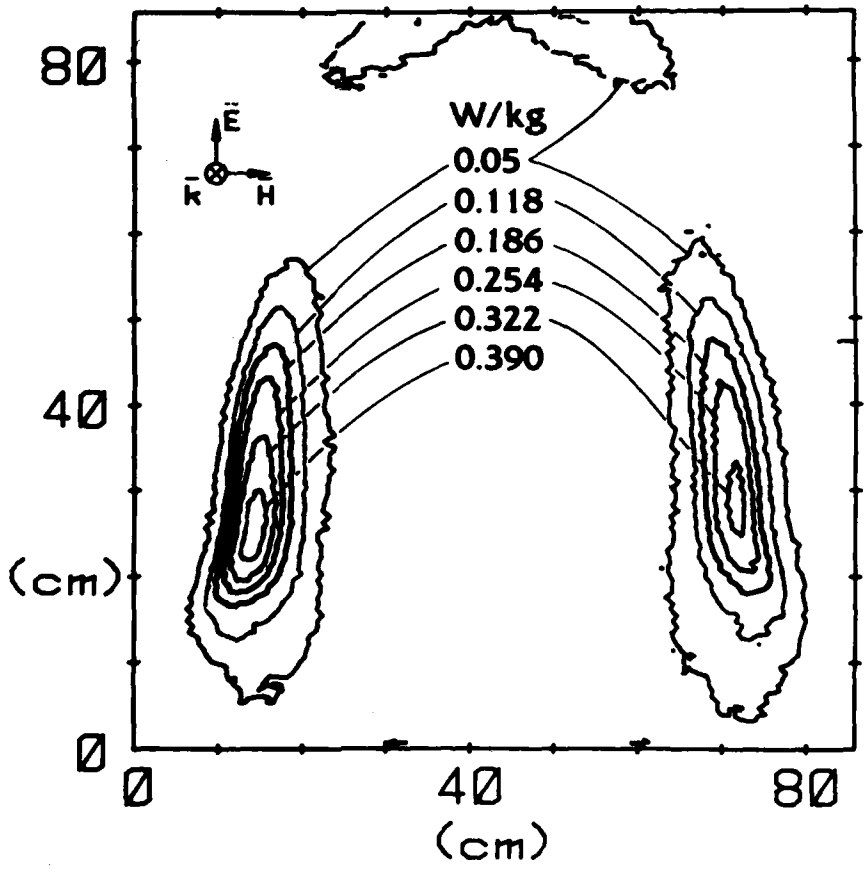

Figure 13. Computer-processed contour plot of SARs for model man exposed to EHK-polarization electromagnetic radiation (midbody close-up).

70 kg MAN h = 1.74 m sf = 5.54

P_{inc} = 1.0 mW/cm^2 f = 442 MHz

THERM 10780-01

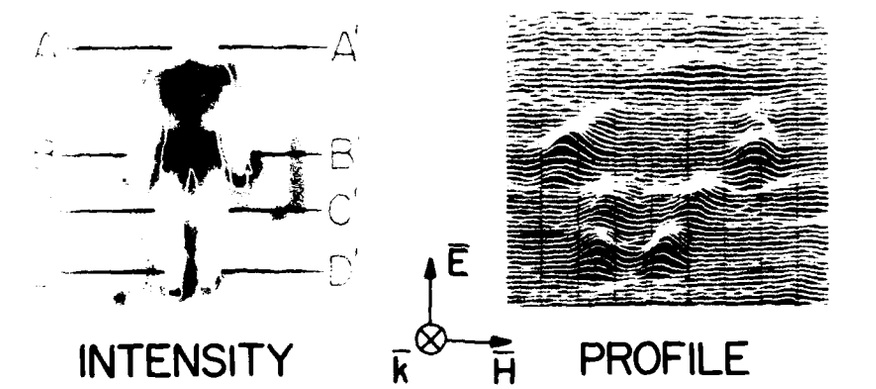

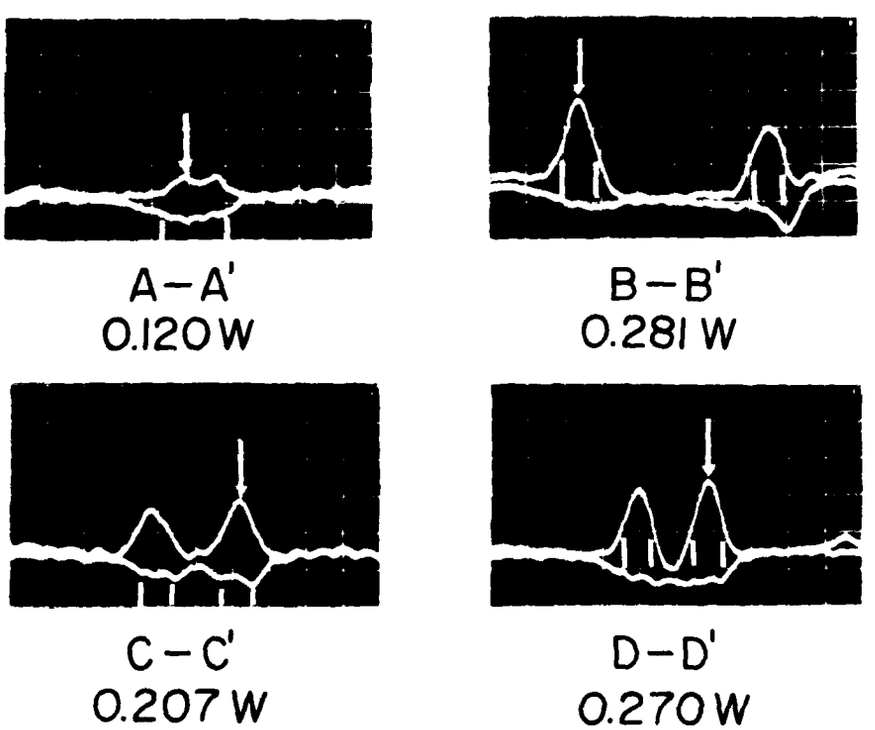

A–A'
0.120 W

B–B'
0.281 W

C–C'
0.207 W

D–D'
0.270 W

Figure 14A. Conventional thermograms from thermograph indicator showing SARs for model man exposed to EHK-polarization electromagnetic radiation.

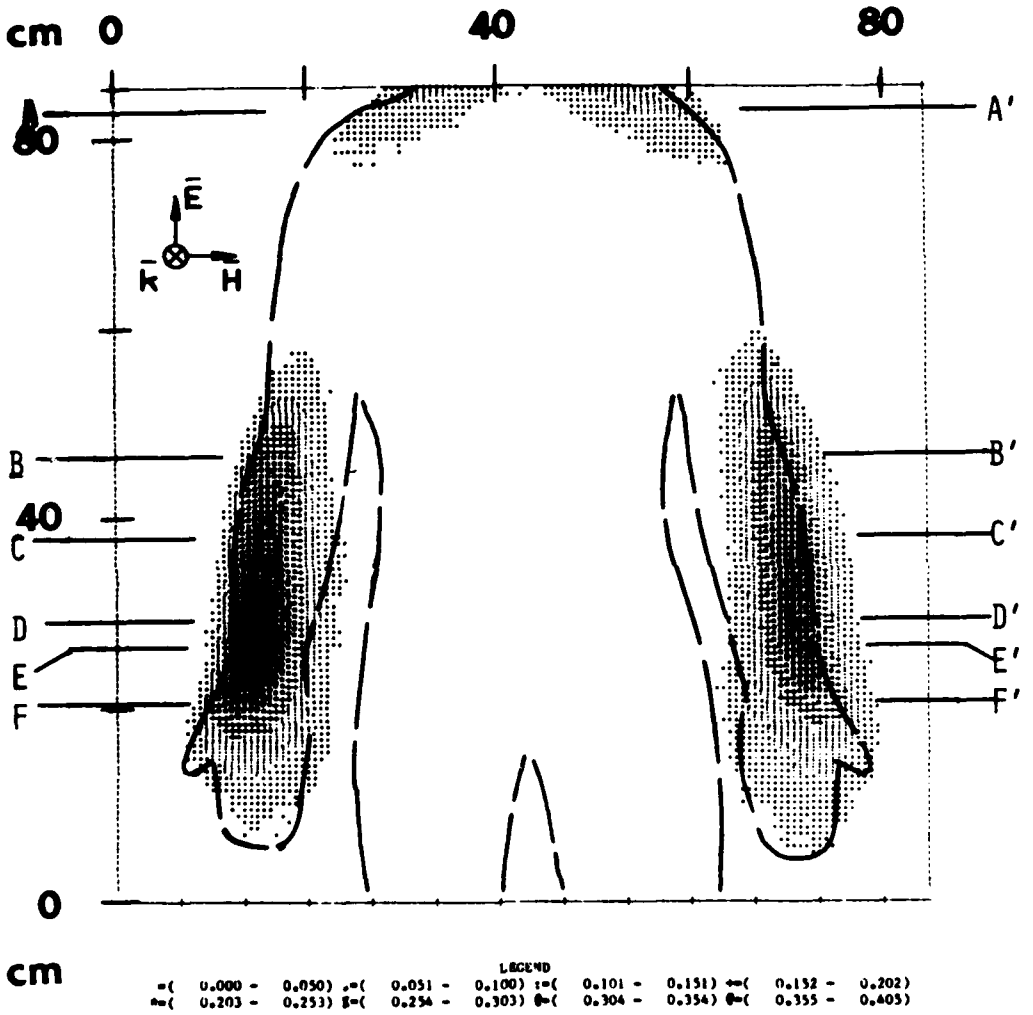

Figure 14B. Computer-processed gray-scale plot of SARs for model man exposed to EHK-polarization electromagnetic radiation (mid-body closeup).

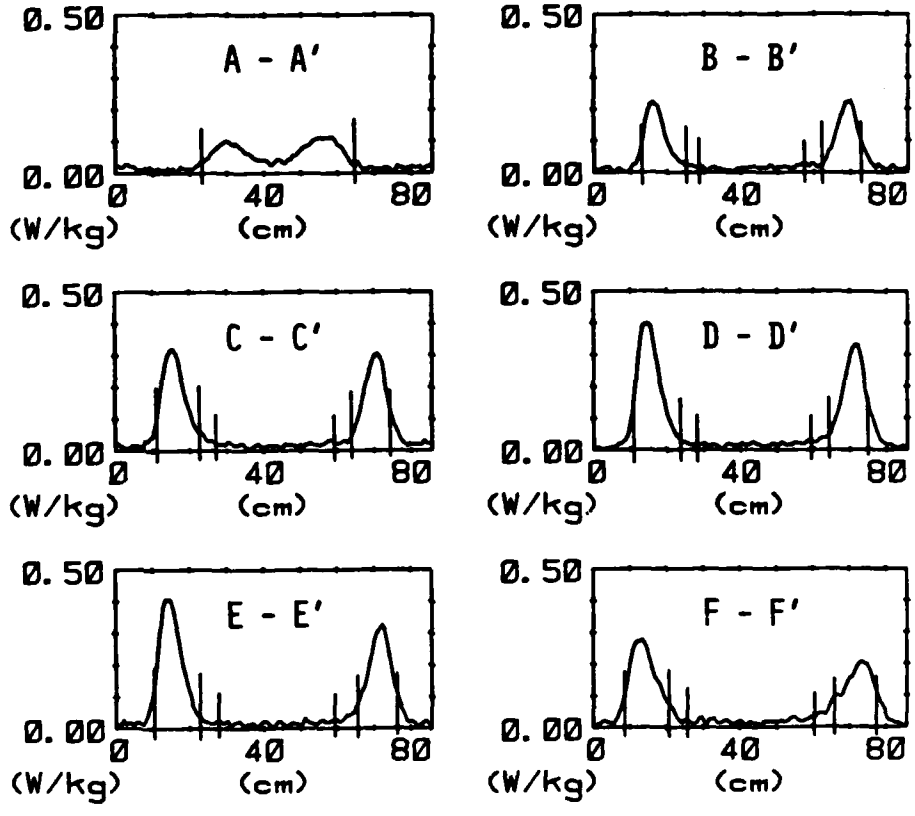

Figure 14C. Computer-processed single-profile scans of SARs for model man exposed to EHK-polarization electromagnetic radiation (midbody closeup).

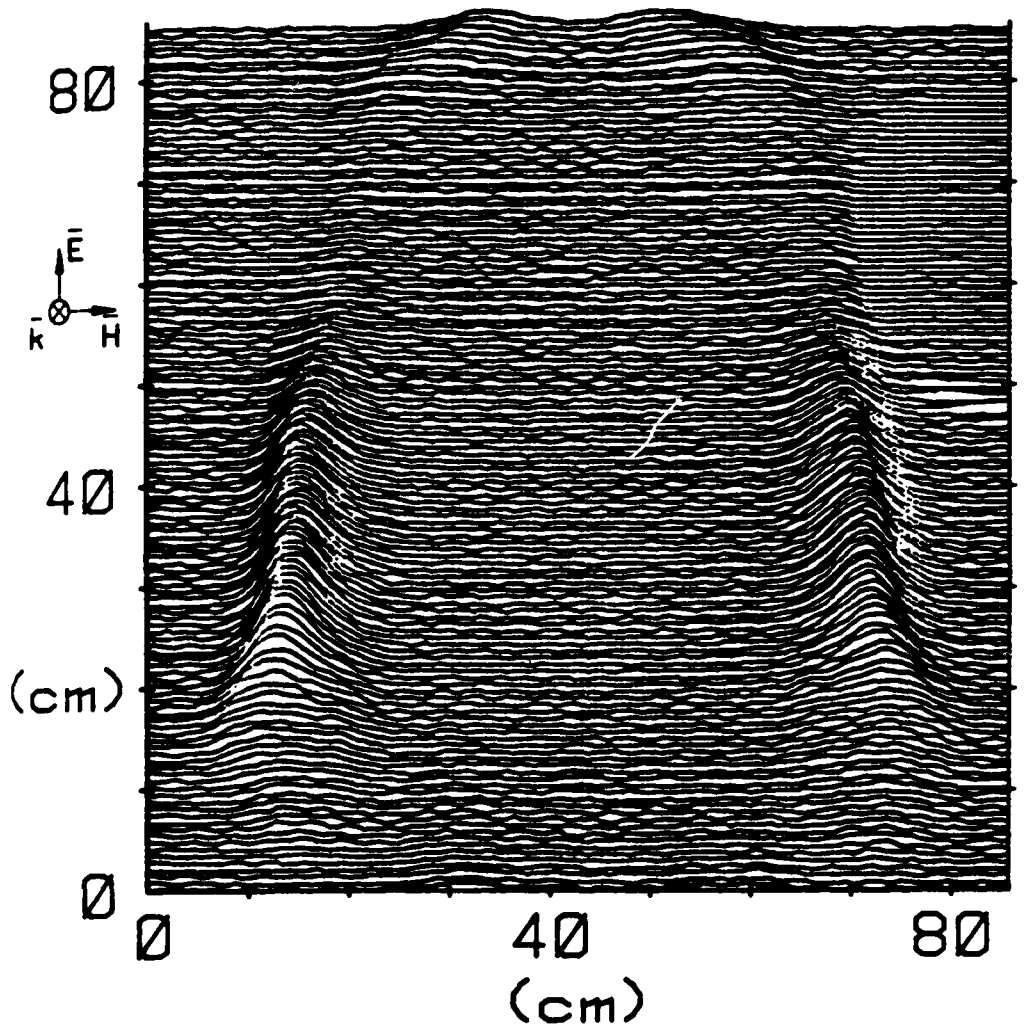

Figure 14D. Computer-processed multiple-profile scan of SARs for model man exposed to EHK-polarization electromagnetic radiation (midbody closeup).

A processed gray-scale plot of the body midsection is reproduced in Fig. 14B, and in Fig. 14C the SAR is shown along specific scan lines (B-scans) in the digitized thermograph. Each thermograph is made up of 128 scan lines. All B-scan plots are labeled to indicate the proper point of comparison with a gray-scale plot of the same image. Profile plots are composed of multiple B-scans, as shown in Fig. 14D, presenting a sort of relief map of SAR over the thermographed object. The profile plots included later in this section show the entire image for all exposures, and closeup scans for some exposures. The plot can be limited to any rectangular area of the image so that the analyst can blow up areas of interest for more detailed examination. Gray-scale plots are printouts that display heating in eight different shades, each shade of gray representing a specific heating (SAR) range. The SAR ranges are displayed at the bottom of each plot, as shown in Fig. 14B. For each exposure the user may also display the plot in terms of temperature, temperature change, SAR, or current density.

Too many data were collected during the period of the project for all to be included in this volume. They have been stored in large computer data files in the Bioelectromagnetics Research Laboratory, and the results for any given exposure situation can be quickly retrieved by the interactive computer program. In Fig. 15 is illustrated a page of the index for such a file, representing a block of 235 processed thermograms taken over a period of one month, as seen by the data analyst. Two thermograms correspond to each image. The first is a scan of the cross section of an unfilled model (Fig. 16). The boundary edges are heated so as to highlight the demarcation of the region filled with synthetic tissue. The exact coordinates of curve defining the boundary, obtained by direct measurement, are stored in the computer. Through an interactive program and the use of a light-pen, this curve is fitted to the thermographic image of the highlighted unfilled model and stored in the computer for later use in the analysis (Fig. 17). The computer-fitting eliminates any error due to changes in image size or shape owing to variation with distance between the thermographic camera and the object or as a result of aberration of the camera lens.

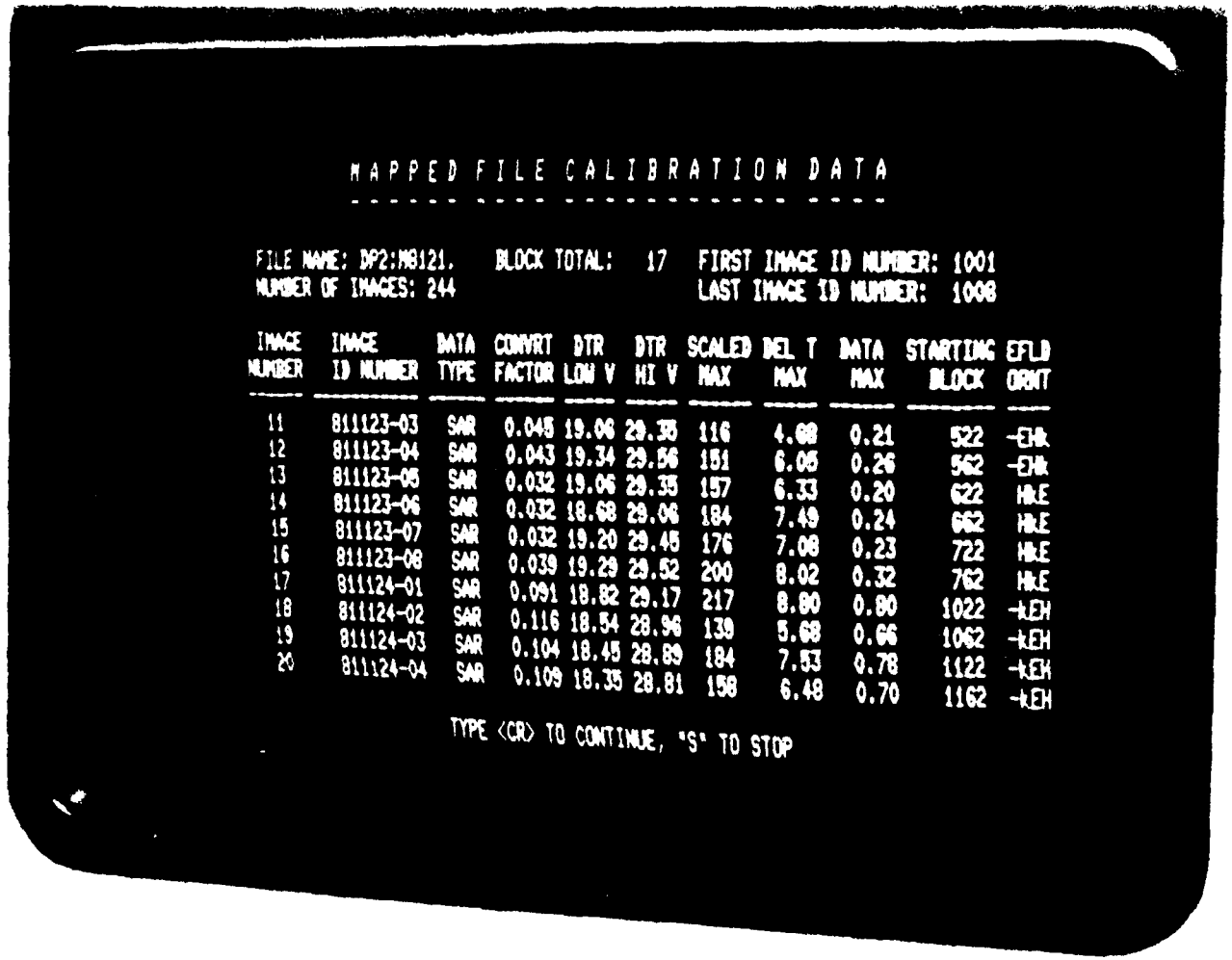

MAPPED FILE CALIBRATION DATA

FILE NAME: DP2:M8121. BLOCK TOTAL: 17 FIRST IMAGE ID NUMBER: 1001
NUMBER OF IMAGES: 244 LAST IMAGE ID NUMBER: 1008

IMAGE NUMBER	IMAGE ID NUMBER	DATA TYPE	CONVRT FACTOR	DTR LOW V	DTR HI V	SCALED MAX	DEL T MAX	DATA MAX	STARTING BLOCK	EFLD ORNT
11	811123-03	SAR	0.045	19.06	29.35	116	4.88	0.21	522	-EHk
12	811123-04	SAR	0.043	19.34	29.56	151	6.05	0.26	562	-EHk
13	811123-05	SAR	0.032	19.06	29.35	157	6.33	0.20	622	HkE
14	811123-06	SAR	0.032	18.68	29.06	184	7.49	0.24	662	HkE
15	811123-07	SAR	0.032	19.20	29.45	176	7.08	0.23	722	HkE
16	811123-08	SAR	0.039	19.29	29.52	200	8.02	0.32	762	HkE
17	811124-01	SAR	0.091	18.82	29.17	217	8.80	0.80	1022	-kEH
18	811124-02	SAR	0.116	18.54	28.96	139	5.68	0.66	1062	-kEH
19	811124-03	SAR	0.104	18.45	28.89	184	7.53	0.78	1122	-kEH
20	811124-04	SAR	0.109	18.35	28.81	158	6.48	0.70	1162	-kEH

TYPE <CR> TO CONTINUE, "S" TO STOP

Figure 15. Computer retrieval of first index page of large thermograph-image data file.

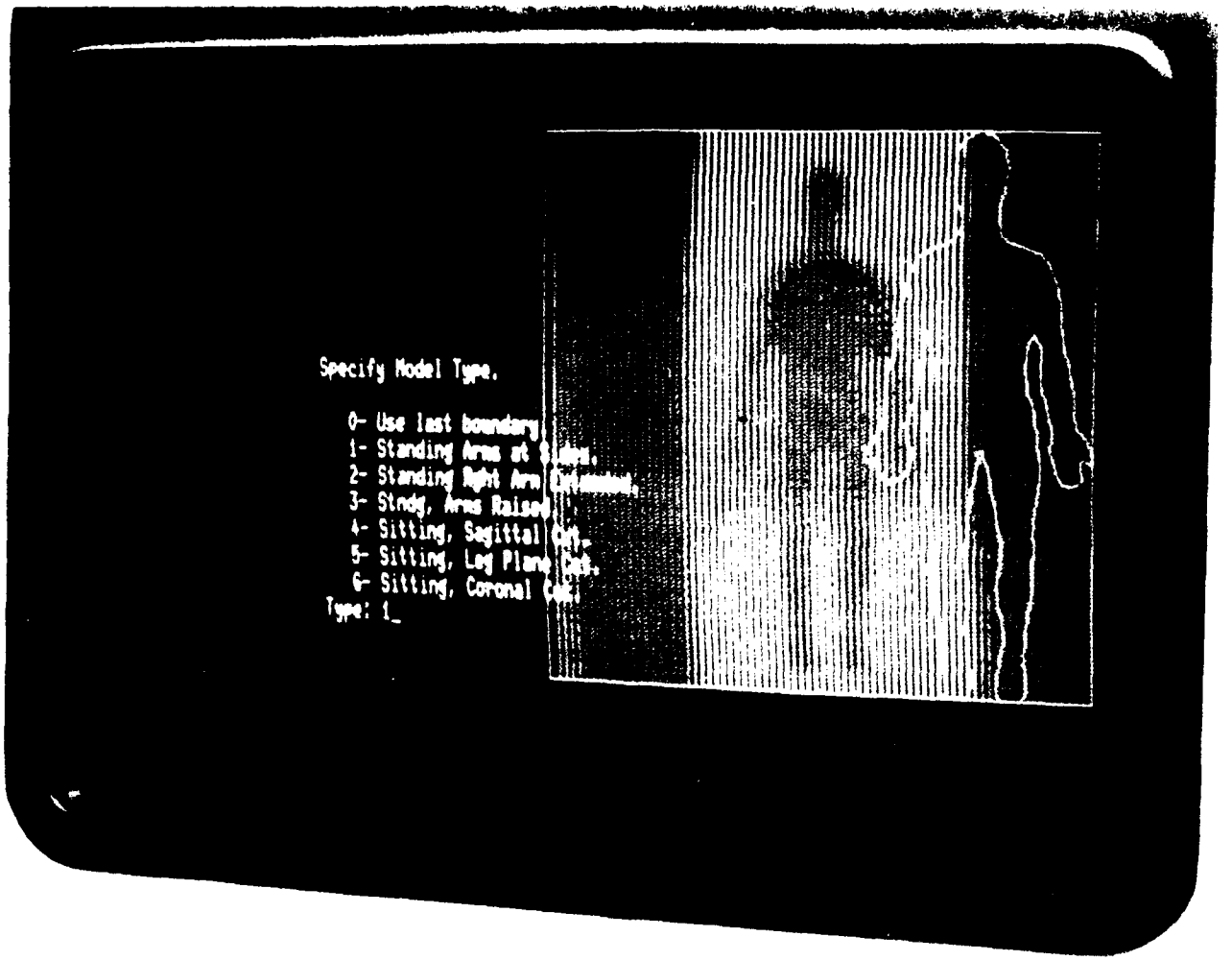

Figure 16. Retrieval of thermogram of empty heated-model Styrofoam section for boundary fitting.

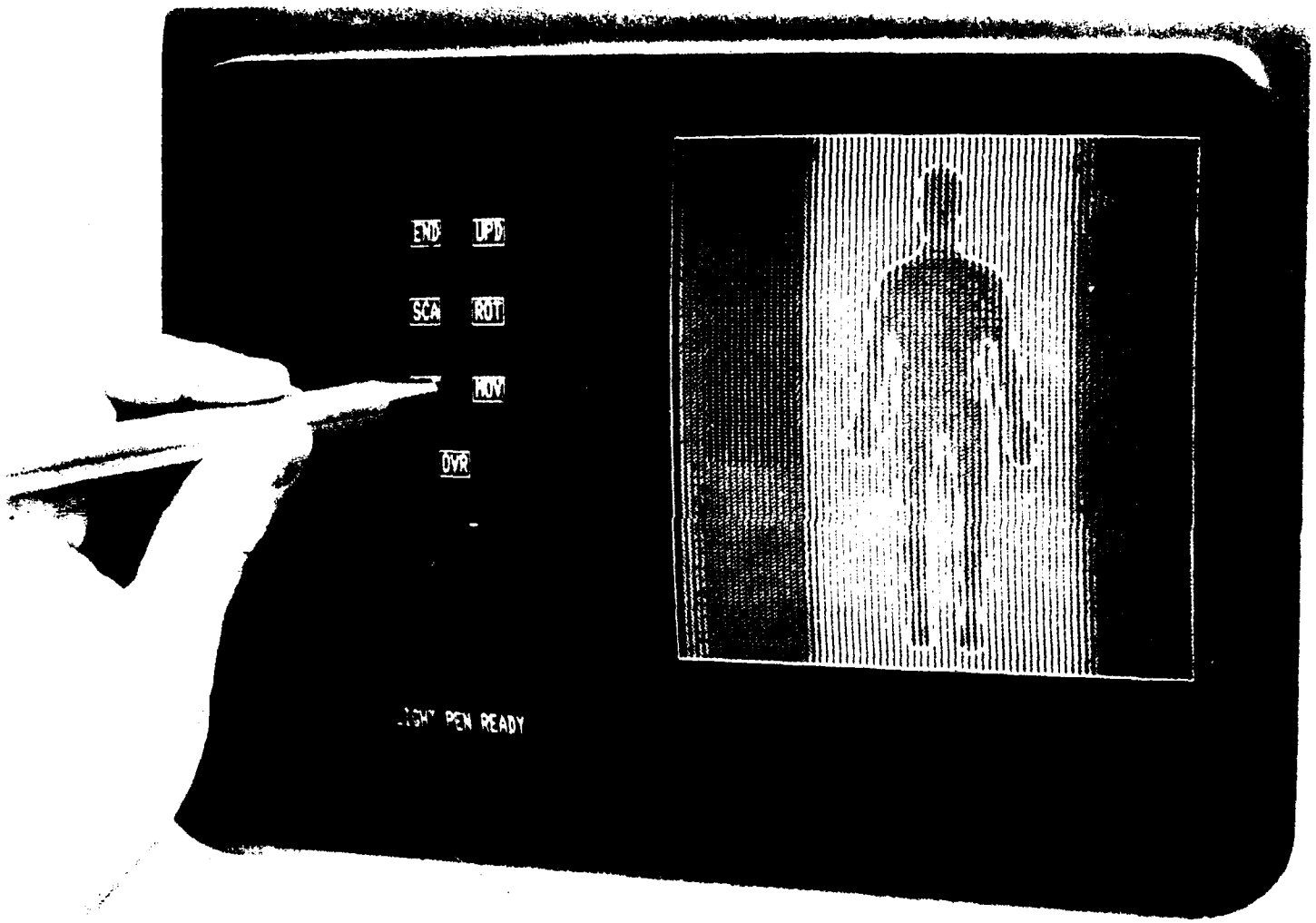

Figure 17. Boundary properly fitted to thermogram image of empty heated model.

The desired image is brought onto the screen from the file (Fig. 18). An interactive command places the boundary around the image. Another interactive command enables the analyst to touch any point on the image with the light-pen; then the pixel column number, row number, SAR per mW/cm^2, and temperature change for the actual measurement will appear at the bottom of the screen (Fig. 19). Another command displays on the screen a complete horizontal-vertical scan (Fig. 20) of the SAR. Through any point touched by the light-pen, the computer gives the mean, maximum, average, and standard deviation of the SARs along the scan. Finally, for greater accuracy, another command enables movable-crosshair selection of points on the image where further information is needed (Fig. 21). Information of interest can be filed or printed in hard-copy form as described previously and in the following sections.

SAR DISTRIBUTION PATTERNS

Thermographs were obtained for various exposed models as described by Guy et al. (1976, 1978). Except for being filled with the gelled synthetic tissue instead of liquid, the models were exposed in much the same way as for the calorimetric average SAR measurements described before. The man models were sectioned along the central frontal planes so as to form front and back half-sections so that the SAR patterns could be seen in the head, neck, thorax, arms, and legs. Some of the sitting models were sectioned through the sagittal plane so that the SAR patterns in the torso, head, neck, arms, and legs could also be obtained.

The models were exposed to 2450-MHz radiation fields in the anechoic chamber for between 20 and 60 s, with input power ranging from 5 to 10 kW. Thermograms were taken before and after exposure and stored on digital tapes, then analyzed and plotted as described in the previous section.

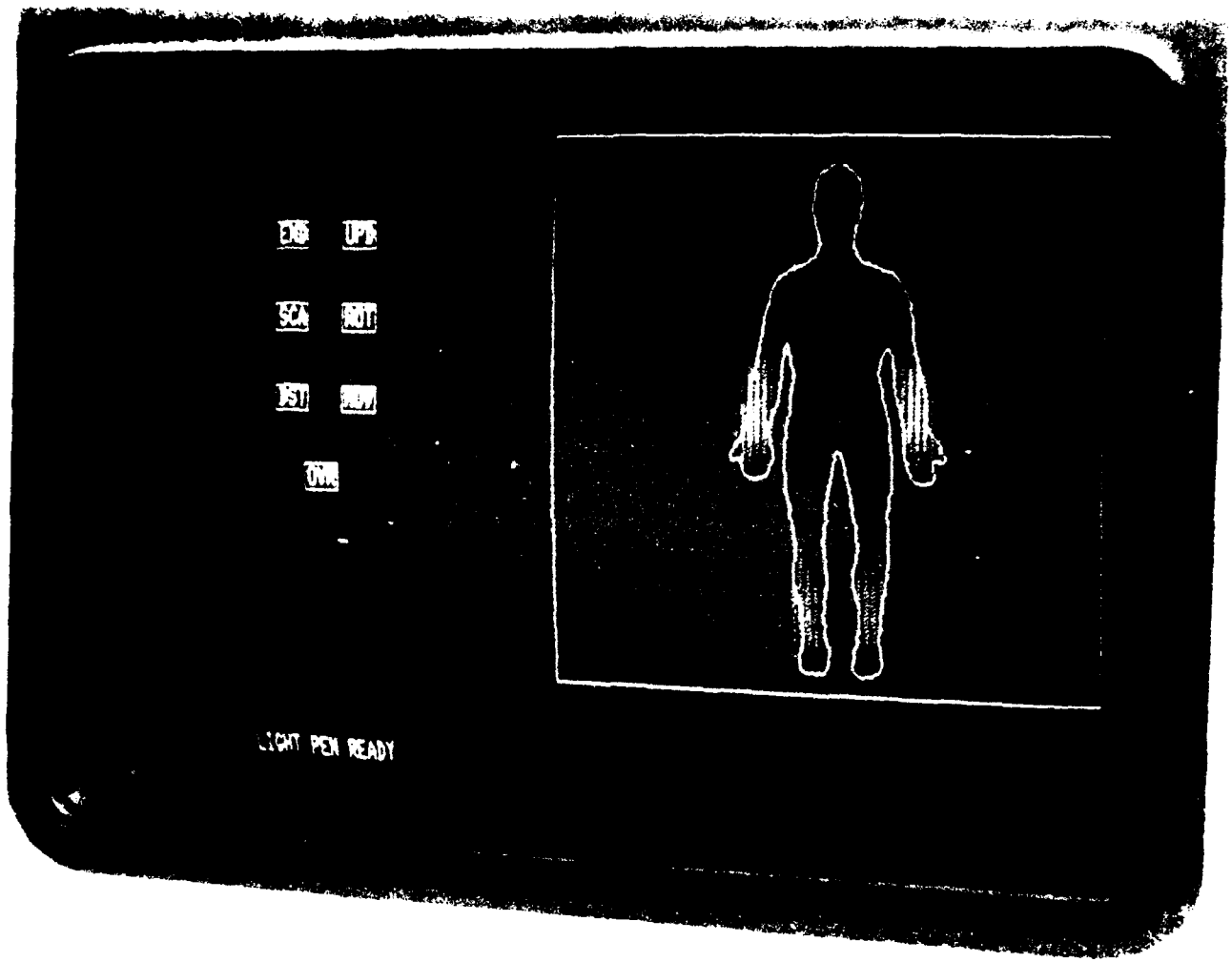

Figure 18. Retrieval of computer-processed SAR patterns with boundary of man.

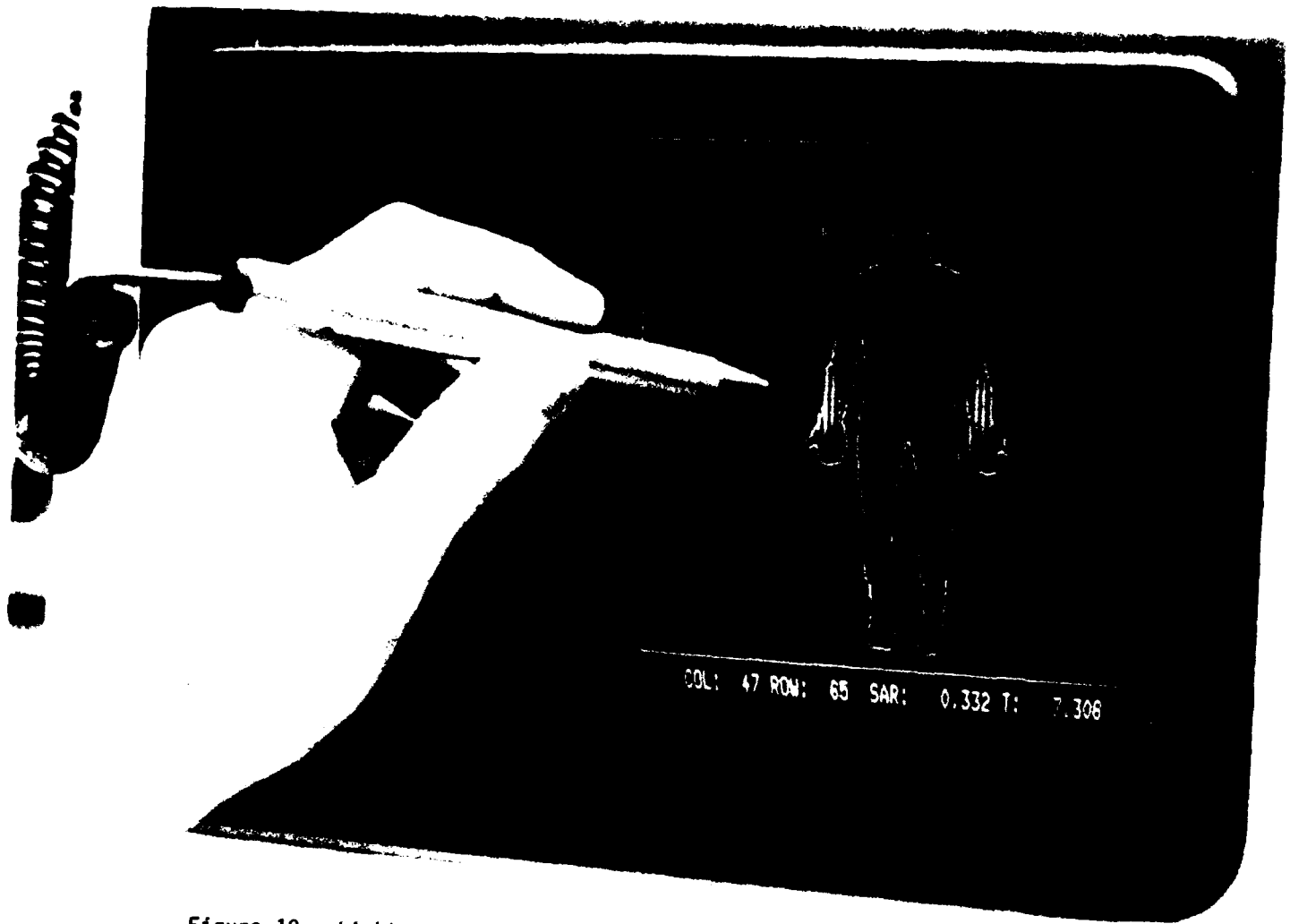

Figure 19. Light-pen used in selection of point on image where SAR information is stored.

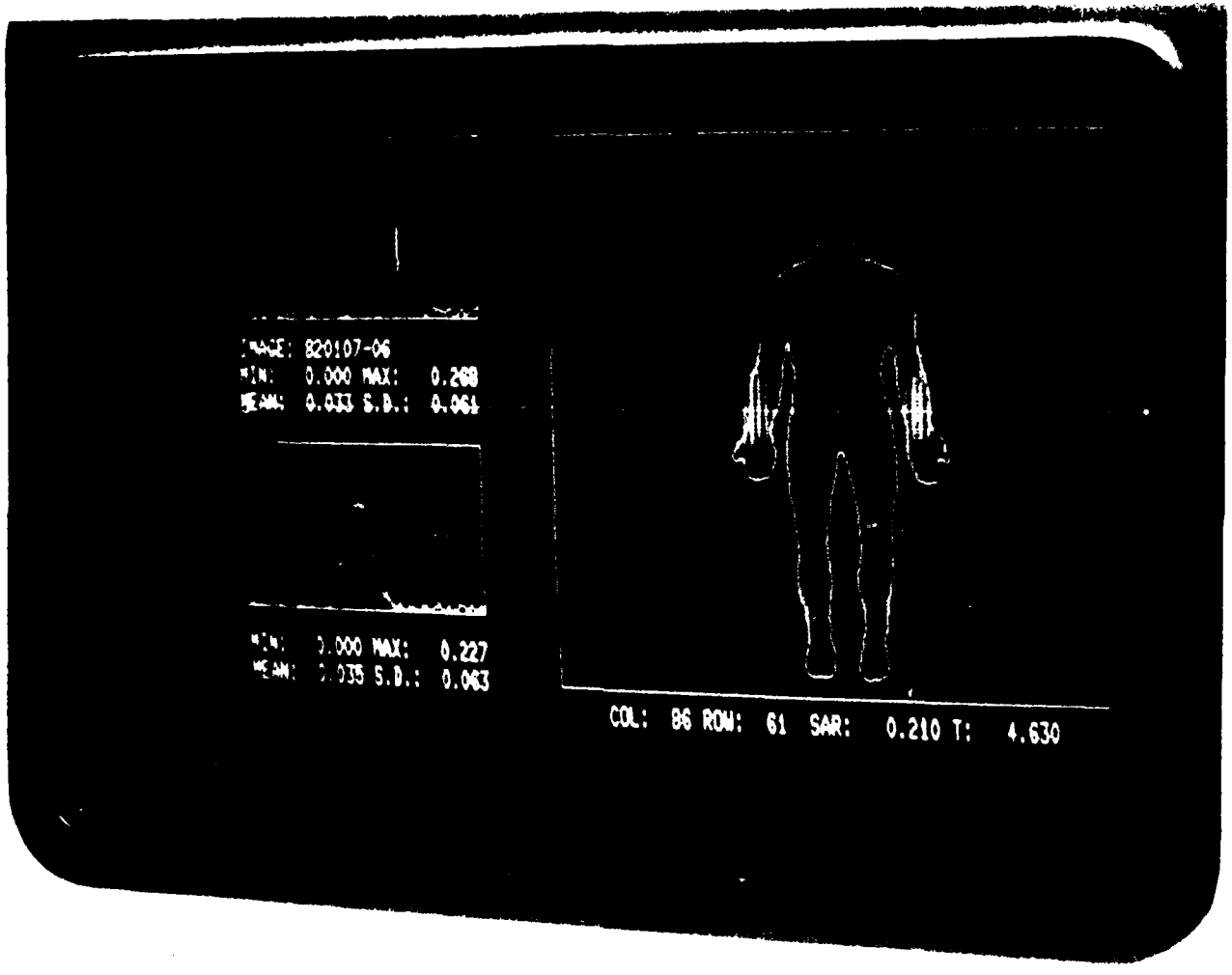

Figure 20. Light-pen selection of point on image where horizontal and vertical SAR scans are desired.

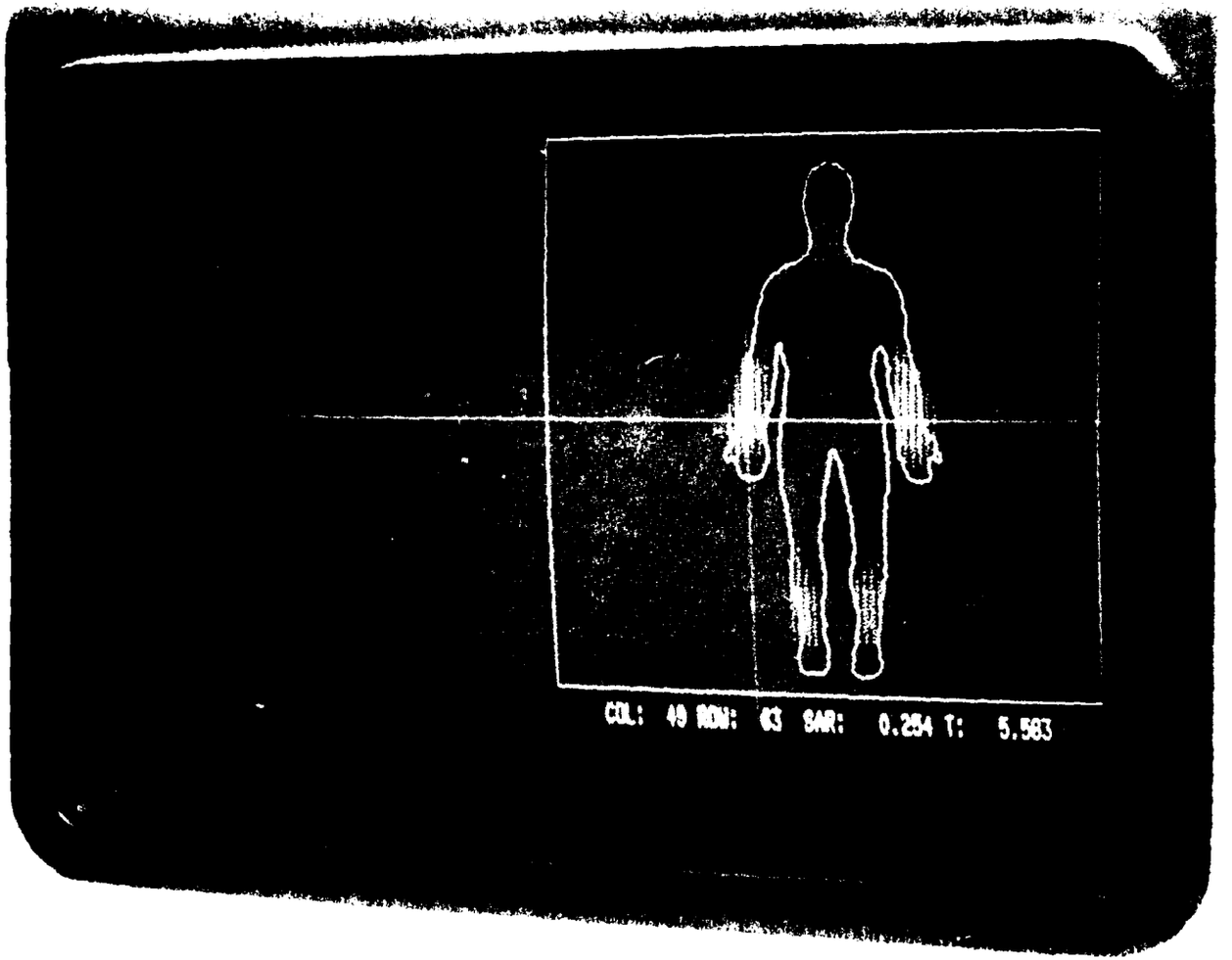

Figure 21. Crosshair selection of points on image where SAR information is desired.

The thermographic data for the 5.44-scale man model exposed under the various polarization conditions are illustrated in Figs. 22A through 62. Most of the graphic data are for whole-body scans, but representative closeup graphics are also presented of the EHK and EKH (arms down) and KEH (one arm extended) polarizations for better detail. The whole-body scans were taken with a standard lens, and the closeup scans with a narrow-angle lens. All of the closeup thermographic data obtained from the images cannot be presented in this report, but maximum SAR values at various portions of the body (Fig. 63) were obtained from the closeup thermograms and are tabulated in Tables 5 through 8.

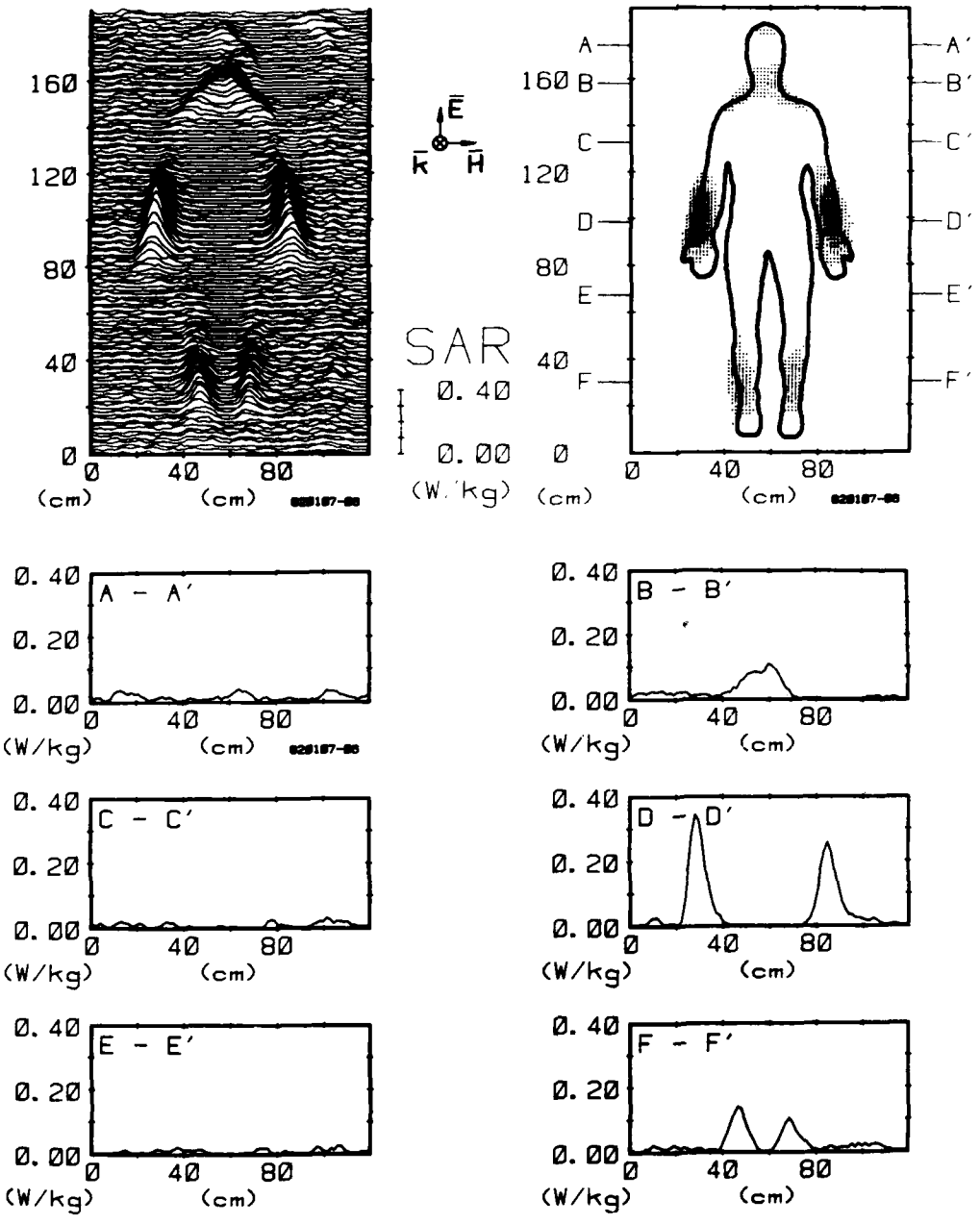

Figure 22A. Computer-processed whole-body thermograms expressing SAR patterns for man with arms down, exposed to 1-mW/cm^2 450-MHz radiation with EHK polarization.

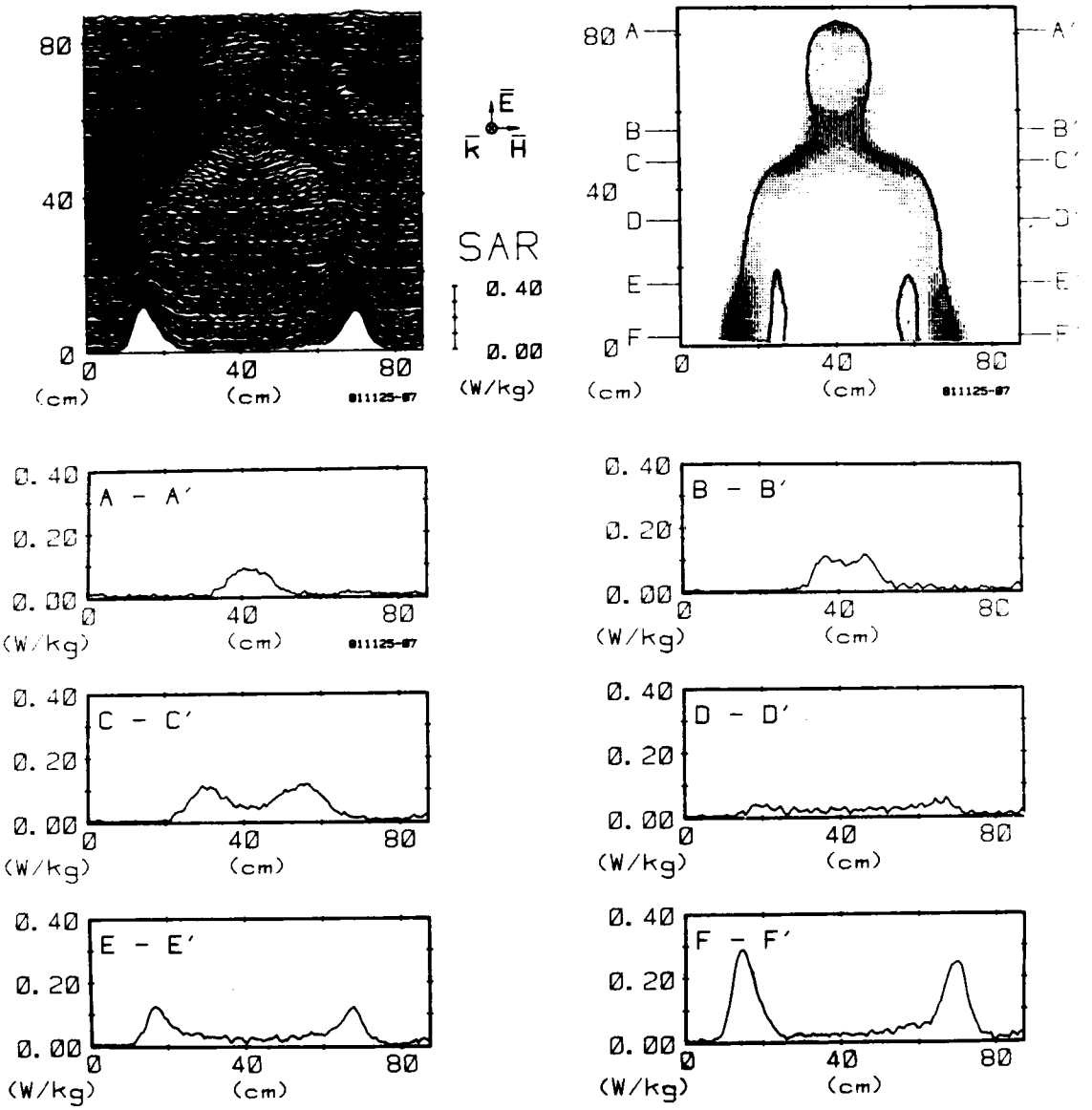

Figure 22B. Computer-processed upper-body thermograms expressing SAR patterns for man with arms down, exposed to 1-mW/cm^2 450-MHz radiation with EHK polarization.

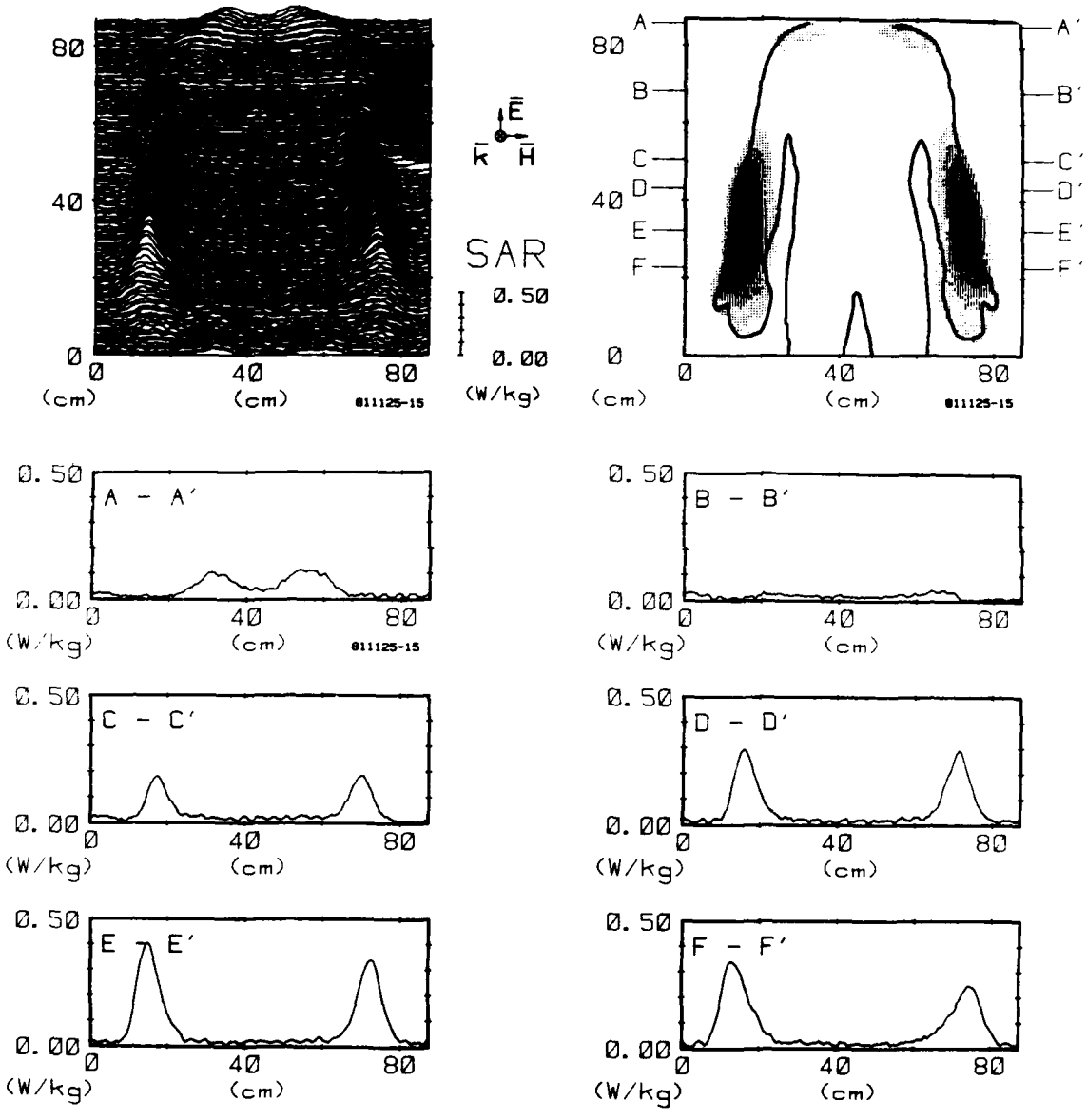

Figure 22C. Computer-processed midbody thermograms expressing SAR patterns for man with arms down, exposed to 1-mW/cm^2 450-MHz radiation with EHK polarization.

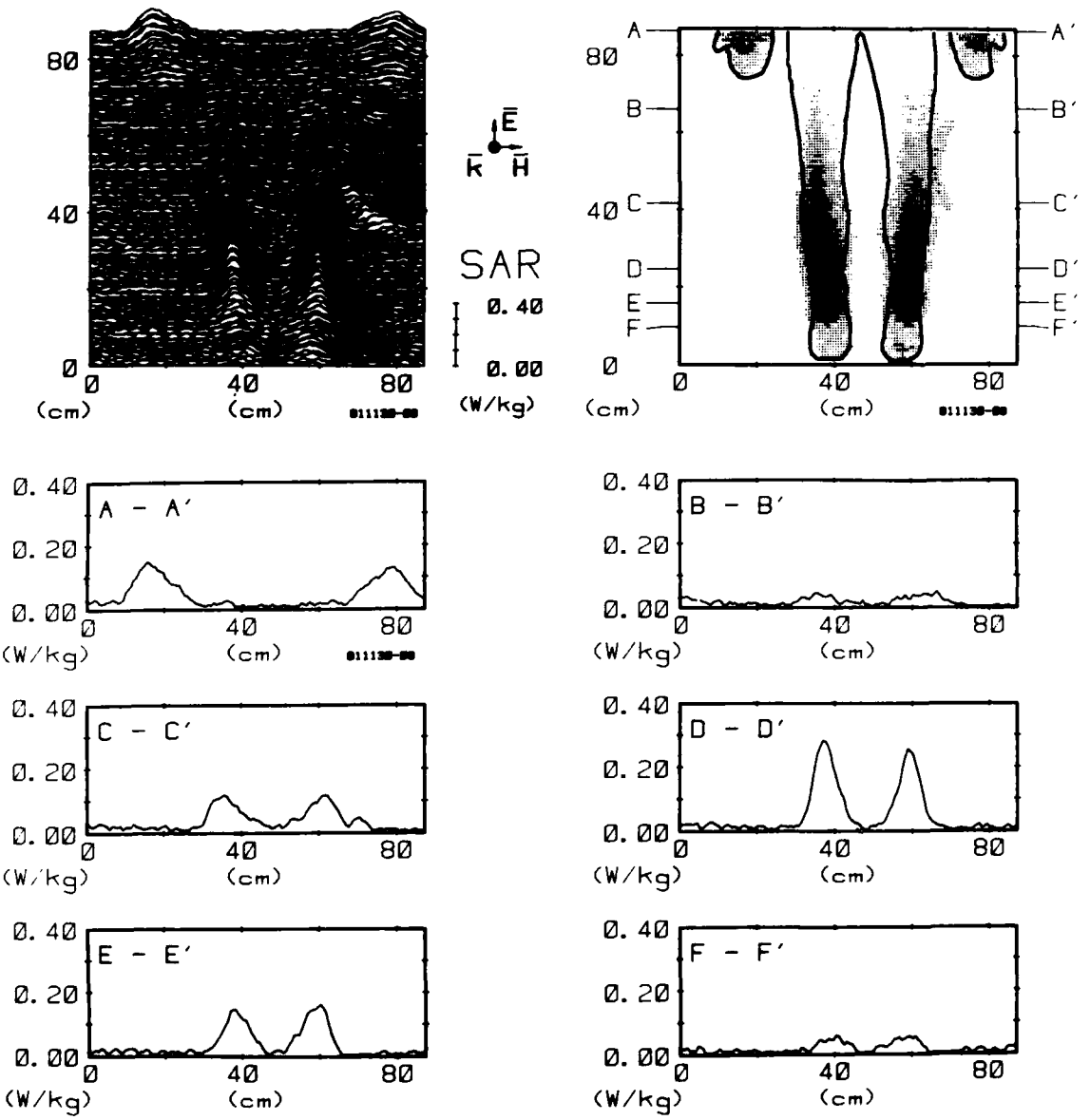

Figure 22D. Computer-processed lower-body thermograms expressing SAR patterns for man with arms down, exposed to 1-mW/cm^2 450-MHz radiation with EHK polarization.

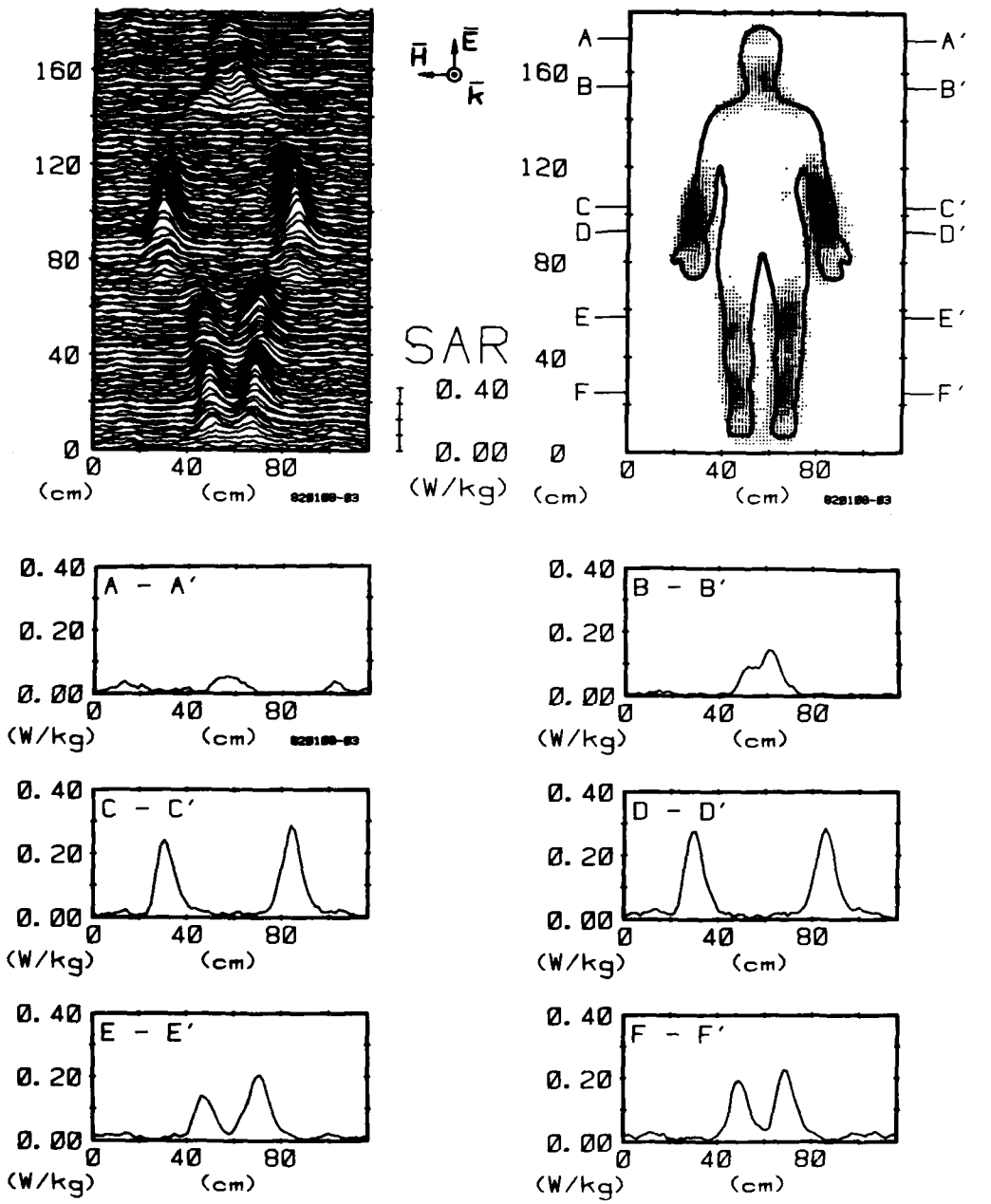

Figure 23. Computer-processed whole-body thermograms expressing SAR patterns for man with arms down, exposed to 1-mW/cm^2 450-MHz radiation with -EHK polarization.

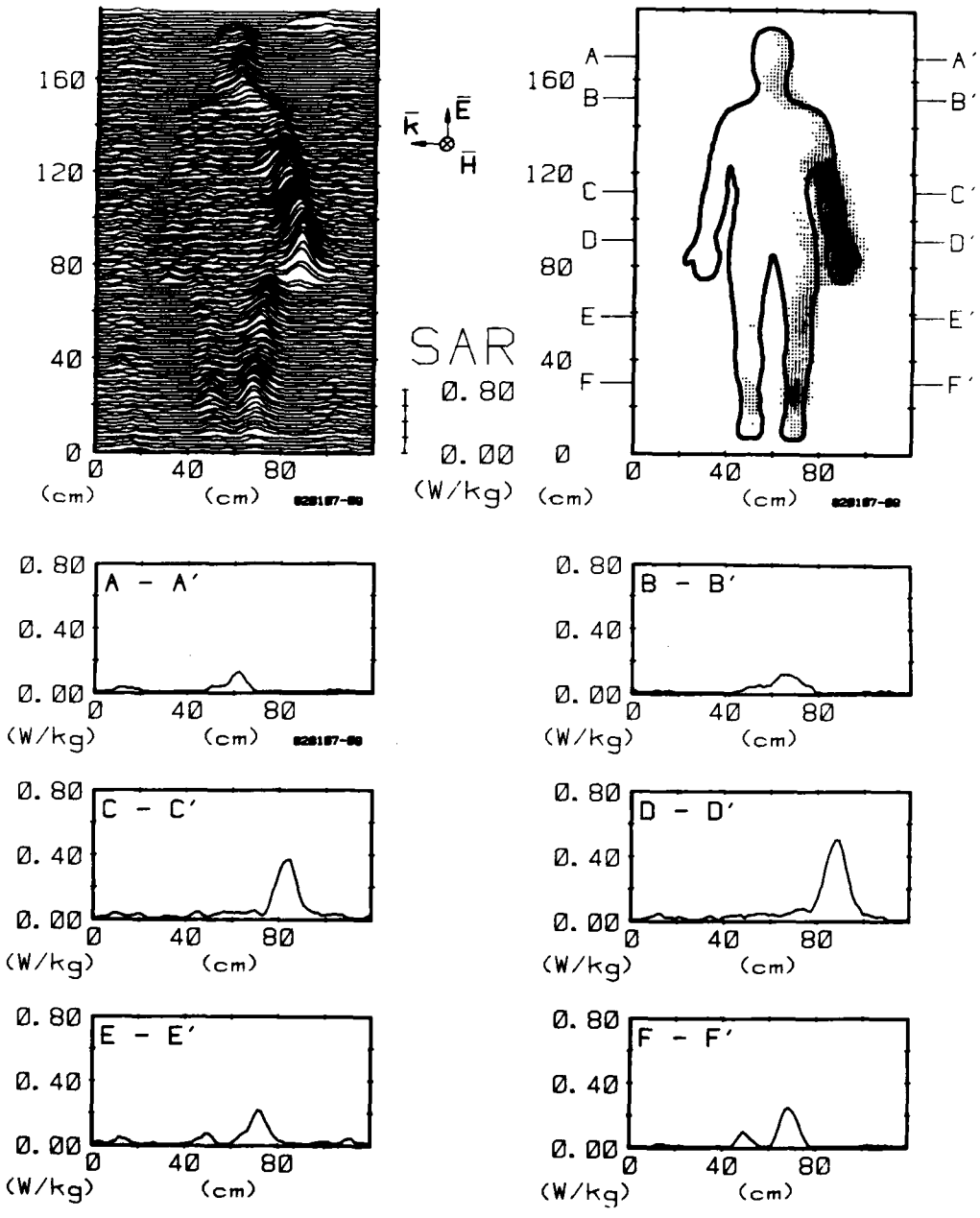

Figure 24A. Computer-processed whole-body thermograms expressing SAR patterns for man with arms down, exposed to 1-mW/cm^2 450-MHz radiation with EKH polarization.

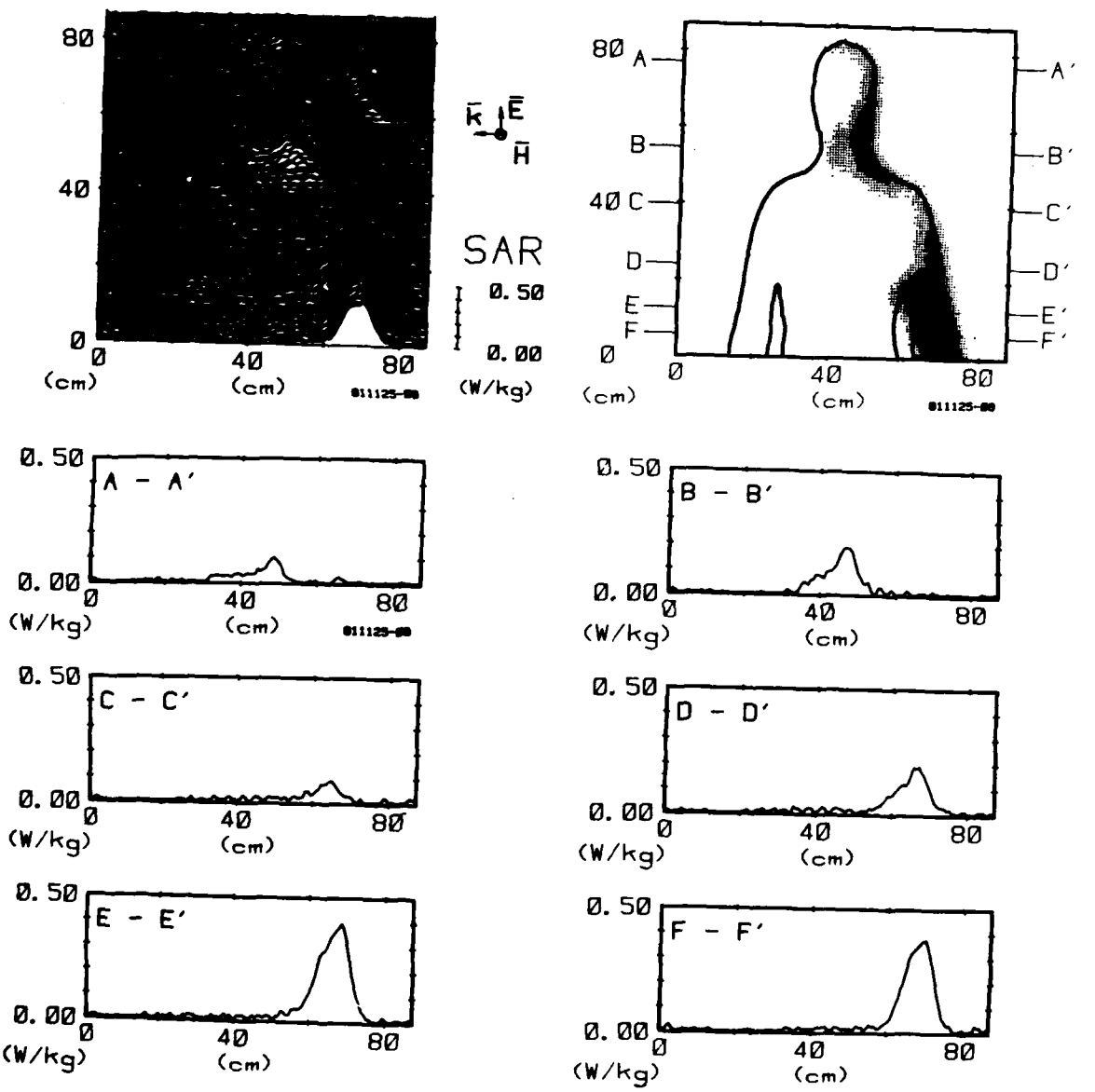

Figure 24B. Computer-processed upper-body thermograms expressing SAR patterns for man with arms down, exposed to 1-mW/cm^2 450-MHz radiation with EKH polarization.

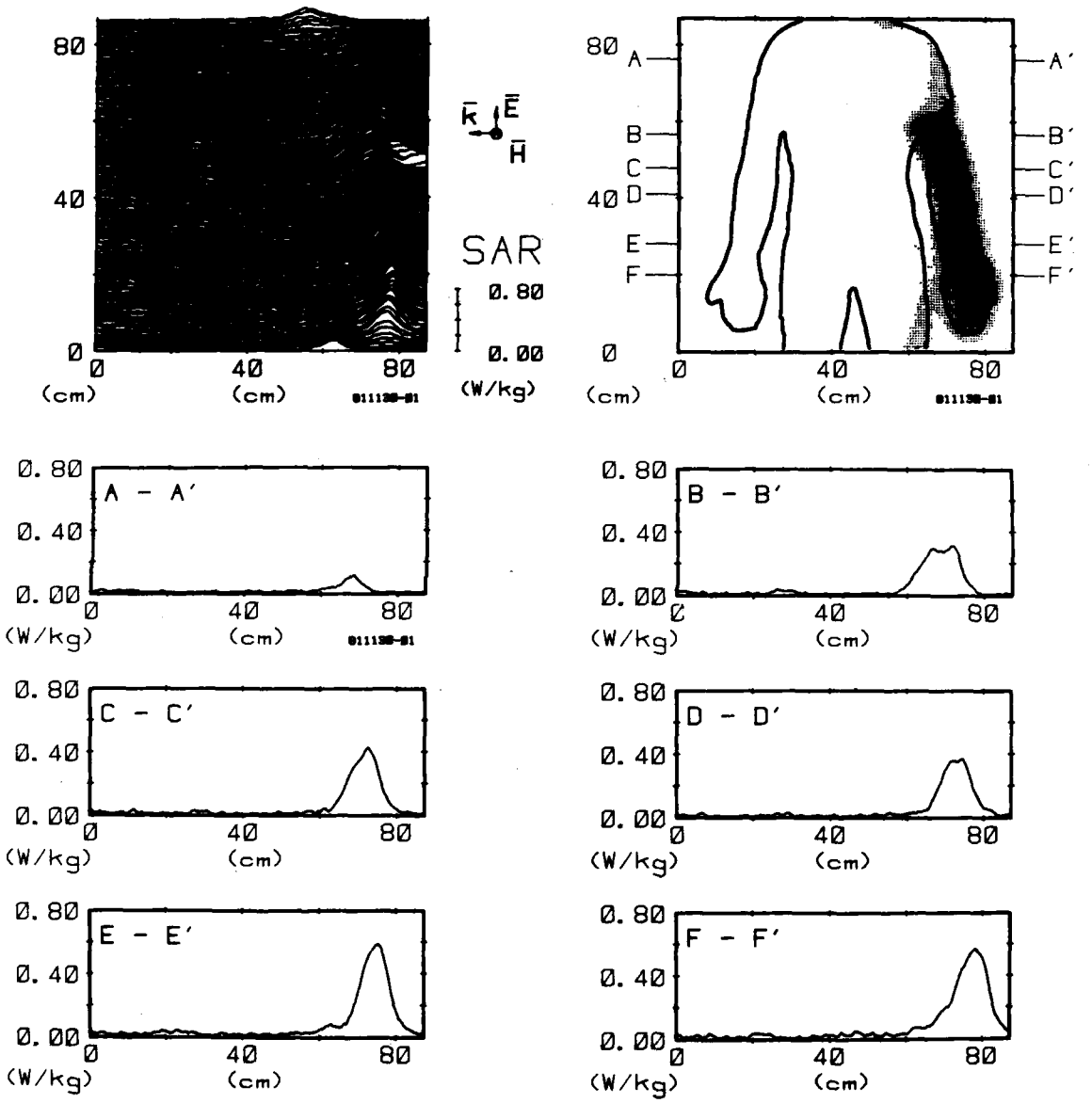

Figure 24C. Computer-processed midbody thermograms expressing SAR patterns for man with arms down, exposed to 1-mW/cm^2 450-MHz radiation with EKH polarization.

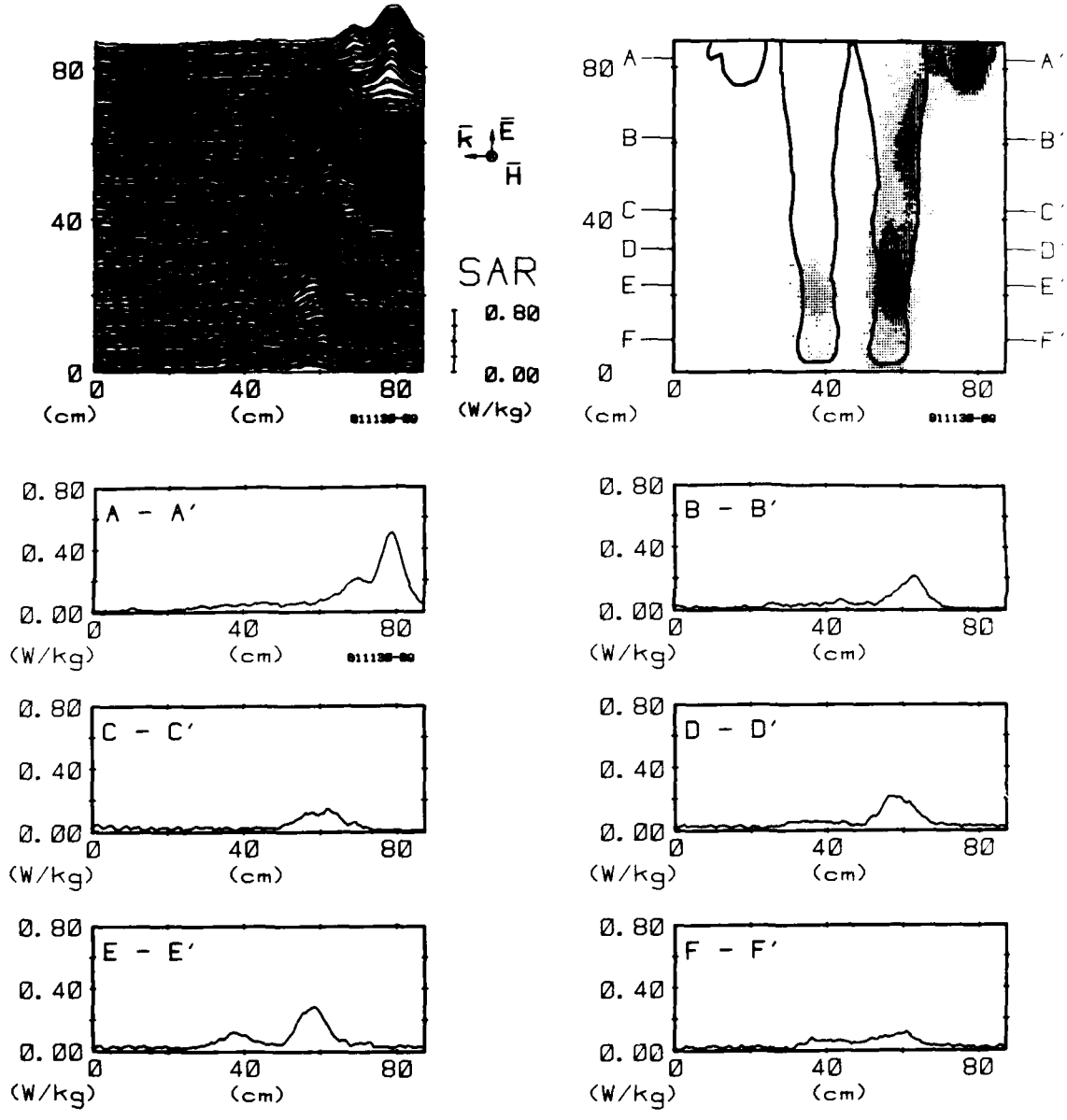

Figure 24D. Computer-processed lower-body thermograms expressing SAR patterns for man with arms down, exposed to 1-mW/cm^2 450-MHz radiation with EKH polarization.

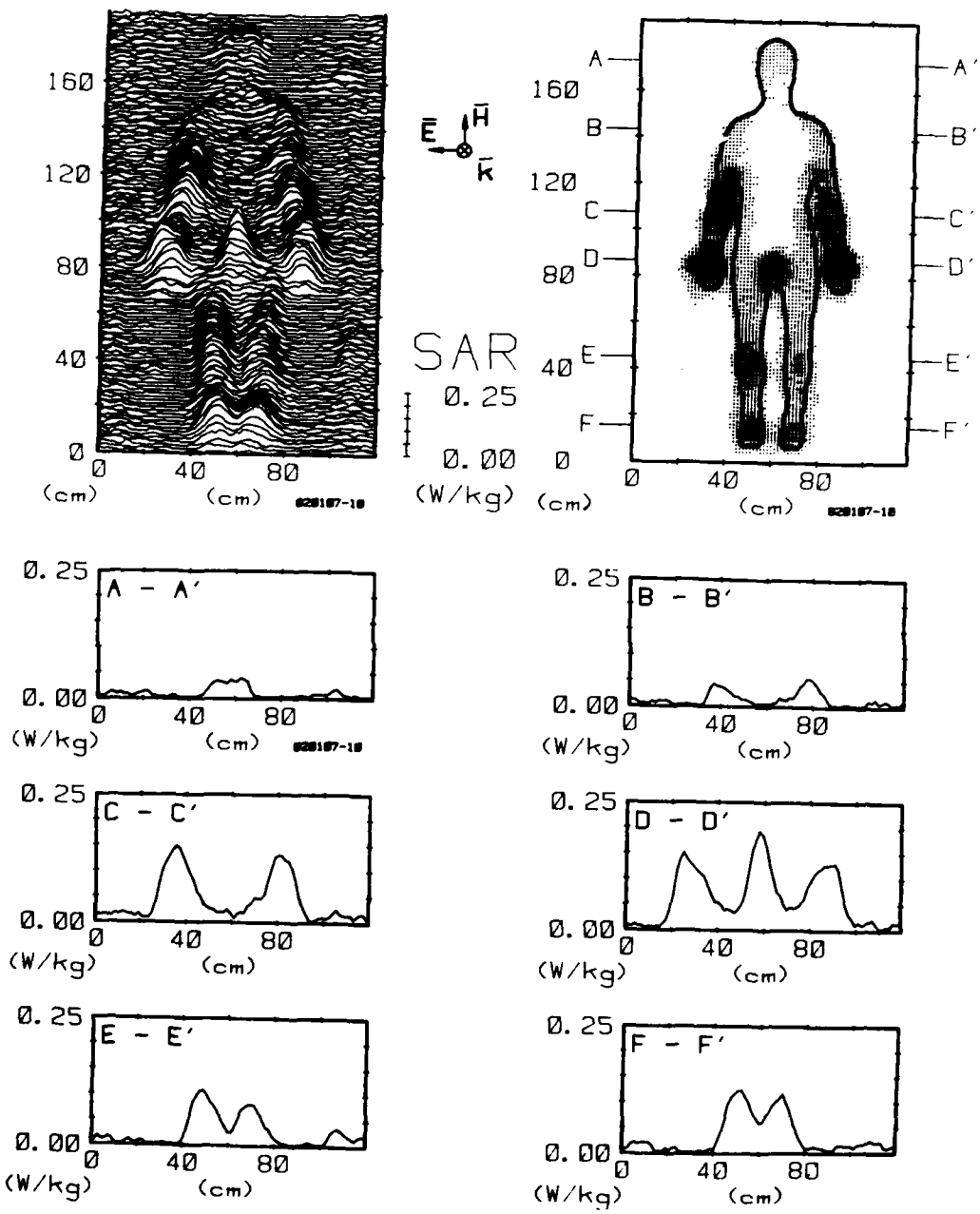

Figure 25. Computer-processed whole-body thermograms expressing SAR patterns for man with arms down, exposed to 1-mW/cm^2 450-MHz radiation with HEK polarization.

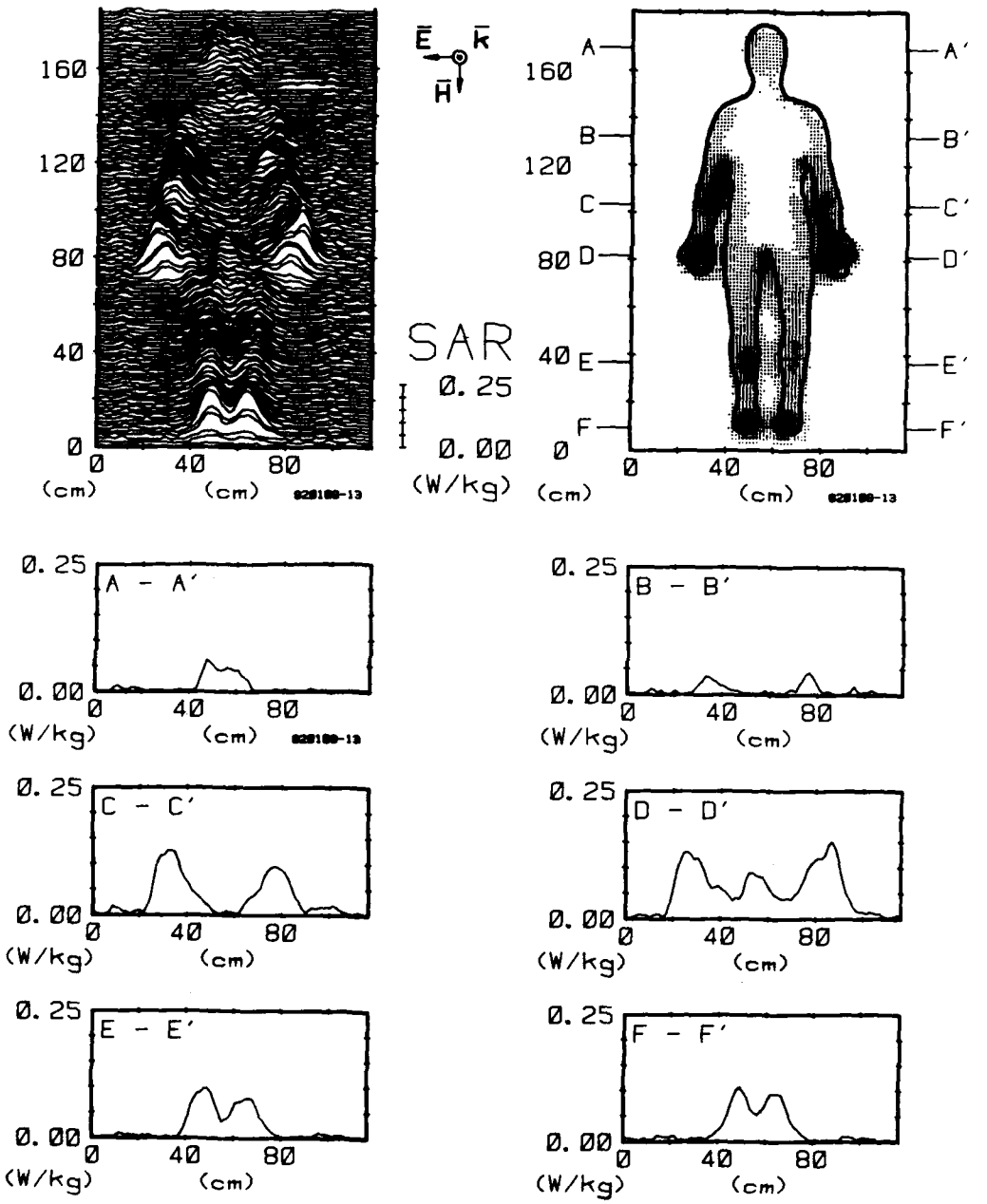

Figure 26. Computer-processed whole-body thermograms expressing SAR patterns for man with arms down, exposed to 1-mW/cm^2 450-MHz radiation with -HEK polarization.

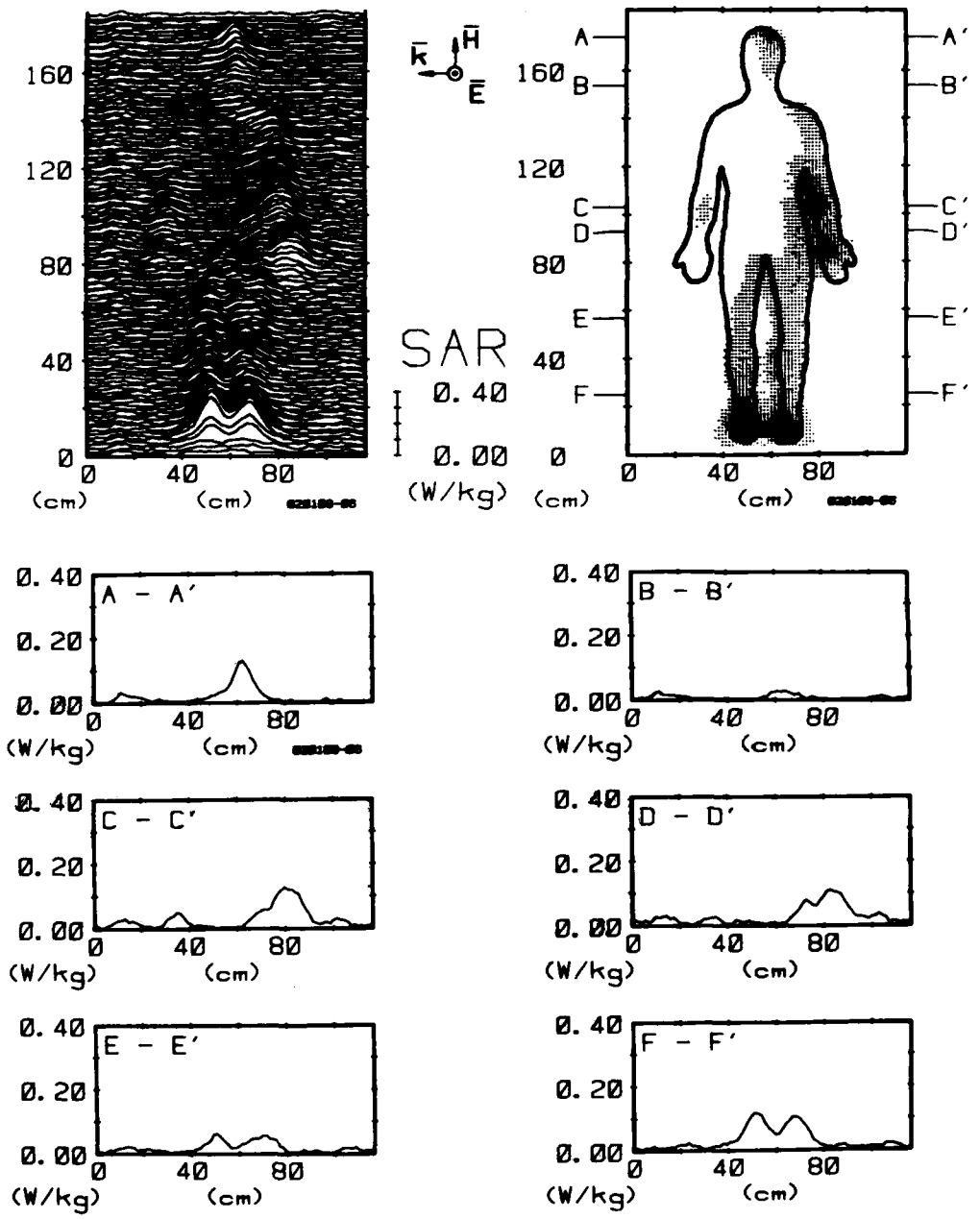

Figure 27. Computer-processed whole-body thermograms expressing SAR patterns for man with arms down, exposed to 1-mW/cm^2 450-MHz radiation with HKE polarization.

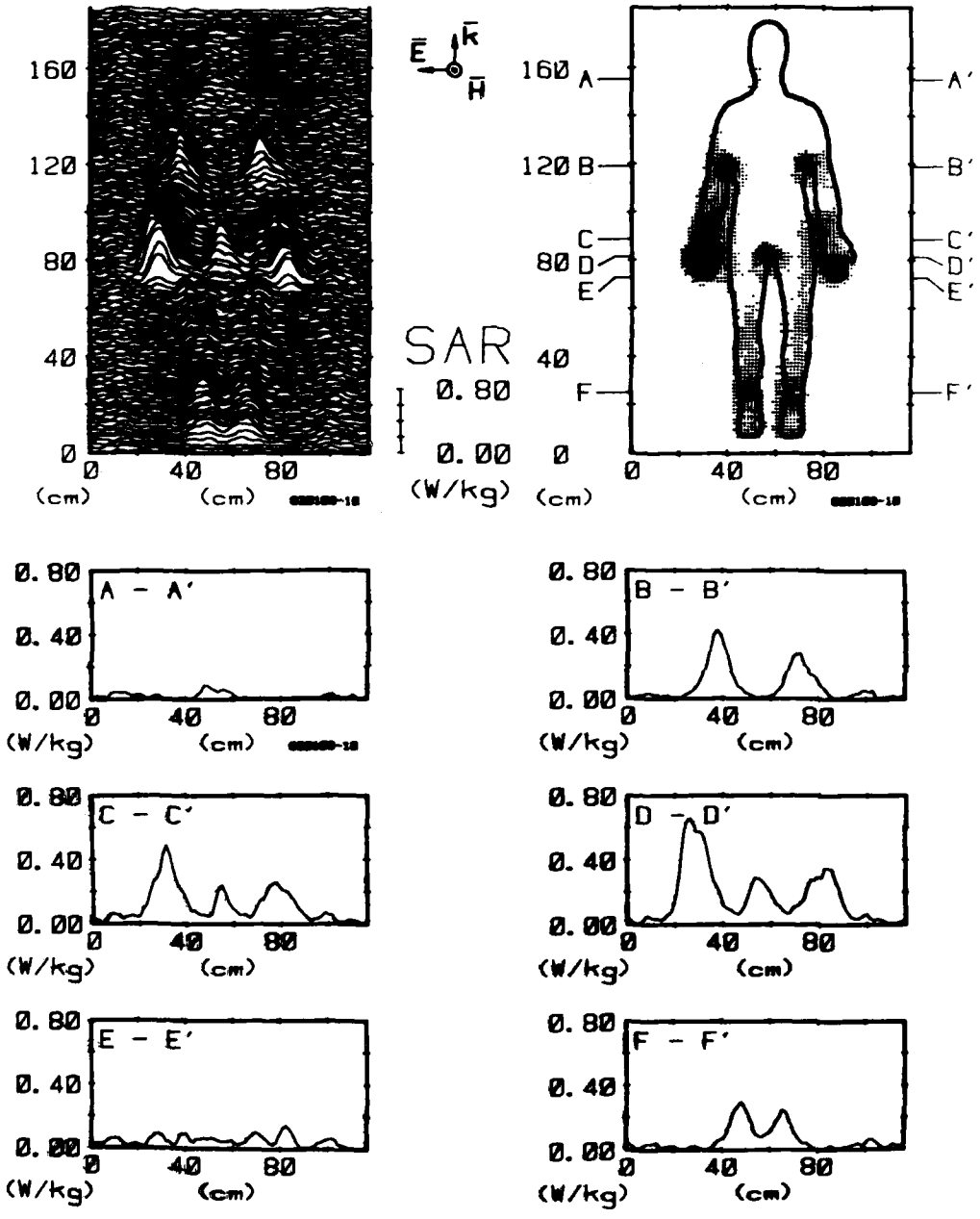

Figure 28. Computer-processed whole-body thermograms expressing SAR patterns for man with arms down, exposed to 1-mW/cm^2 450-MHz radiation with KEH polarization.

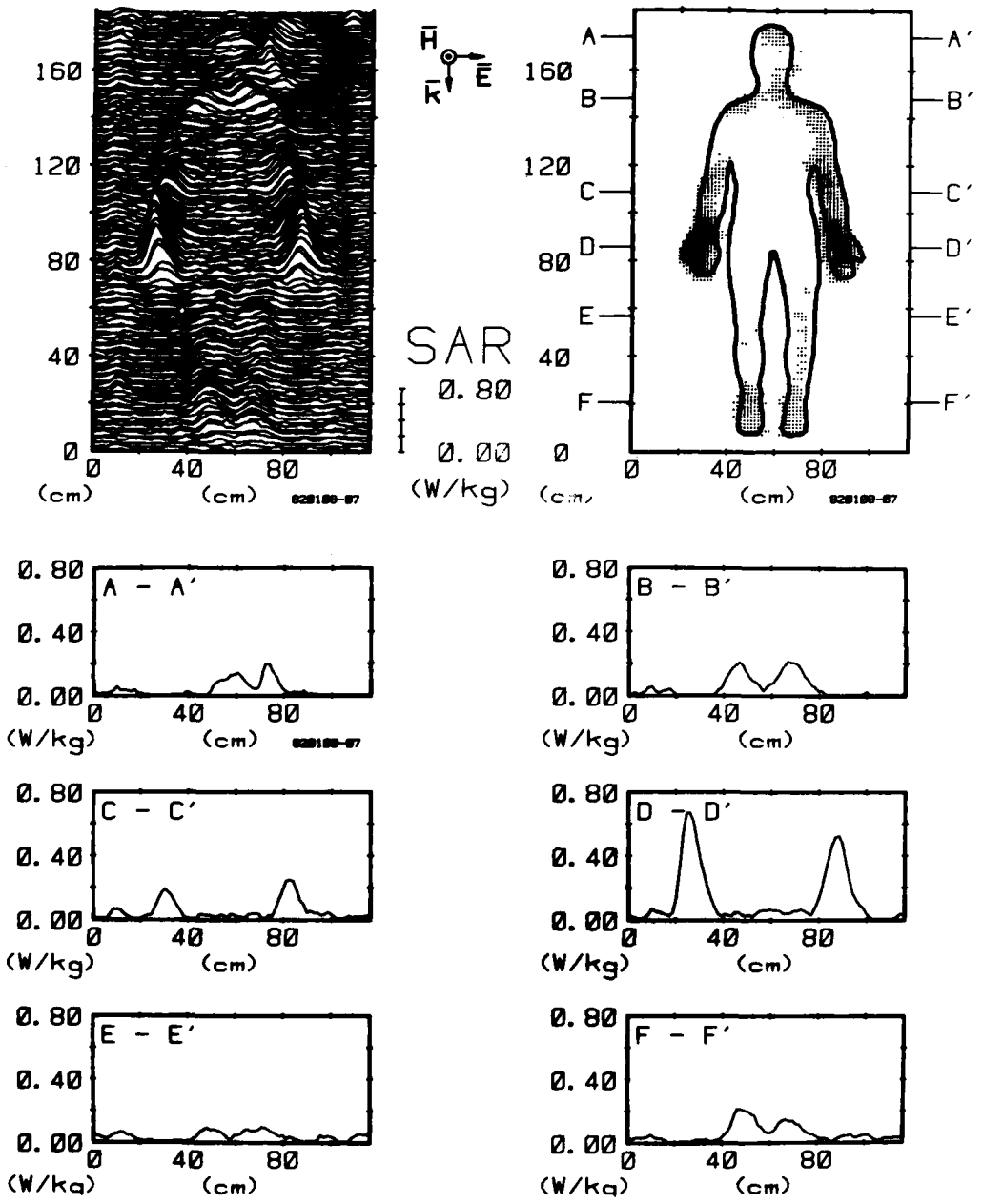

Figure 29. Computer-processed whole-body thermograms expressing SAR patterns for man with arms down, exposed to 1-mW/cm^2 450-MHz radiation with -KEH polarization.

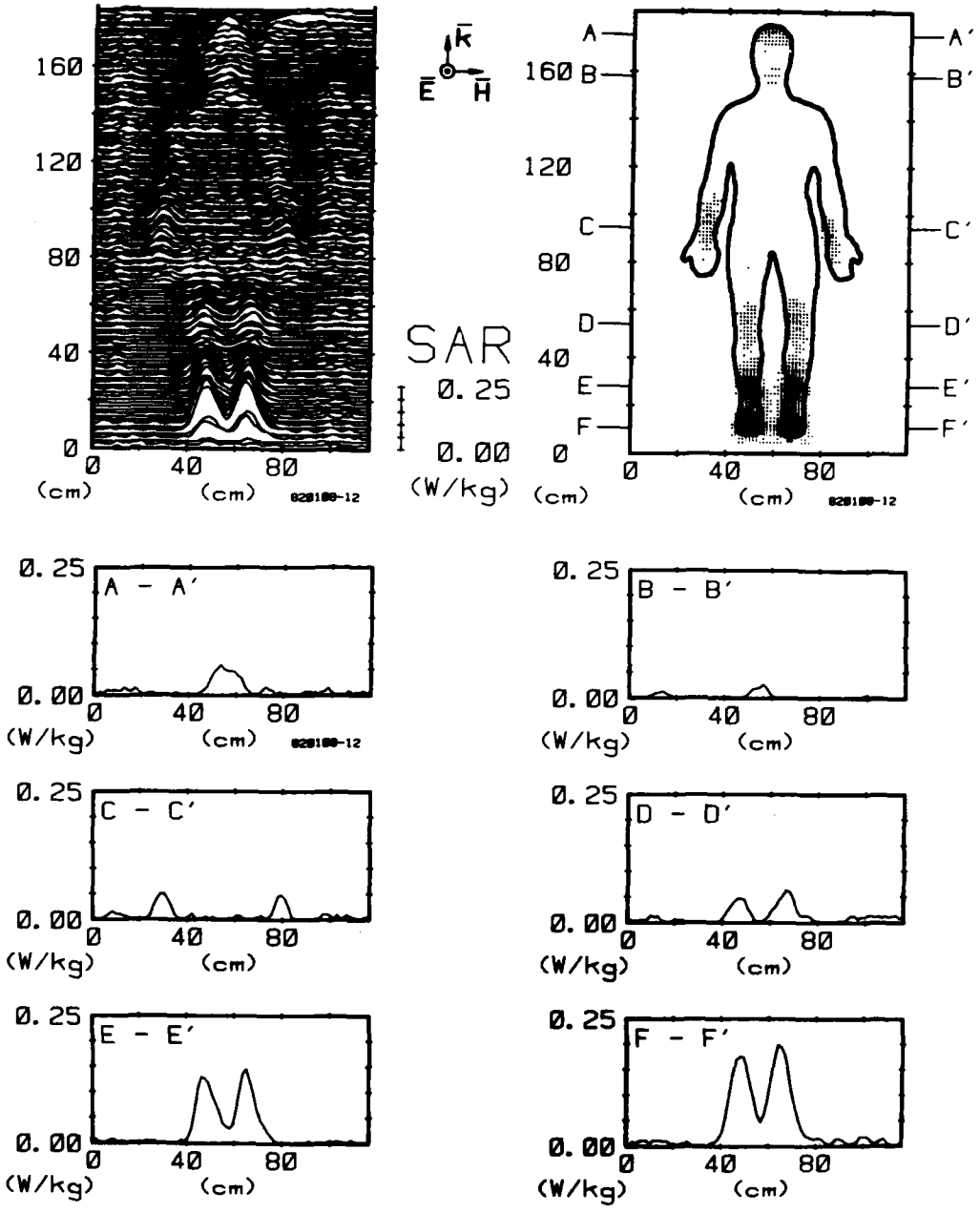

Figure 30. Computer-processed whole-body thermograms expressing SAR patterns for man with arms down, exposed to 1-mW/cm^2 450-MHz radiation with KHE polarization.

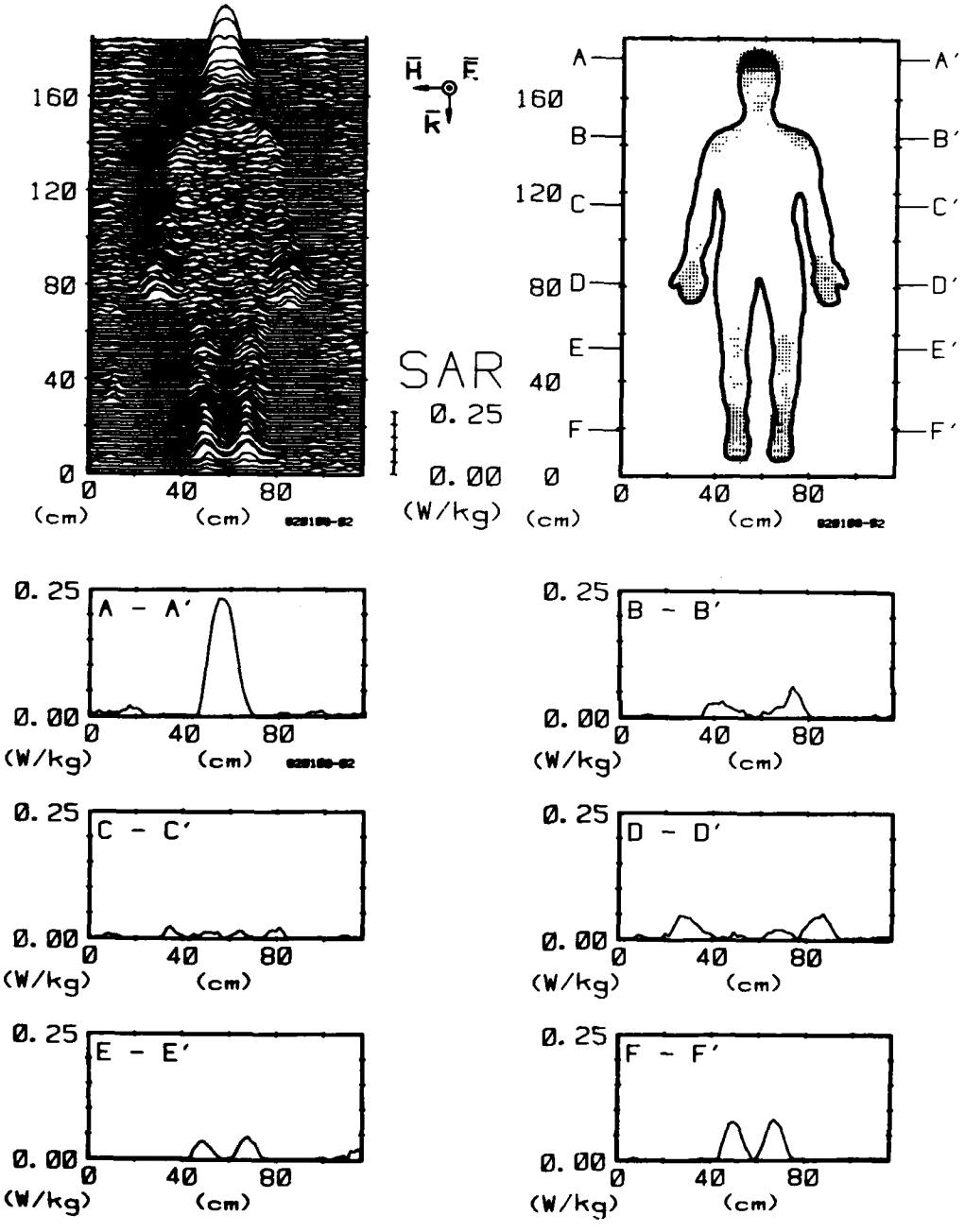

Figure 31. Computer-processed whole-body thermograms expressing SAR patterns for man with arms down, exposed to 1-mW/cm^2 450-MHz radiation with -KHE polarization.

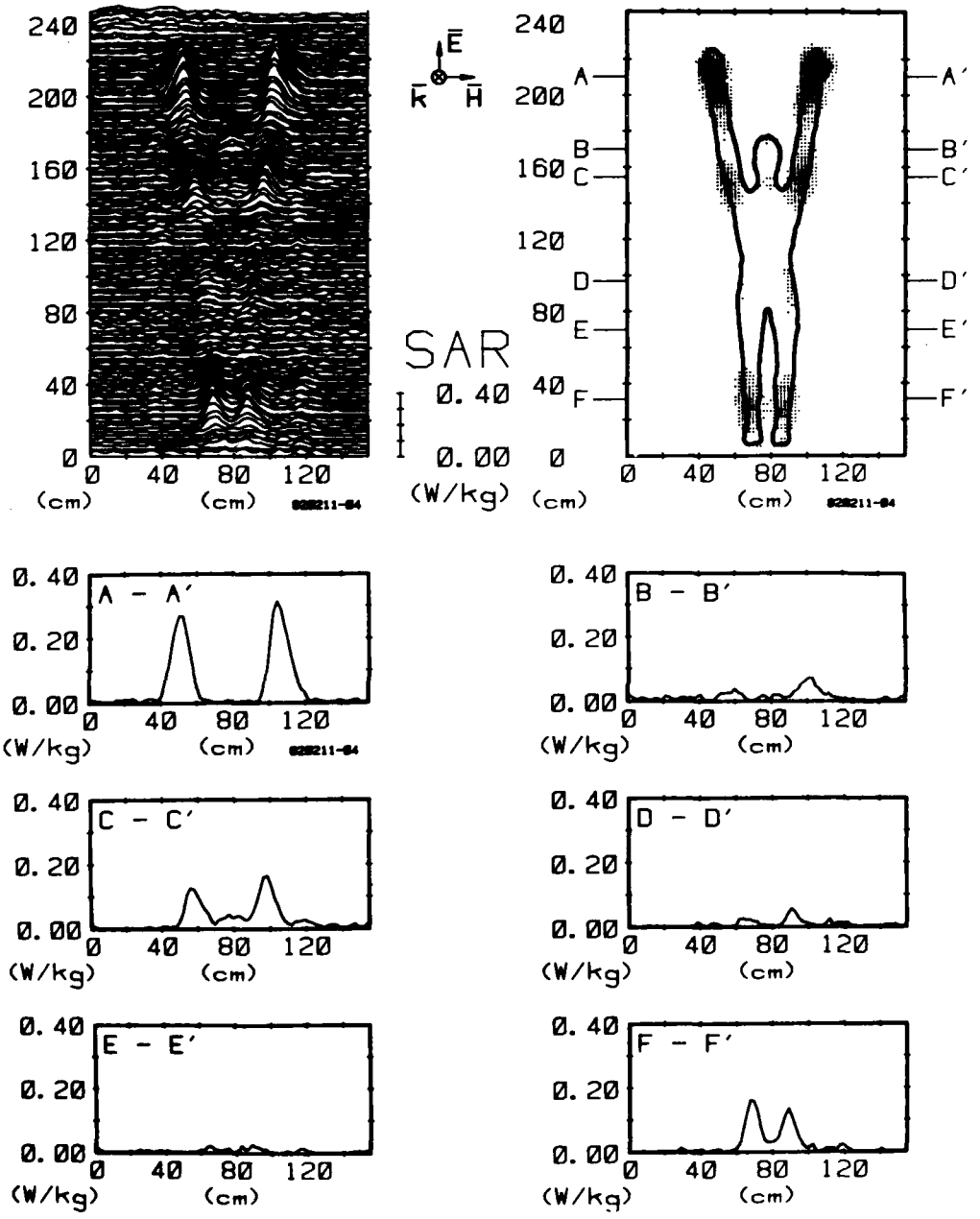

Figure 32. Computer-processed whole-body thermograms expressing SAR patterns for man with arms up, exposed to 1-mW/cm^2 450-MHz radiation with EHK polarization.

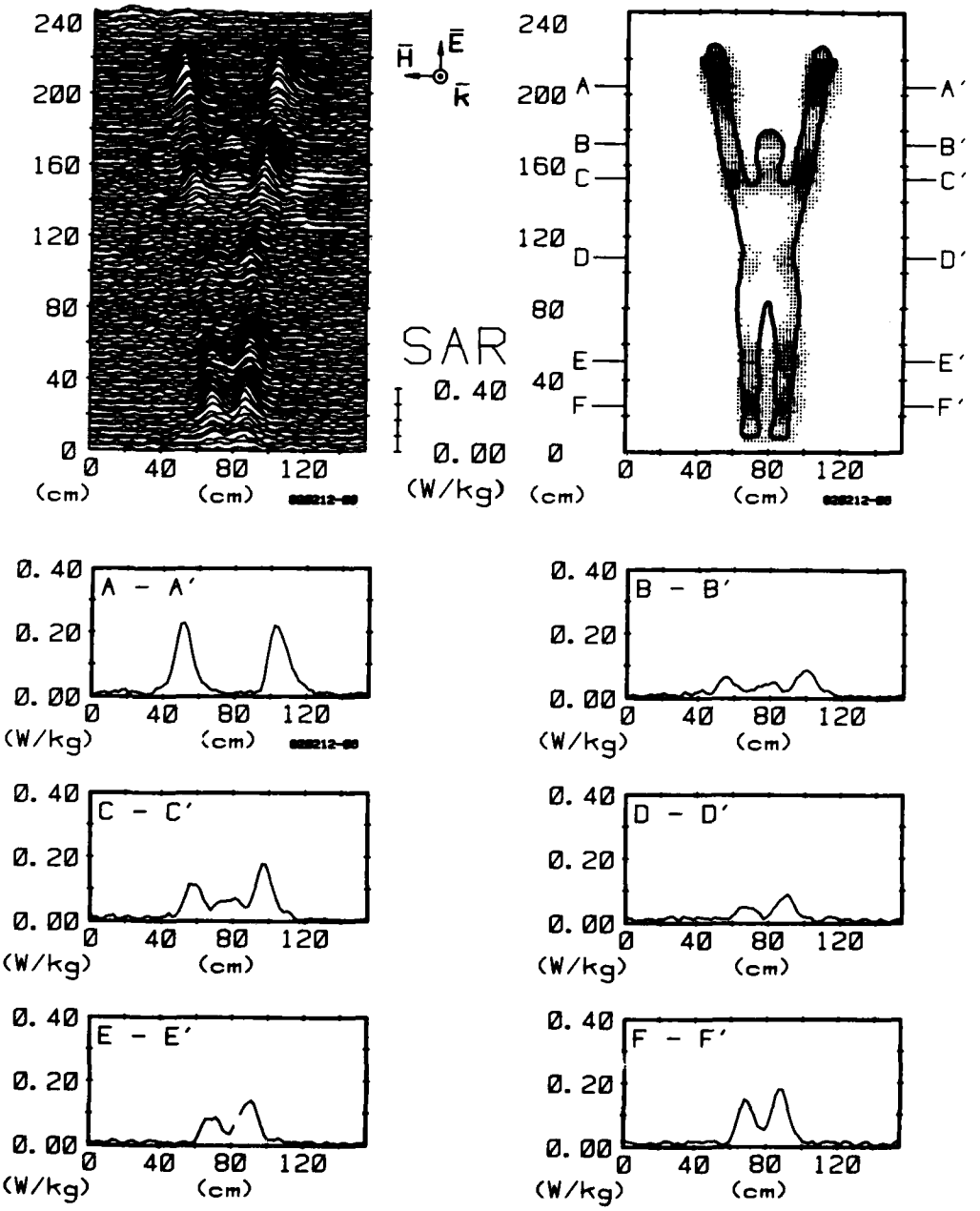

Figure 33. Computer-processed whole-body thermograms expressing SAR patterns for man with arms up, exposed to 1-mW/cm^2 450-MHz radiation with -EHK polarization.

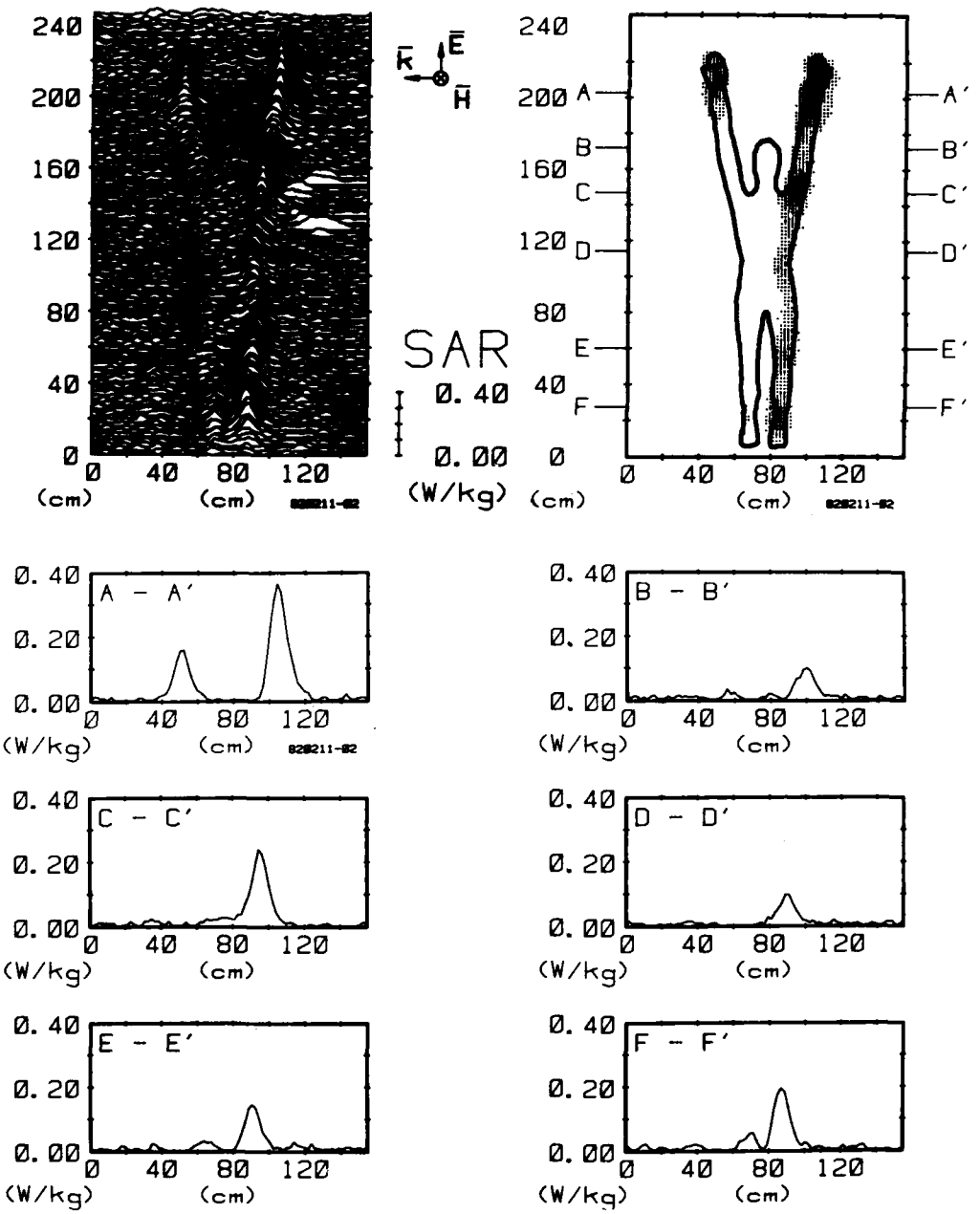

Figure 34. Computer-processed whole-body thermograms expressing SAR patterns for man with arms up, exposed to 1-mW/cm^2 450-MHz radiation with EKH polarization.

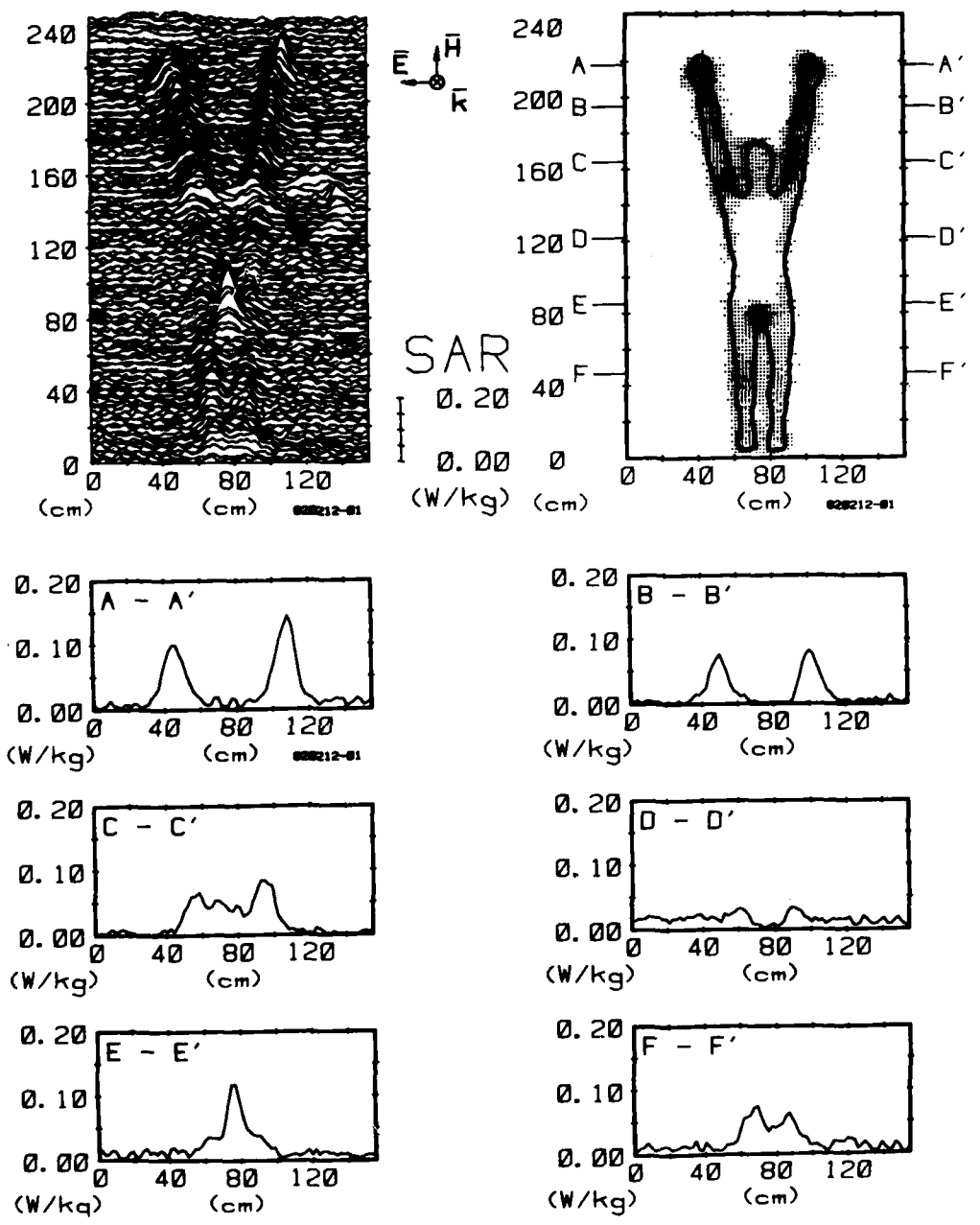

Figure 35. Computer-processed whole-body thermograms expressing SAR patterns for man with arms up, exposed to 1-mW/cm^2 450-MHz radiation with HEK polarization.

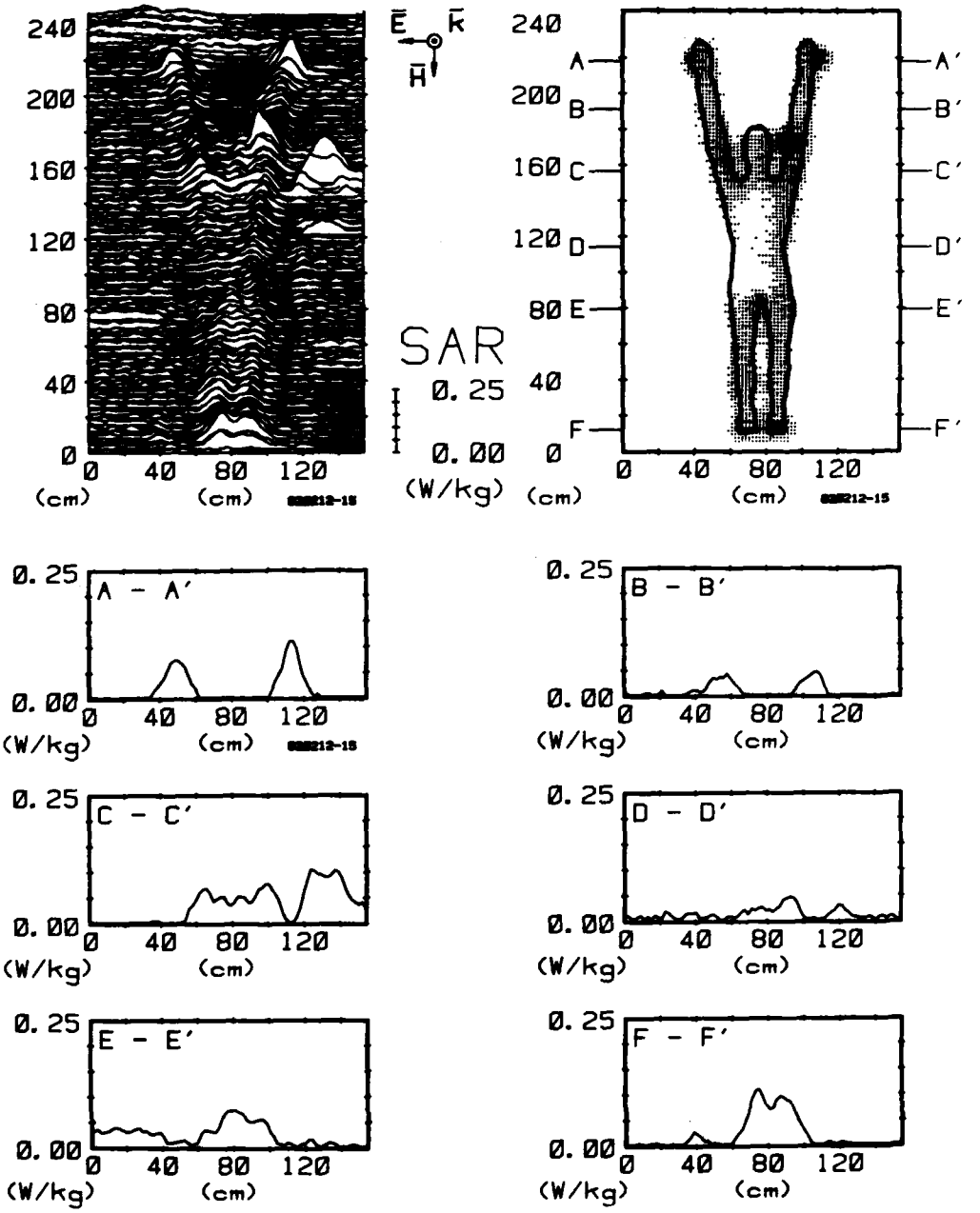

Figure 36. Computer-processed whole-body thermograms expressing SAR patterns for man with arms up exposed to 1-mW/cm^2 450-MHz radiation with -HEK polarization.

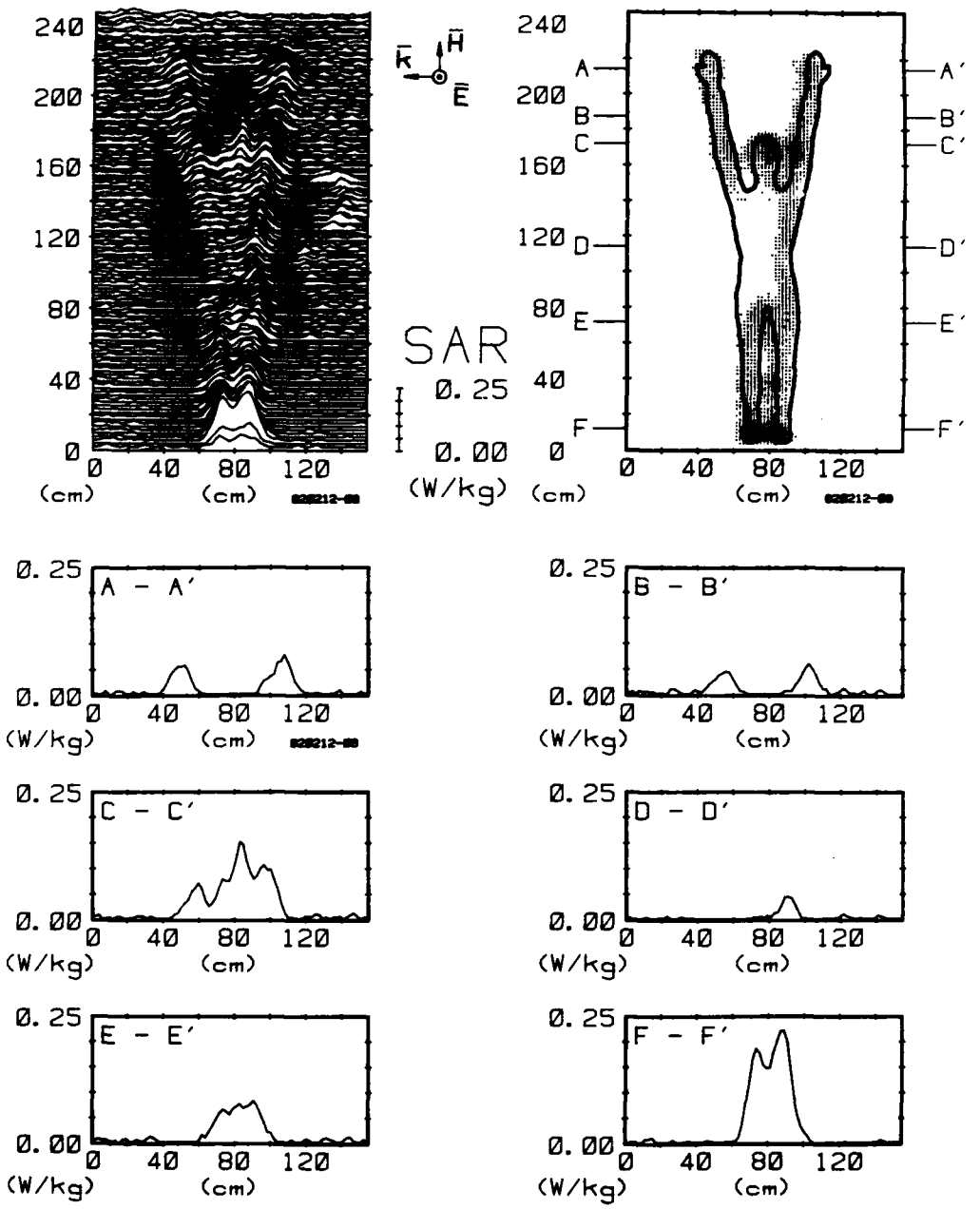

Figure 37. Computer-processed whole-body thermograms expressing SAR patterns for man with arms up, exposed to 1-mW/cm^2 450-MHz radiation with HKE polarization.

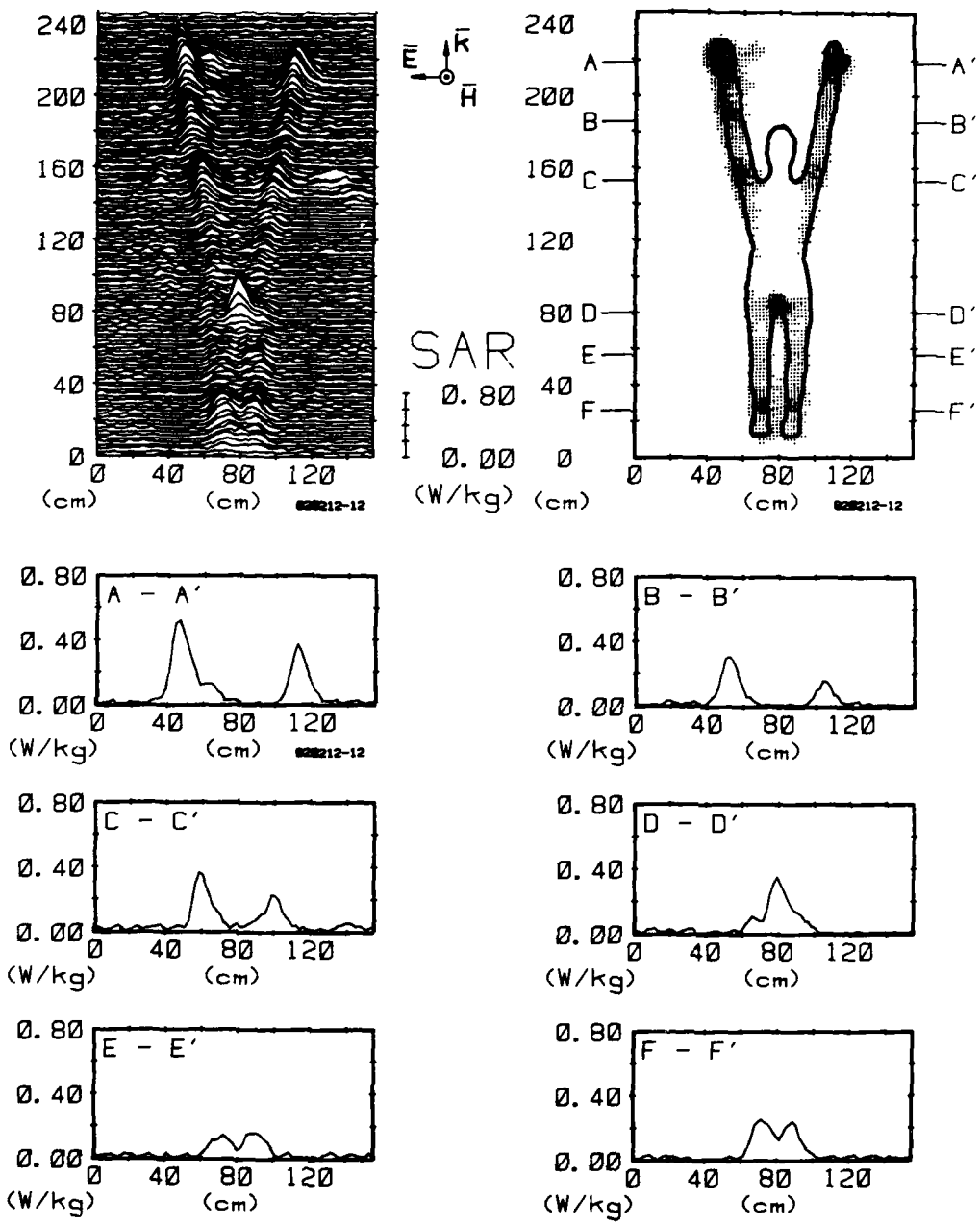

Figure 38. Computer-processed whole-body thermograms expressing SAR patterns for man with arms up, exposed to 1-mW/cm^2 450-MHz radiation with KEH polarization.

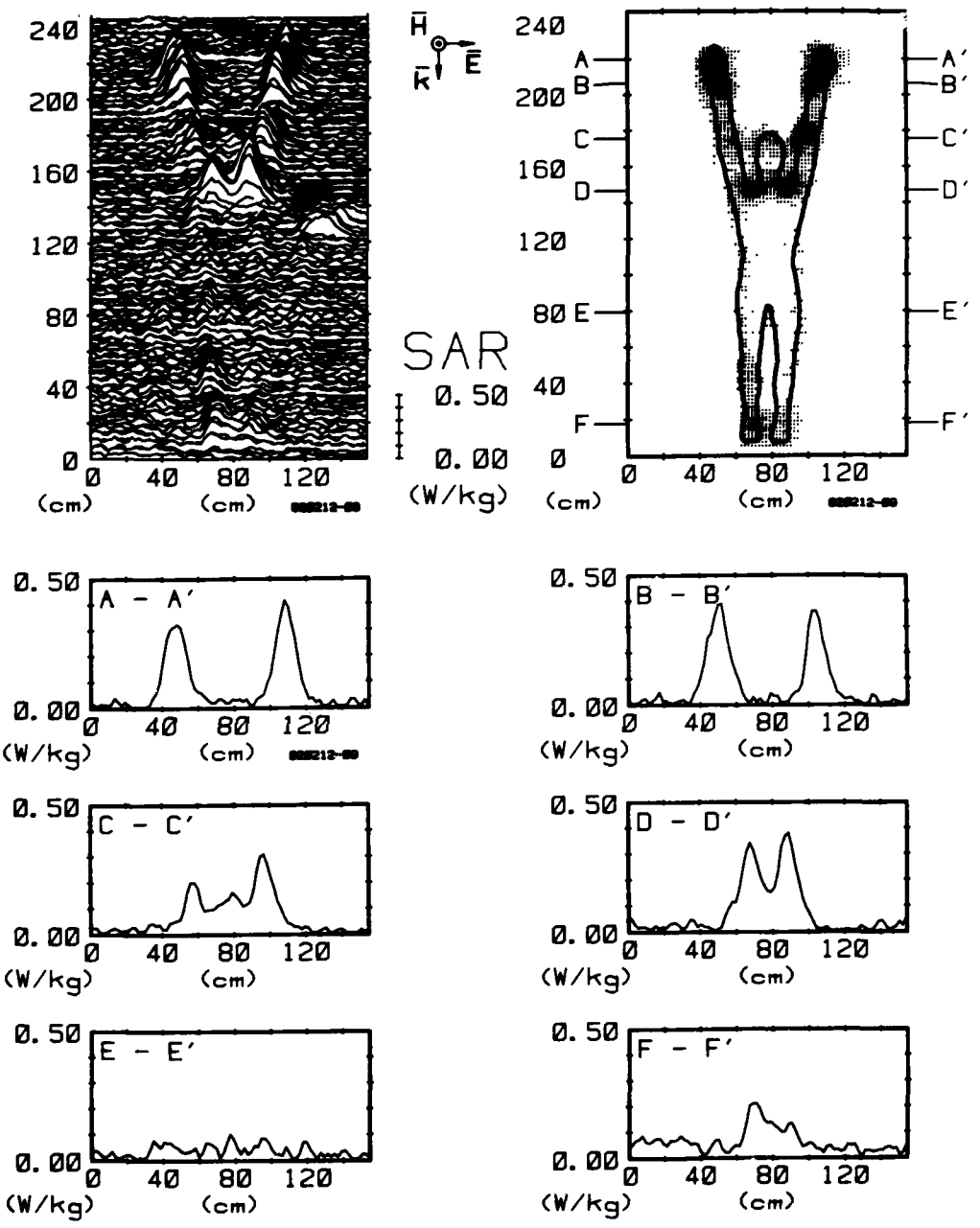

Figure 39. Computer-processed whole-body thermograms expressing SAR patterns for man with arms up, exposed to 1-mW/cm^2 450-MHz radiation with -KEH polarization.

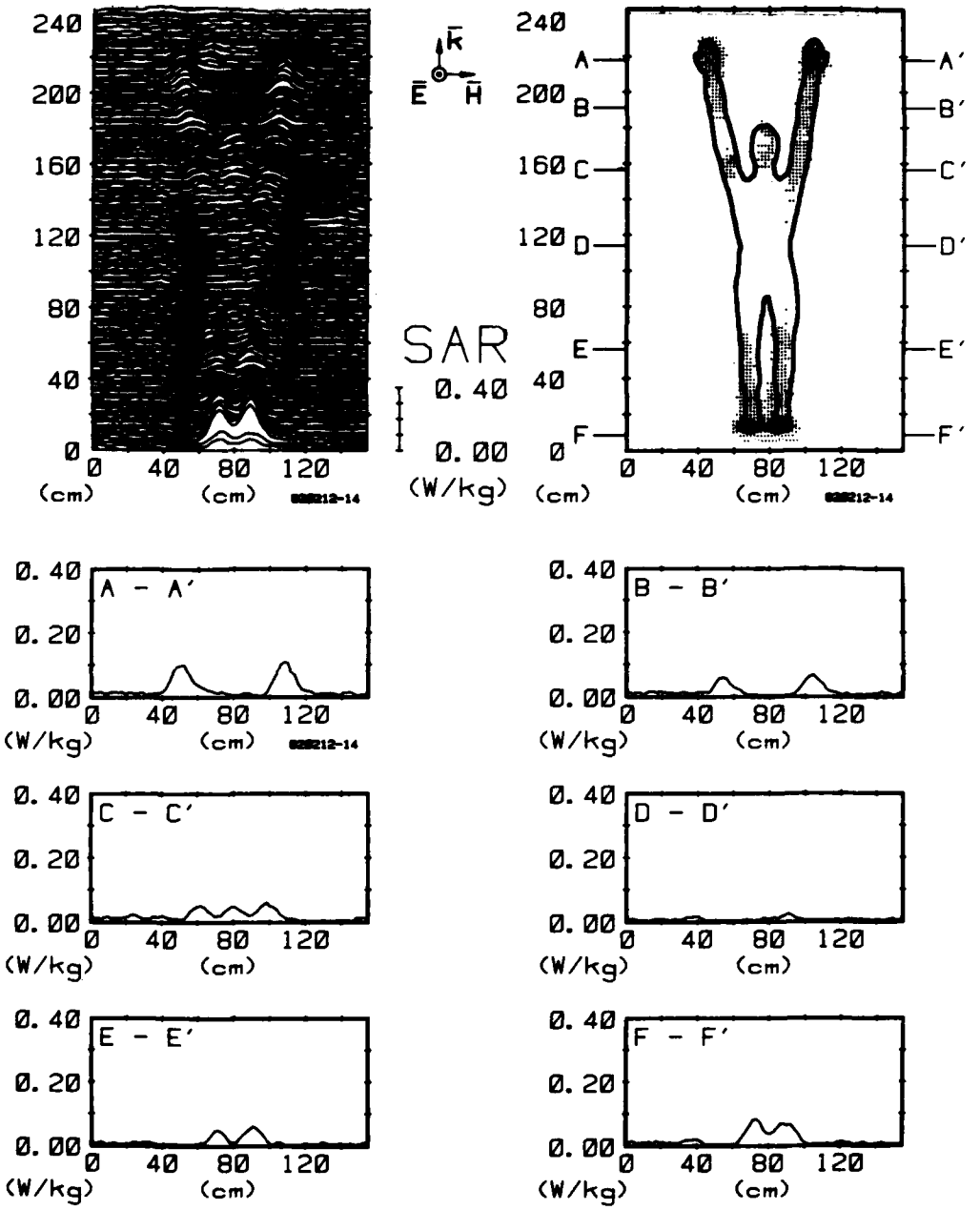

Figure 40. Computer-processed whole-body thermograms expressing SAR patterns for man with arms up, exposed to 1-mW/cm^2 450-MHz radiation with KHE polarization.

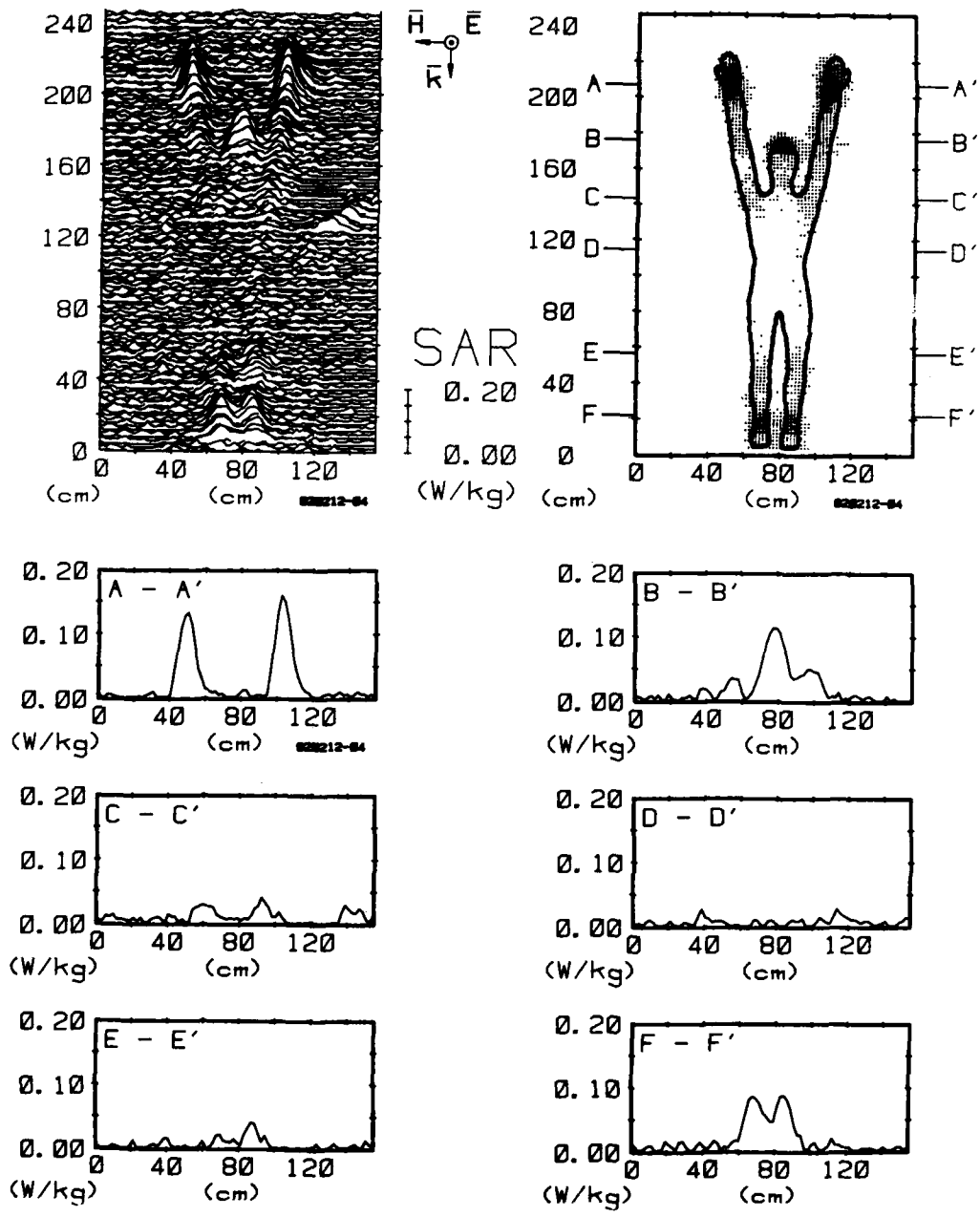

Figure 41. Computer-processed whole-body thermograms expressing SAR patterns for man with arms up, exposed to 1-mW/cm^2 450-MHz radiation with -KHE polarization.

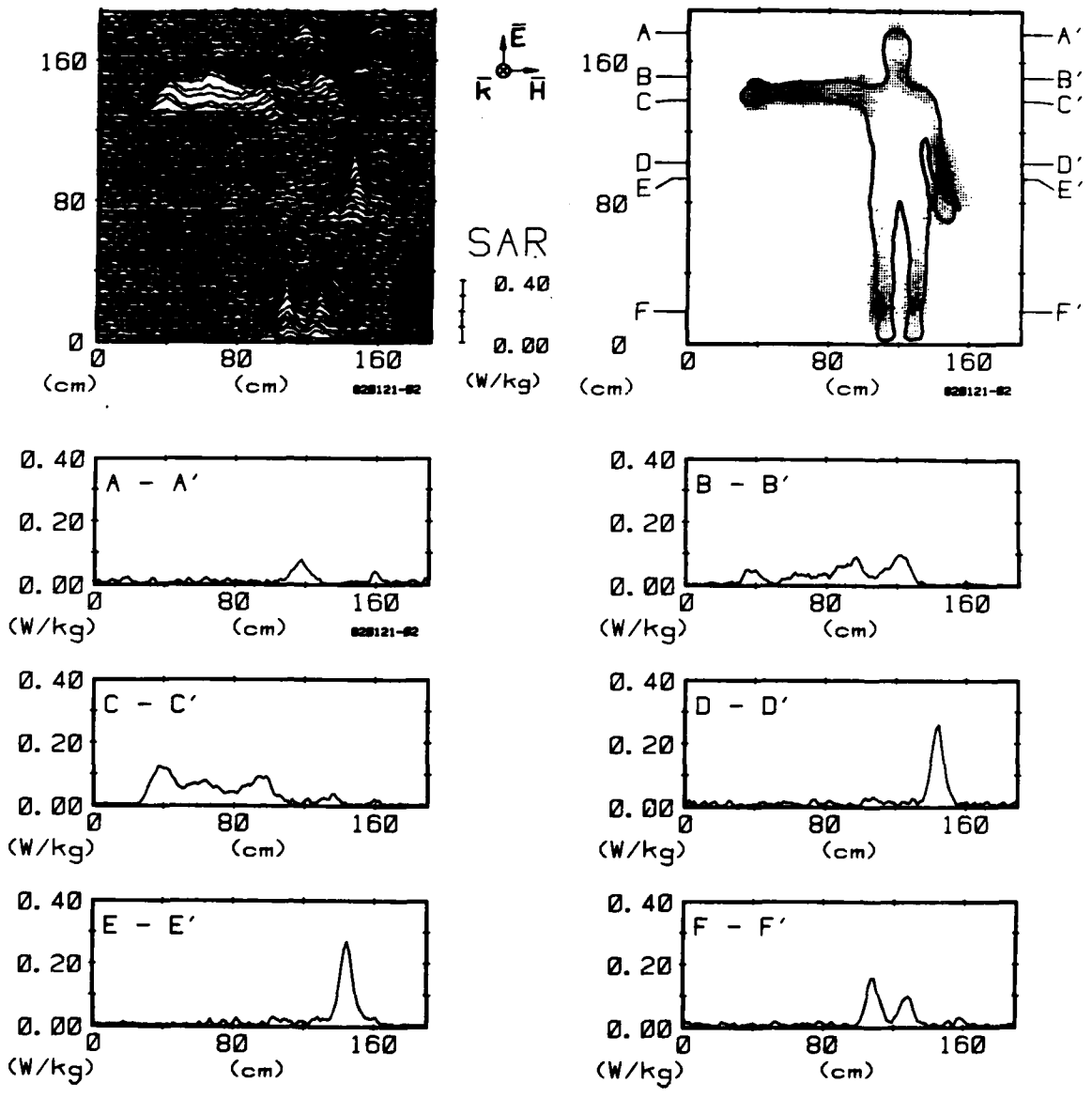

Figure 42. Computer-processed whole-body thermograms expressing SAR patterns for man with one arm extended, exposed to 1-mW/cm^2 450-MHz radiation with EHK polarization.

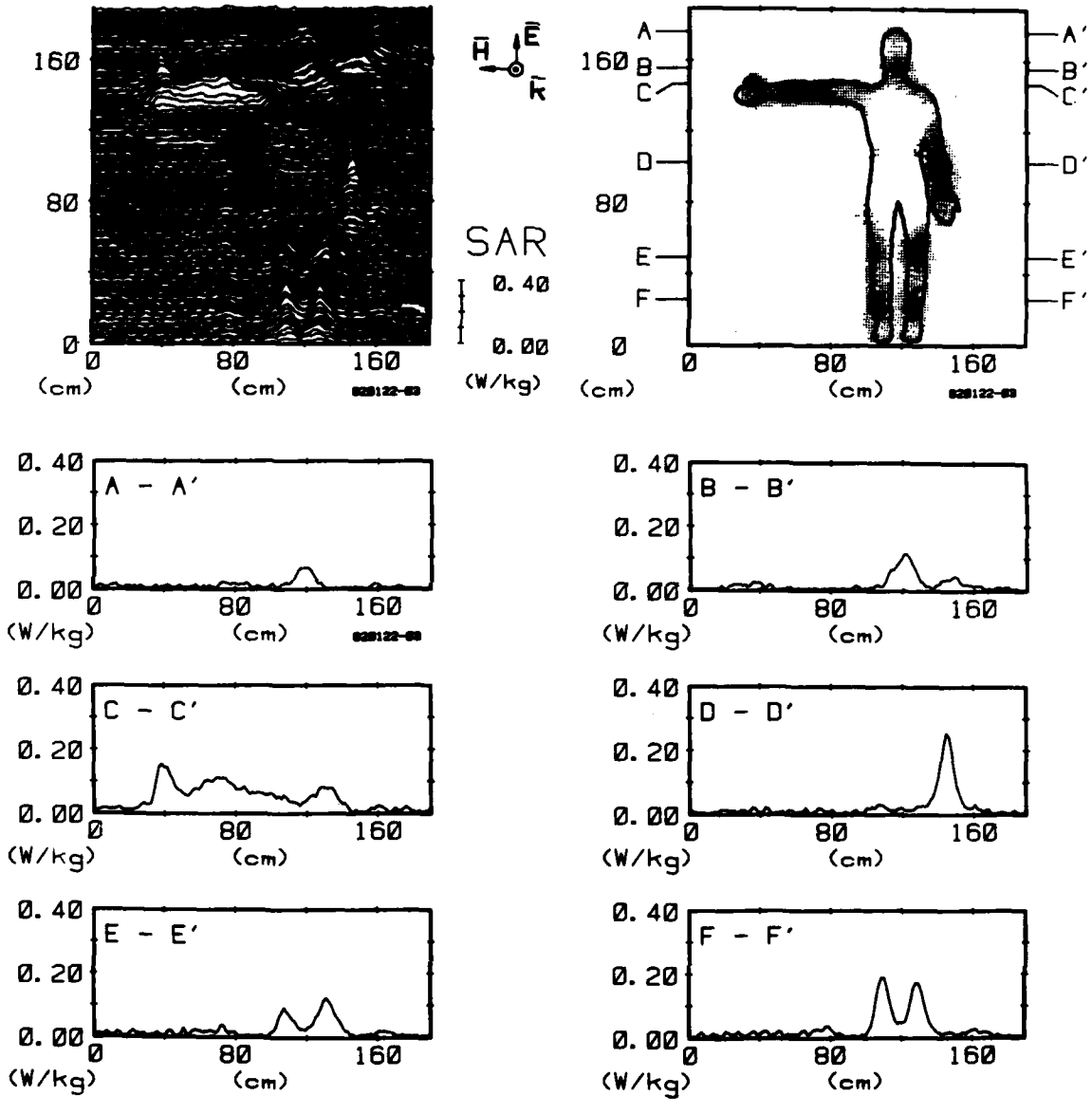

Figure 43. Computer-processed whole-body thermograms expressing SAR patterns for man with one arm extended, exposed to 1-mW/cm^2 450-MHz radiation with -EHK polarization.

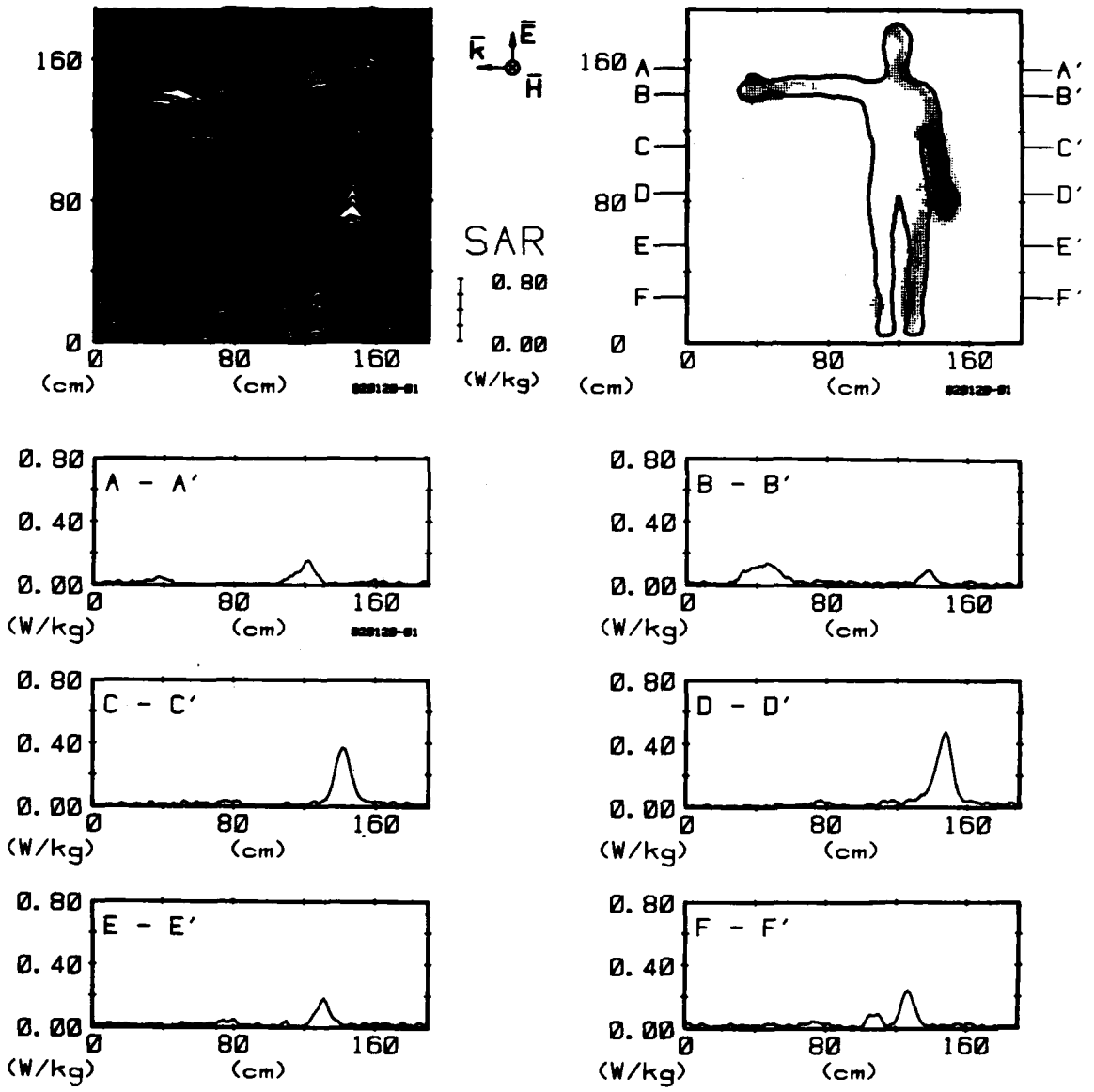

Figure 44. Computer-processed whole-body thermograms expressing SAR patterns for man with one arm extended, exposed to 1-mW/cm^2 450-MHz radiation with EKH polarization.

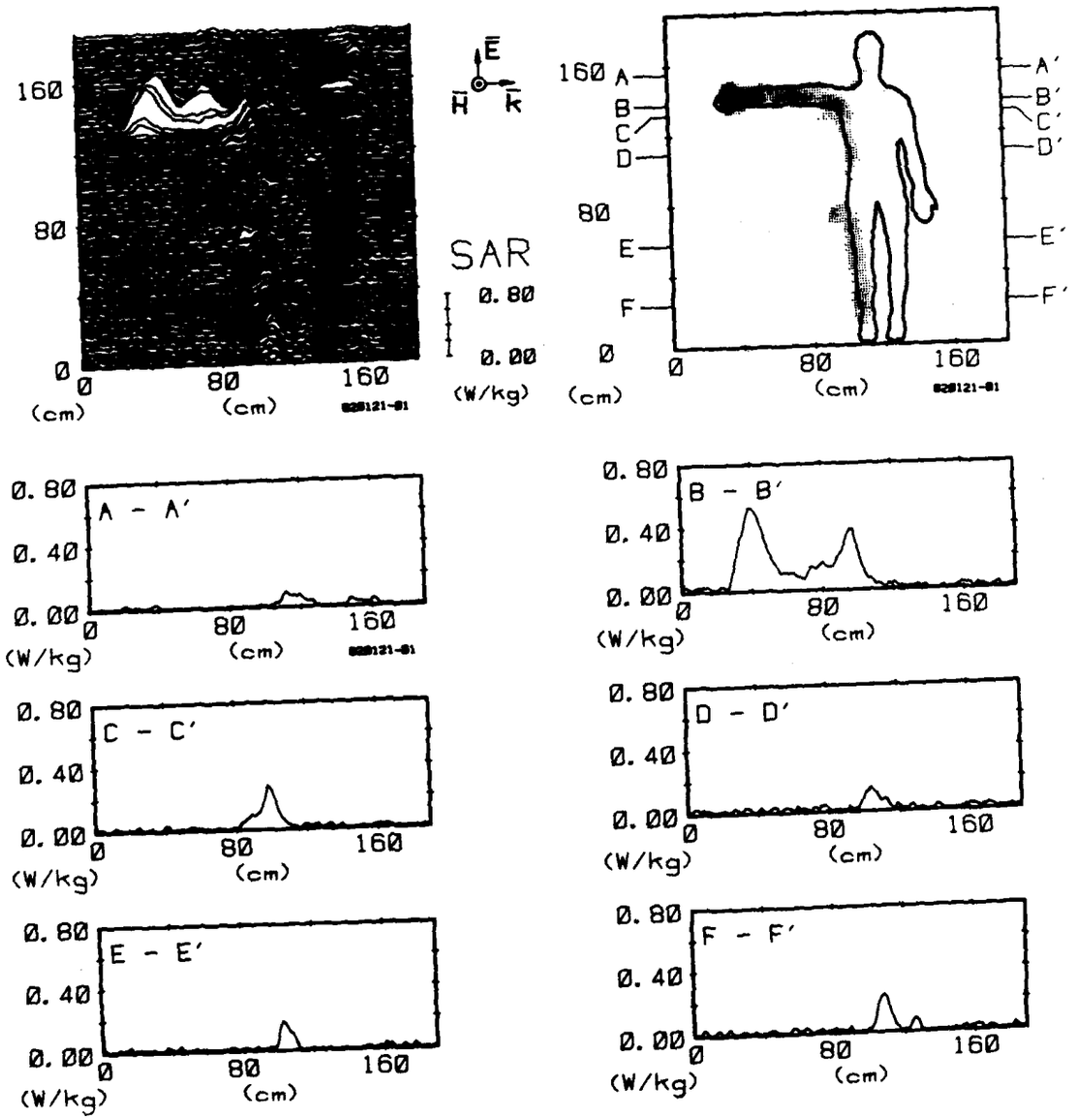

Figure 45. Computer-processed whole-body thermograms expressing SAR patterns for man with one arm extended, exposed to 1-mW/cm^2 450-MHz radiation with -EKH polarization.

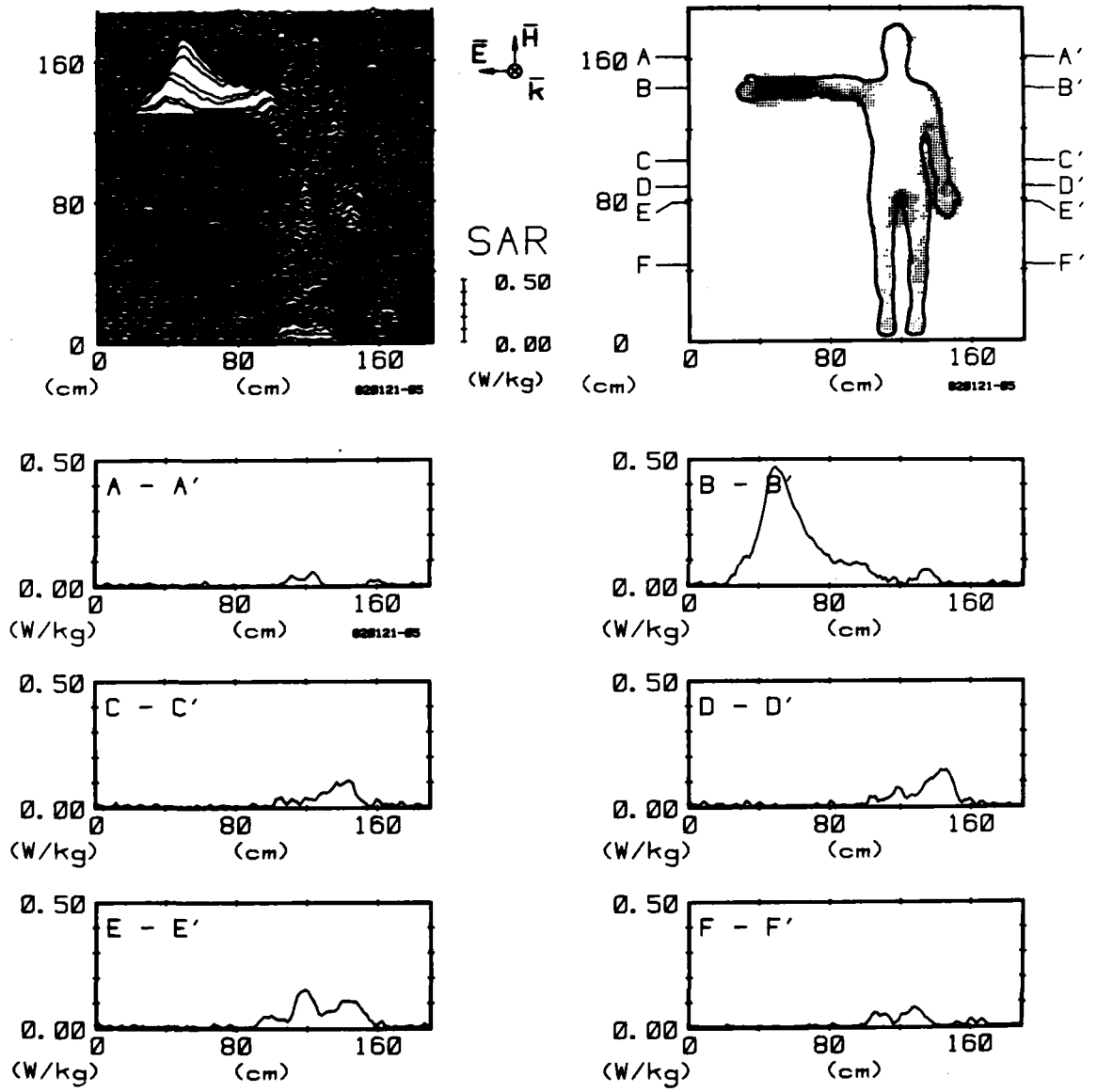

Figure 46. Computer-processed whole-body thermograms expressing SAR patterns for man with one arm extended, exposed to 1-mW/cm^2 450-MHz radiation wth HEK polarization.

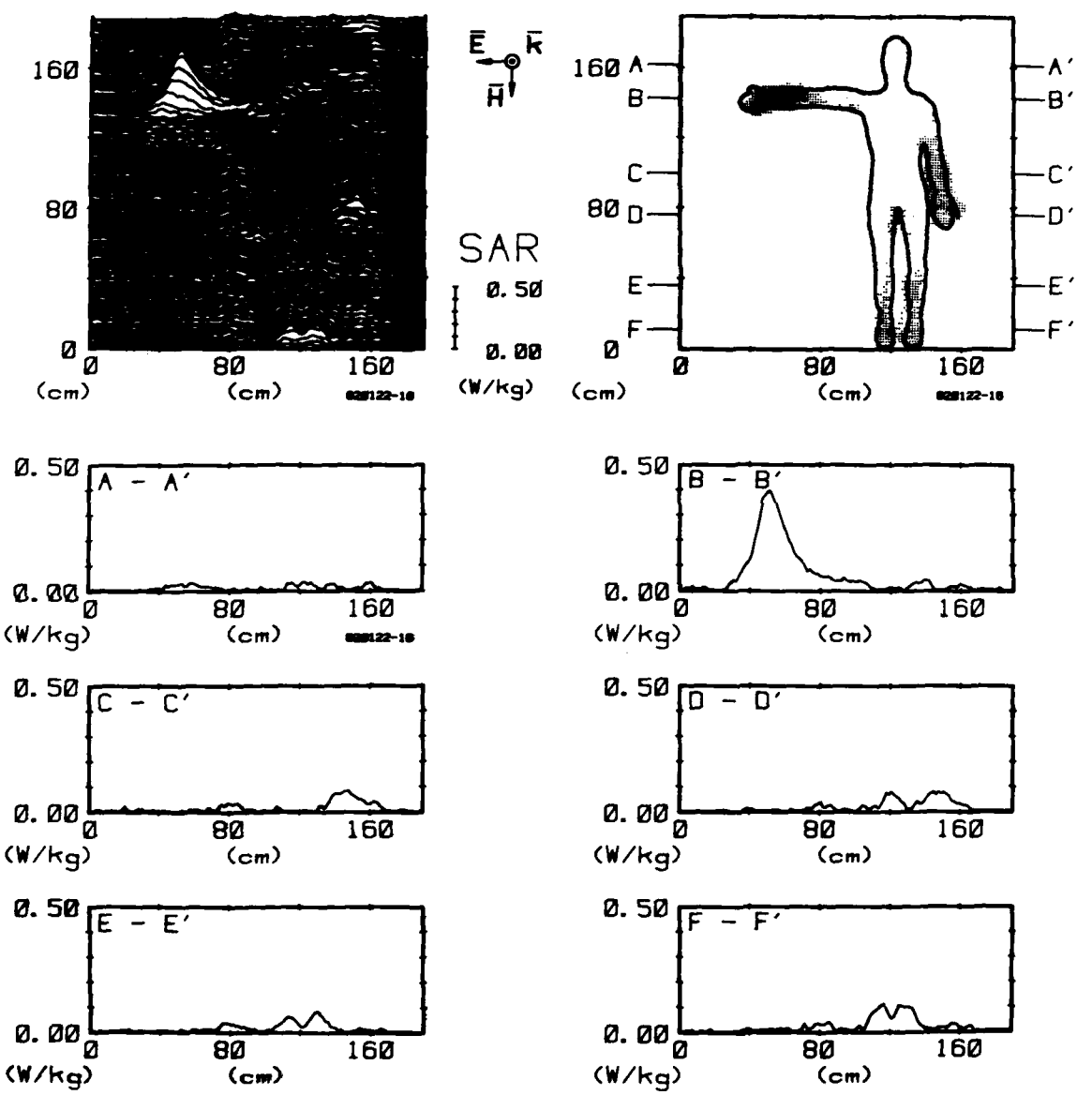

Figure 47. Computer-processed whole-body thermograms expressing SAR patterns for man with one arm extended, exposed to 1-mW/cm^2 450-MHz radiation with -HEK polarization.

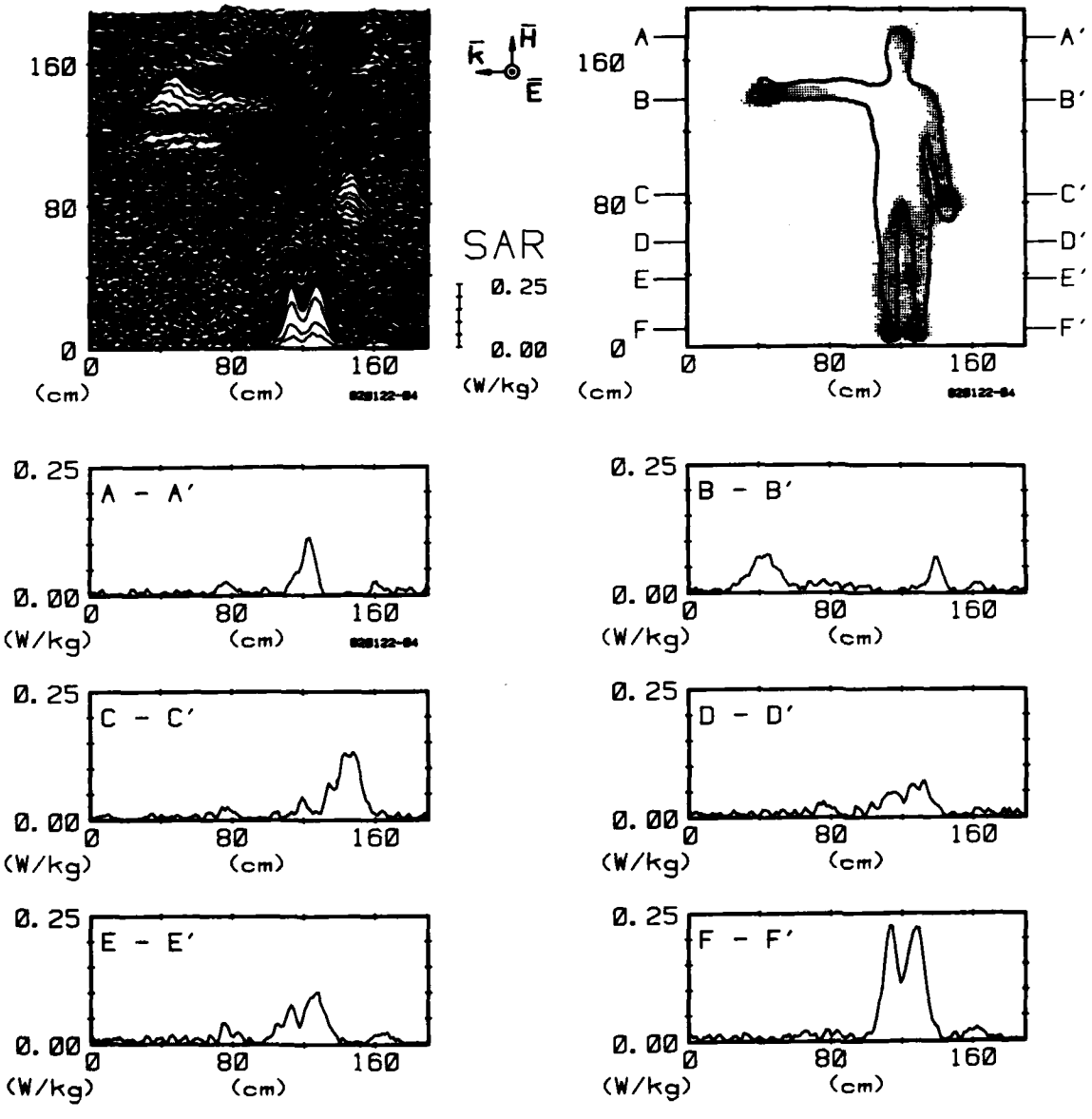

Figure 48. Computer-processed whole-body thermograms expressing SAR patterns for man with one arm extended, exposed to 1-mW/cm^2 450-MHz radiation with HKE polarization.

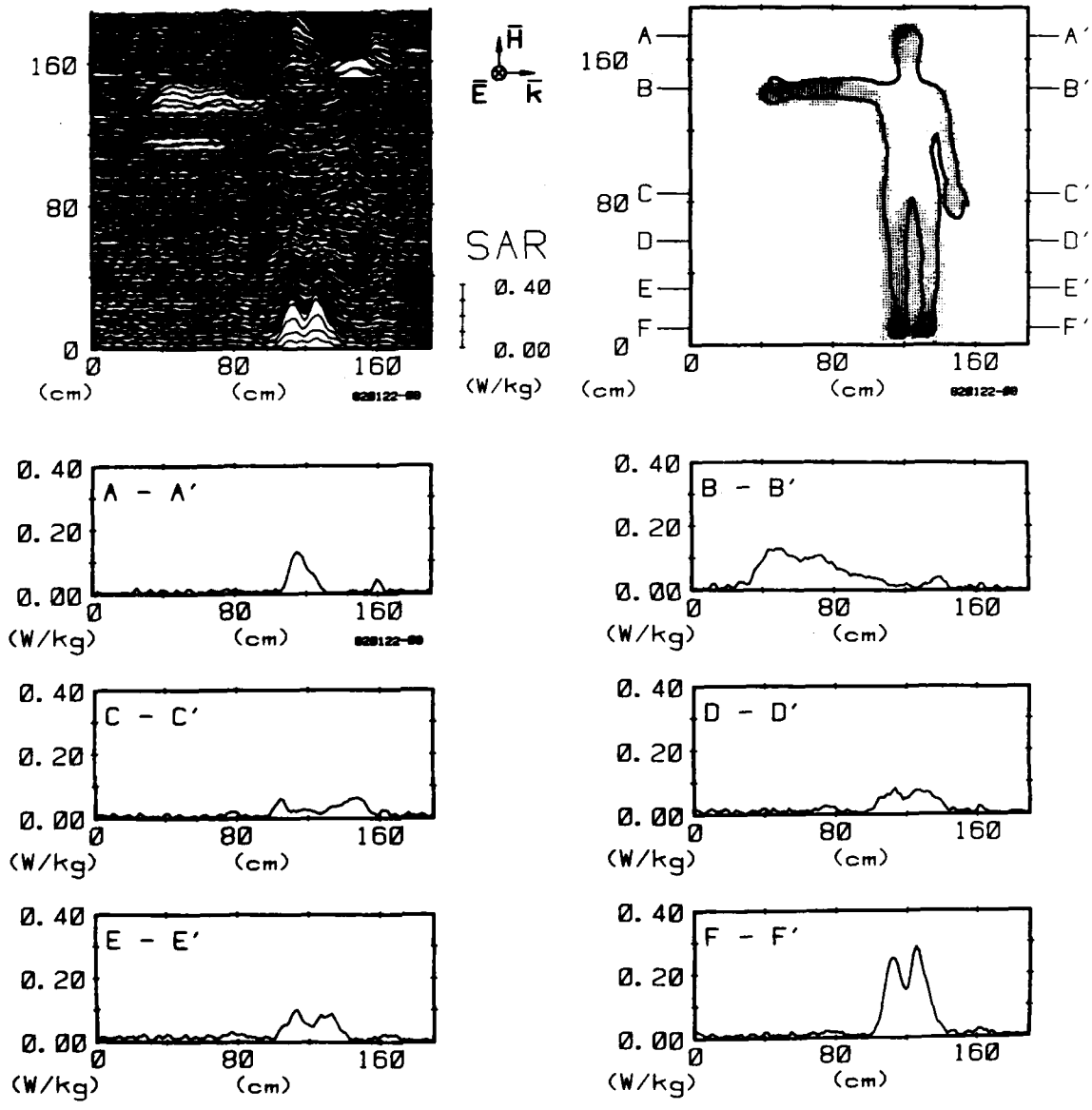

Figure 49. Computer-processed whole-body thermograms expressing SAR patterns for man with one arm extended, exposed to 1-mW/cm^2 450-MHz radiation with -HKE polarization.

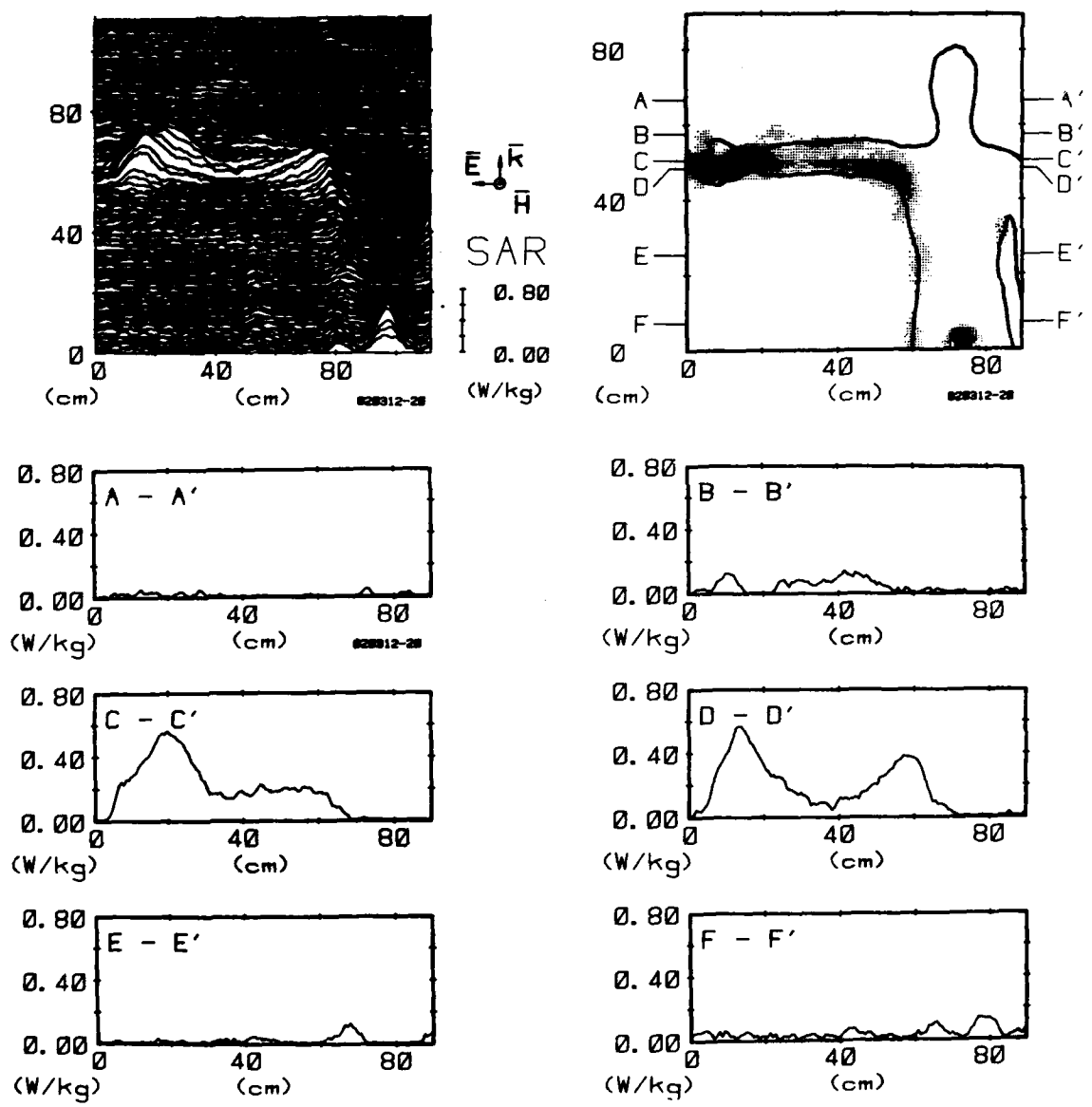

Figure 50A. Computer-processed whole-body thermograms expressing SAR patterns for man with one arm extended, exposed to 1-mW/cm^2 450-MHz radiation with KEH polarization.

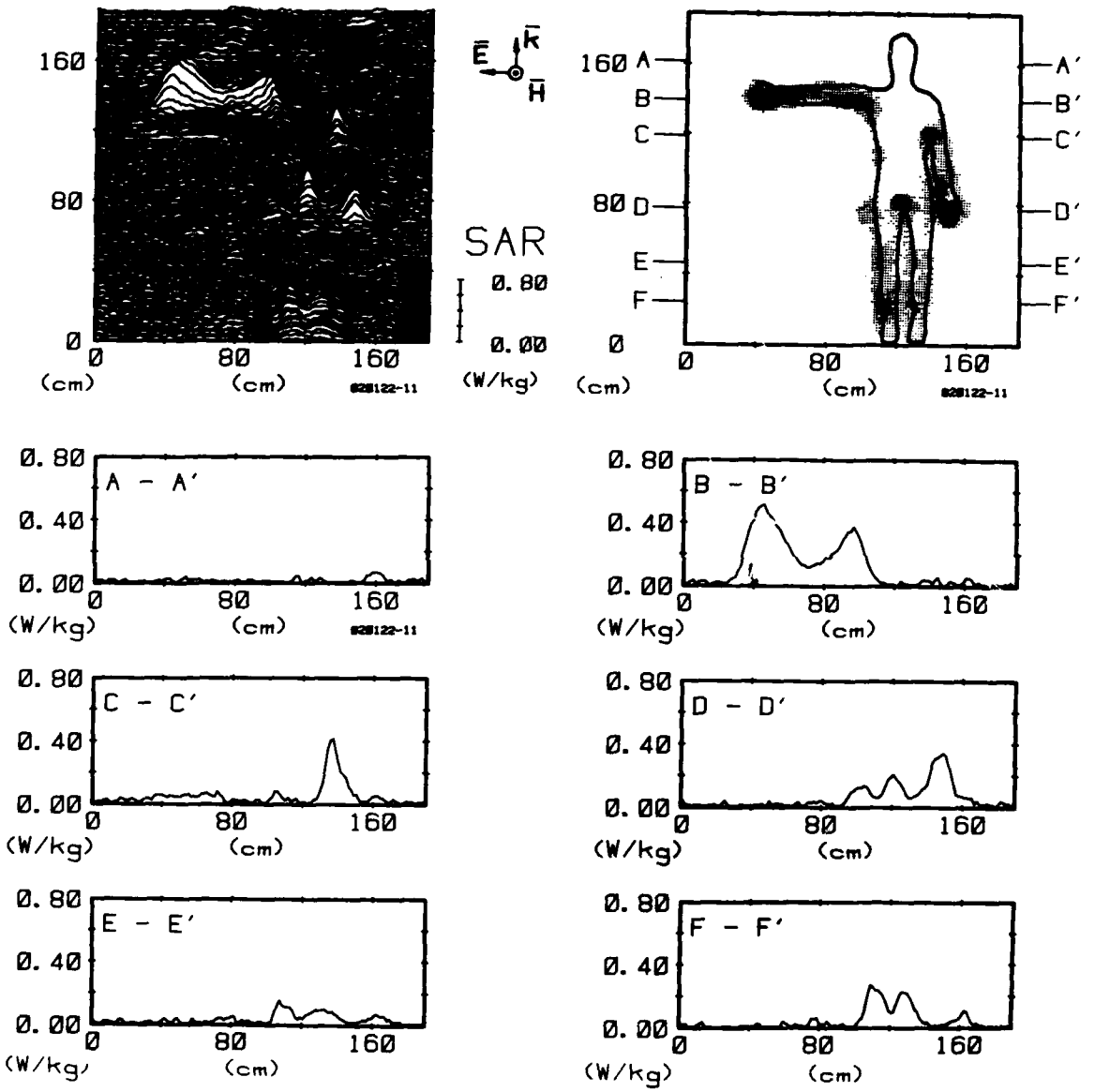

Figure 50B. Computer-processed upper-body thermograms expressing SAR patterns for man with one arm extended, exposed to 1-mW/cm^2 450-MHz radiation with KEH polarization.

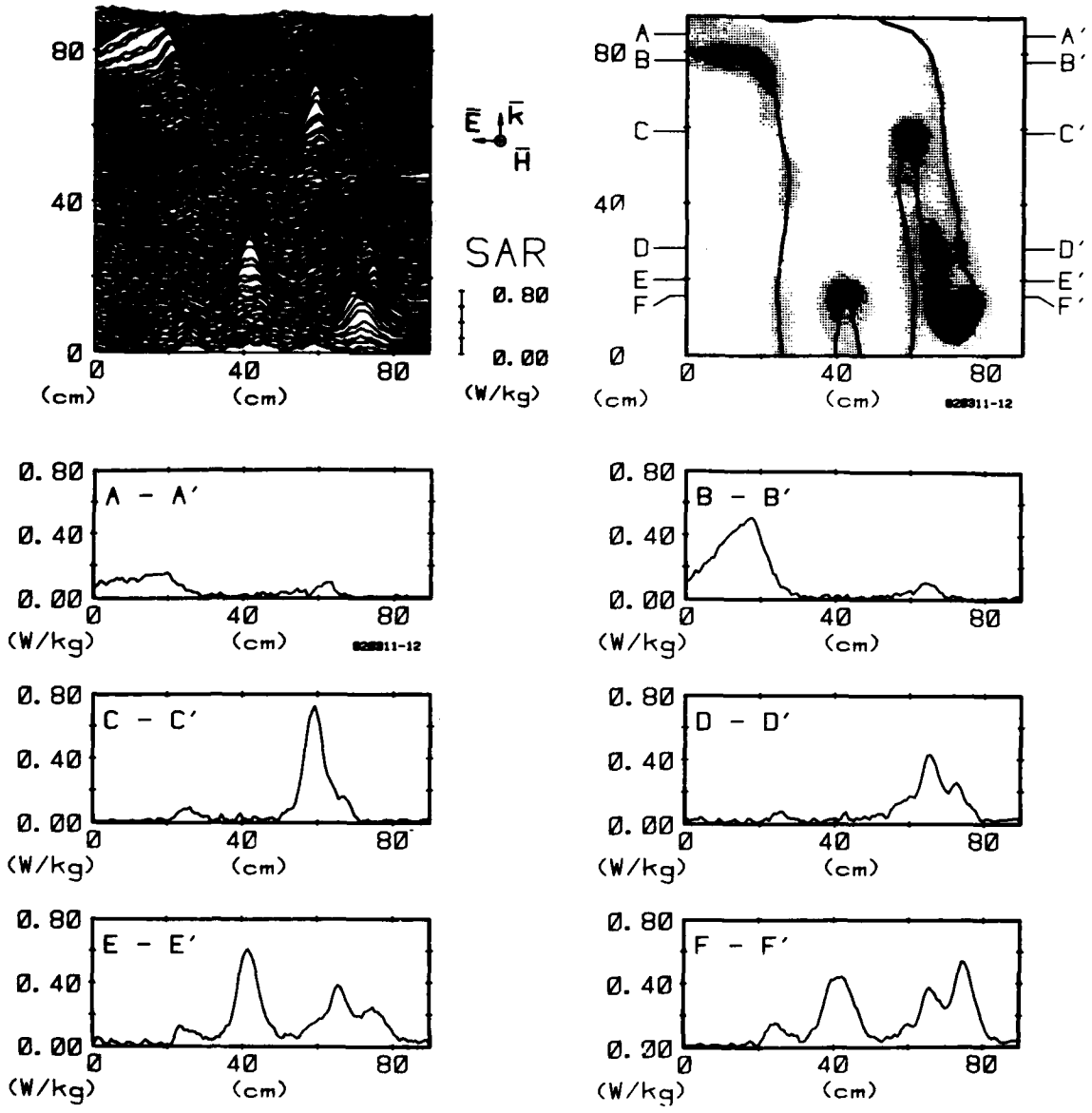

Figure 50C. Computer-processed midbody thermograms expressing SAR patterns for man with one arm extended, exposed to 1-mW/cm^2 450-MHz radiation with KEH polarization.

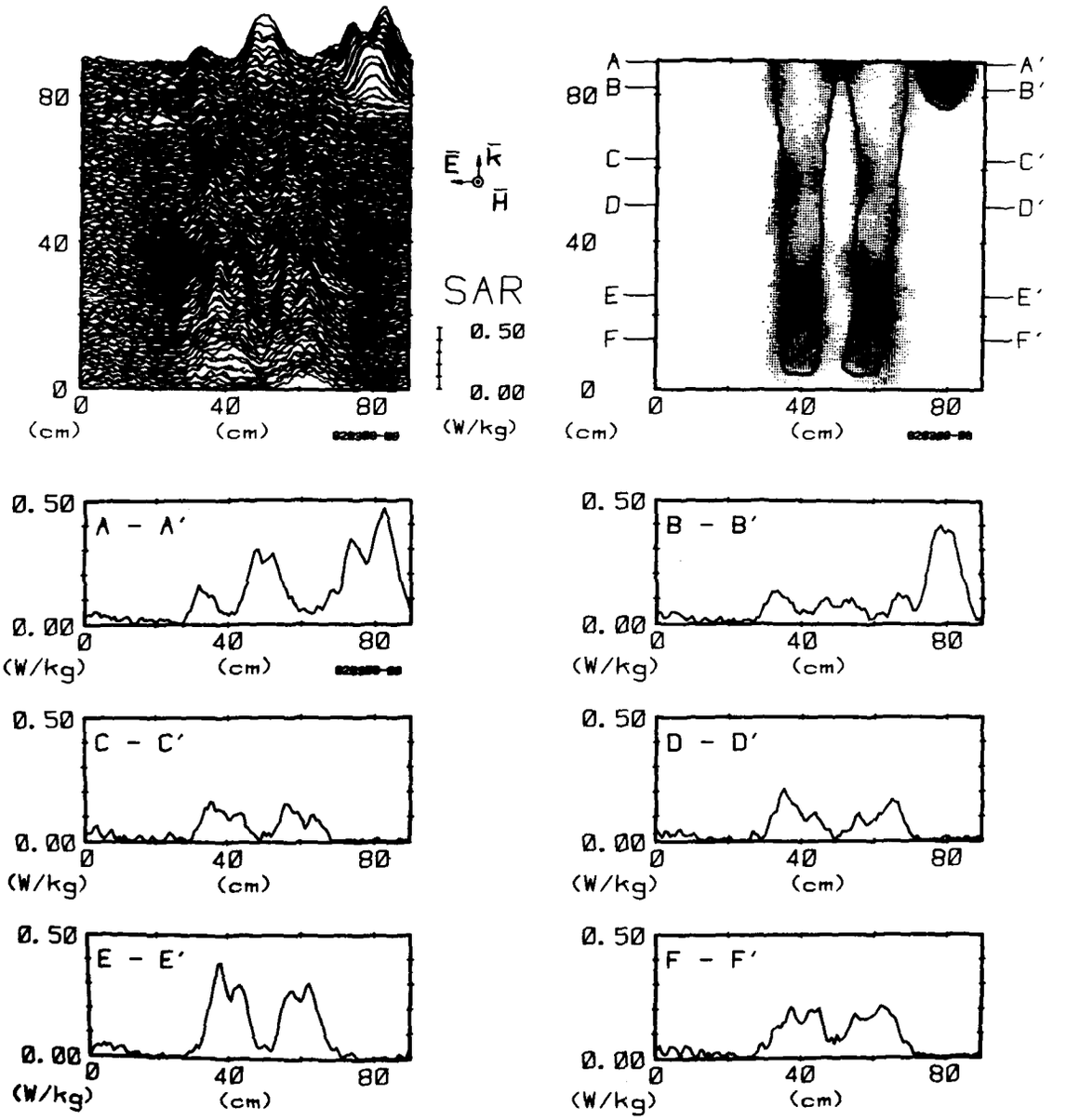

Figure 50D. Computer-processed lower-body thermograms expressing SAR patterns for man with one arm extended, exposed to 1-mW/cm^2 450-MHz radiation with KEH polarization.

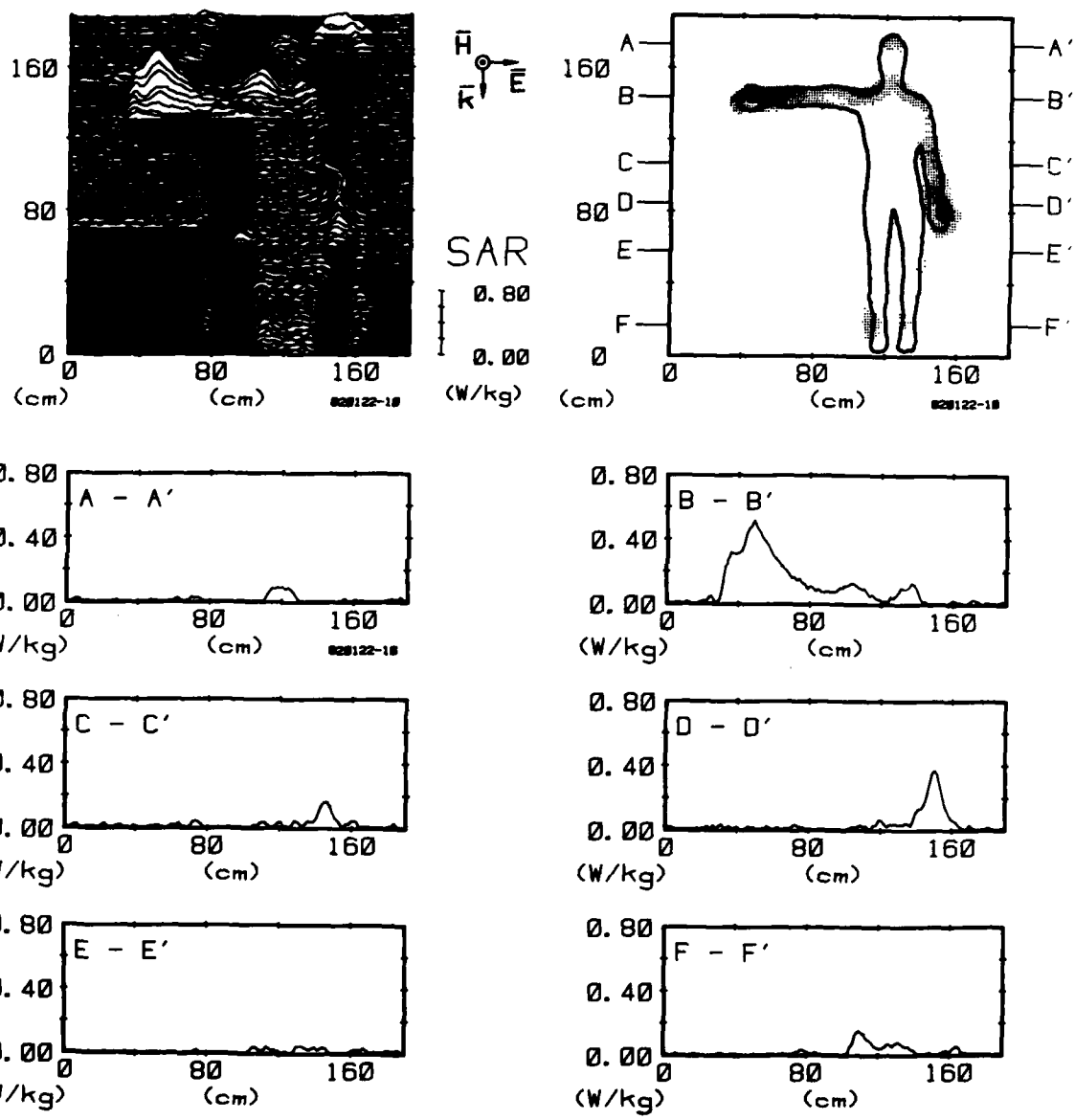

Figure 51. Computer-processed whole-body thermograms expressing SAR patterns for man with one arm extended, exposed to 1-mW/cm^2 450-MHz radiation with -KEH polarization.

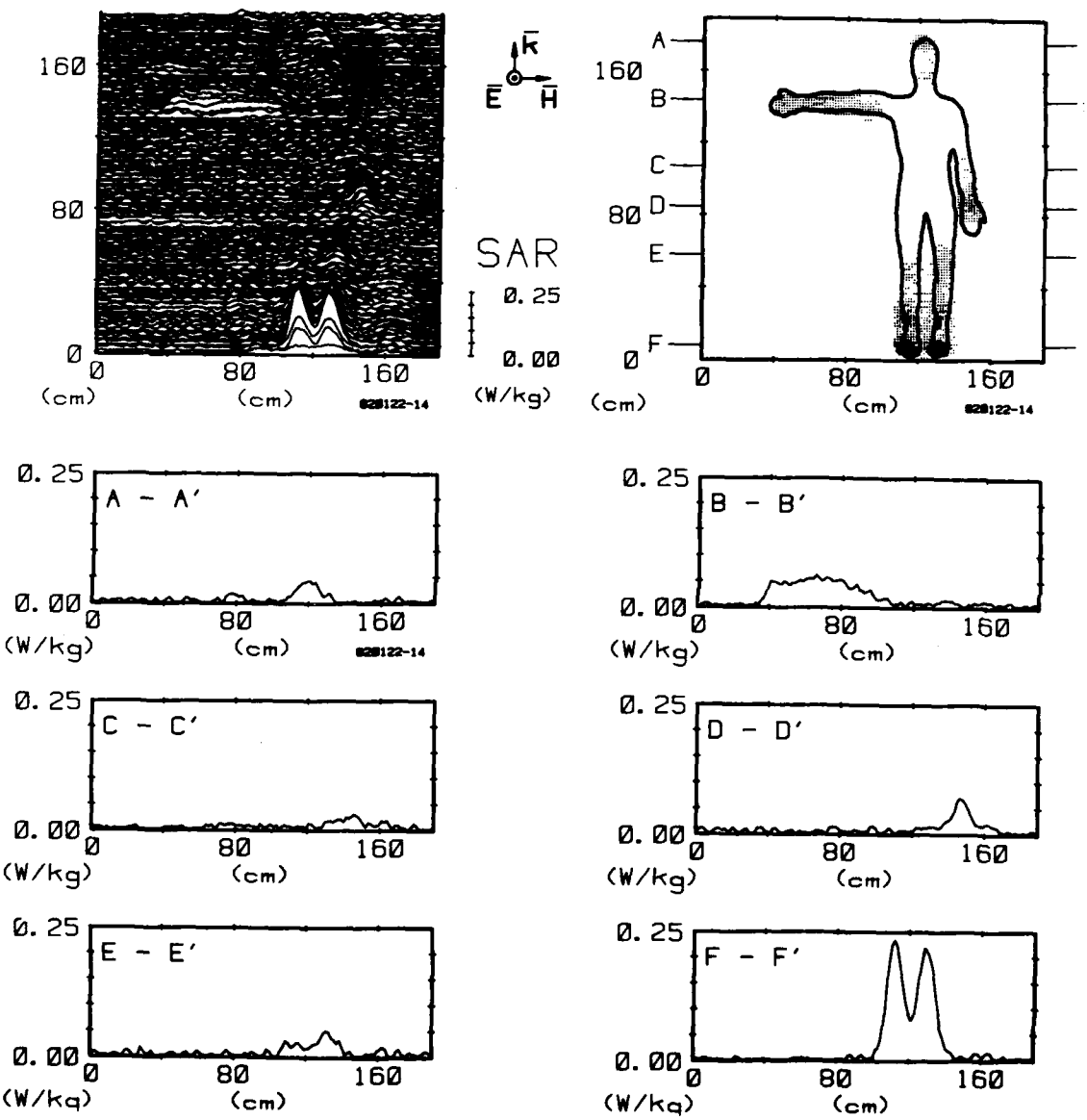

Figure 52. Computer-processed whole-body thermograms expressing SAR patterns for man with one arm extended, exposed to 1-mW/cm^2 450-MHz radiation with KHE polarization.

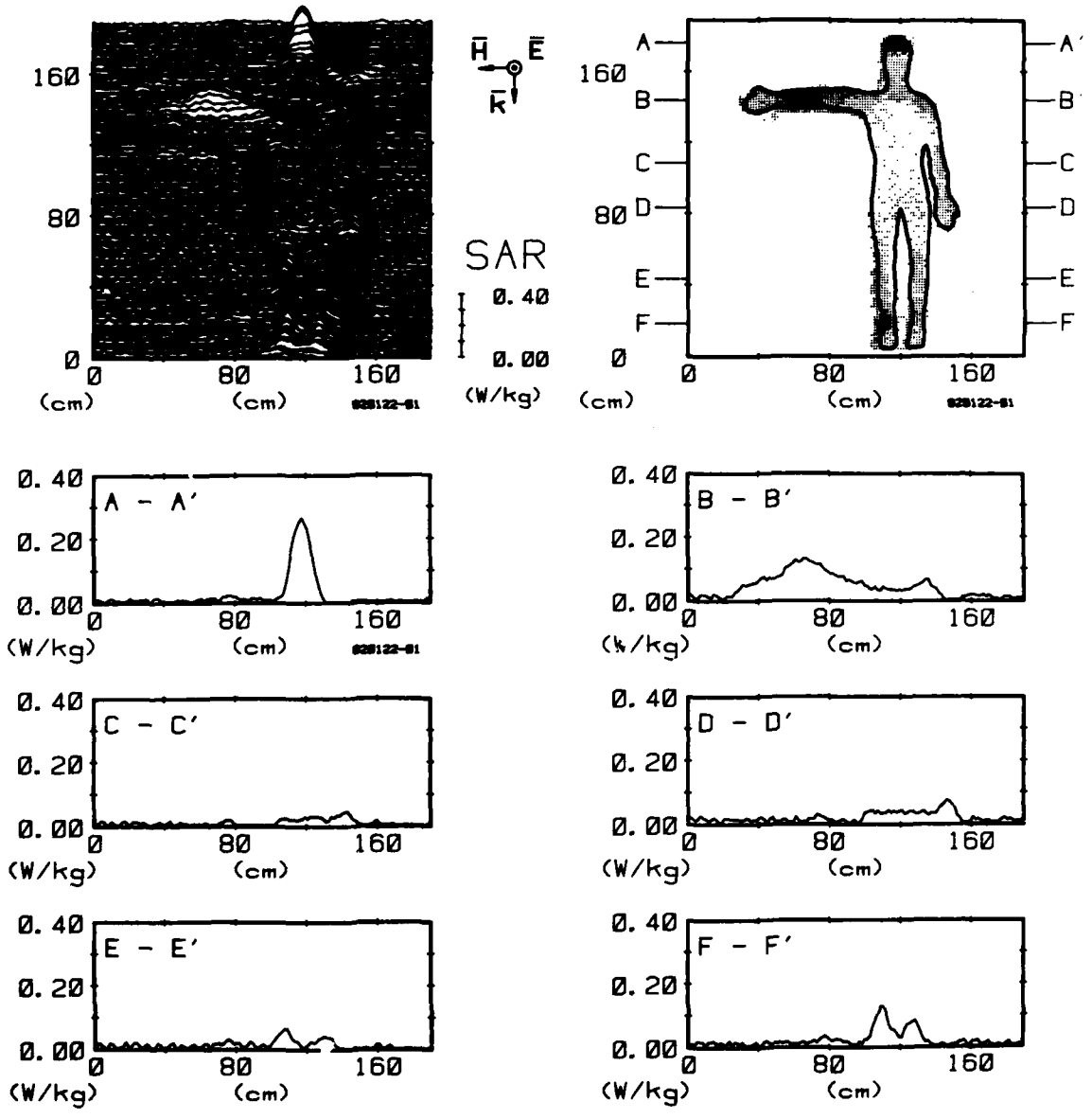

Figure 53. Computer-processed whole-body thermograms expressing SAR patterns for man with one arm extended, exposed to 1-mW/cm^2 450-MHz radiation with -KHE polarization.

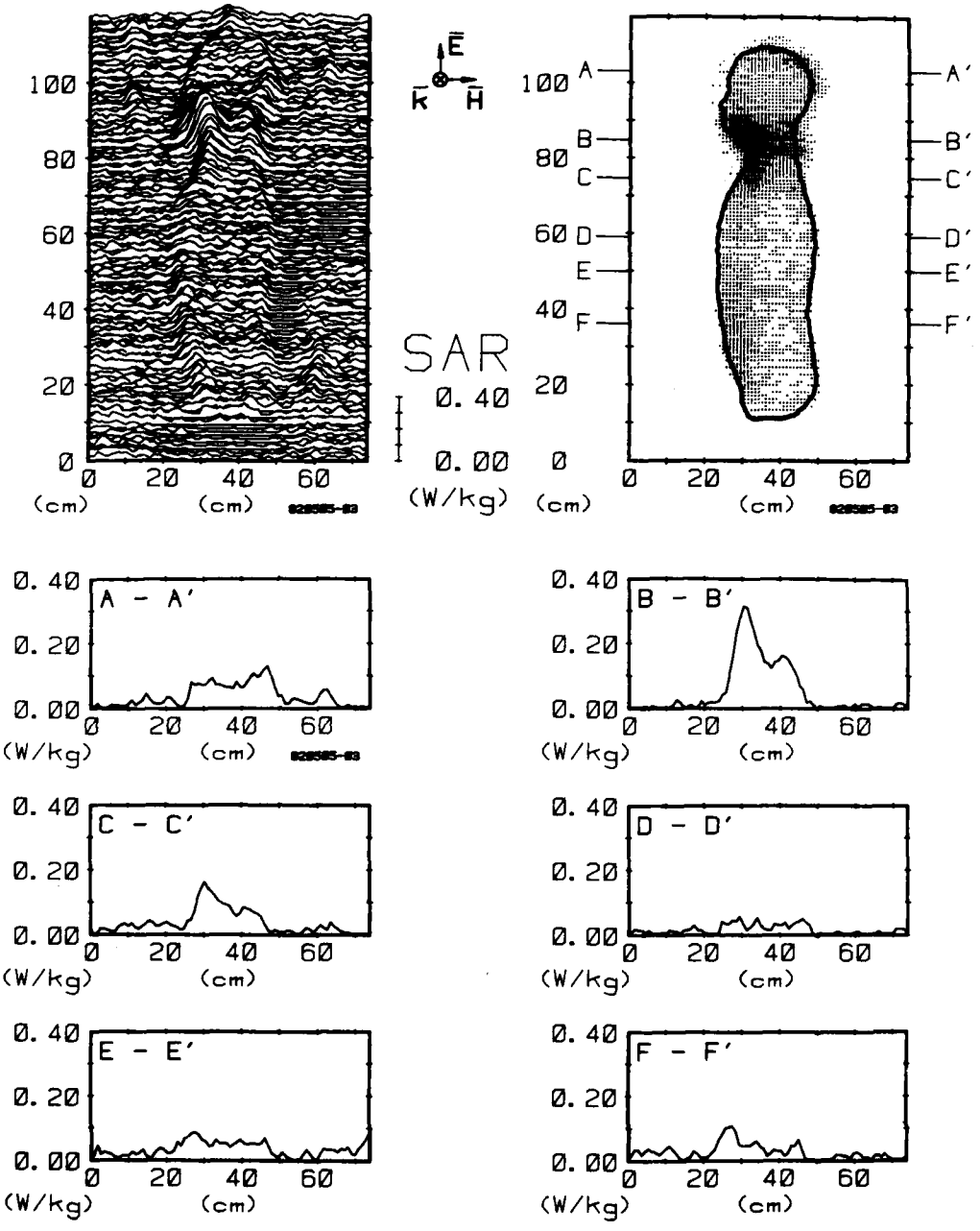

Figure 54. Computer-processed whole-body thermograms expressing SAR patterns for man sitting (sagittal plane), exposed to 1-mW/cm^2 450-MHz radiation with EHK polarization.

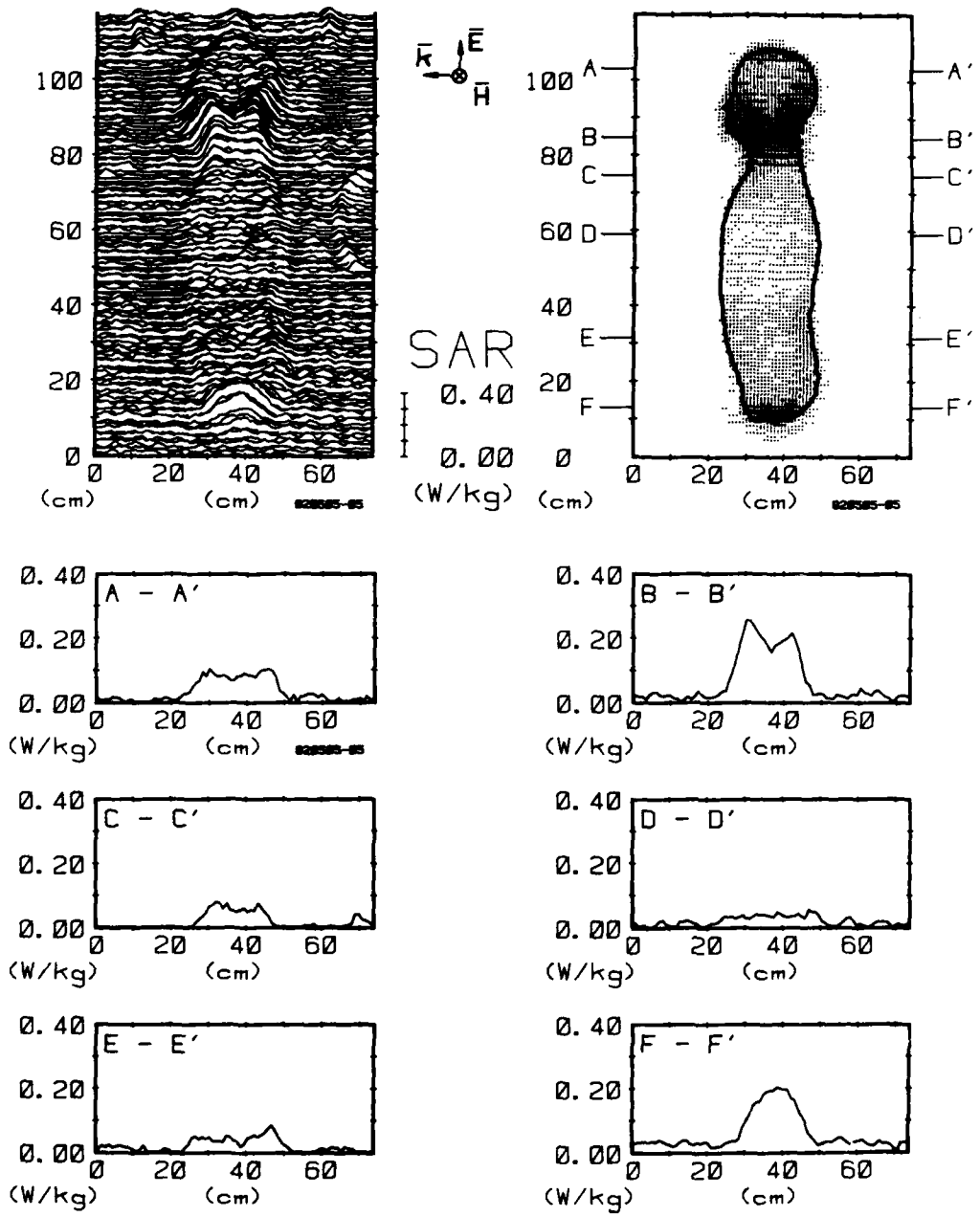

Figure 55. Computer-processed whole-body thermograms expressing SAR patterns for man sitting (sagittal plane), exposed to 1-mW/cm^2 450-MHz radiation with -EHK polarization.

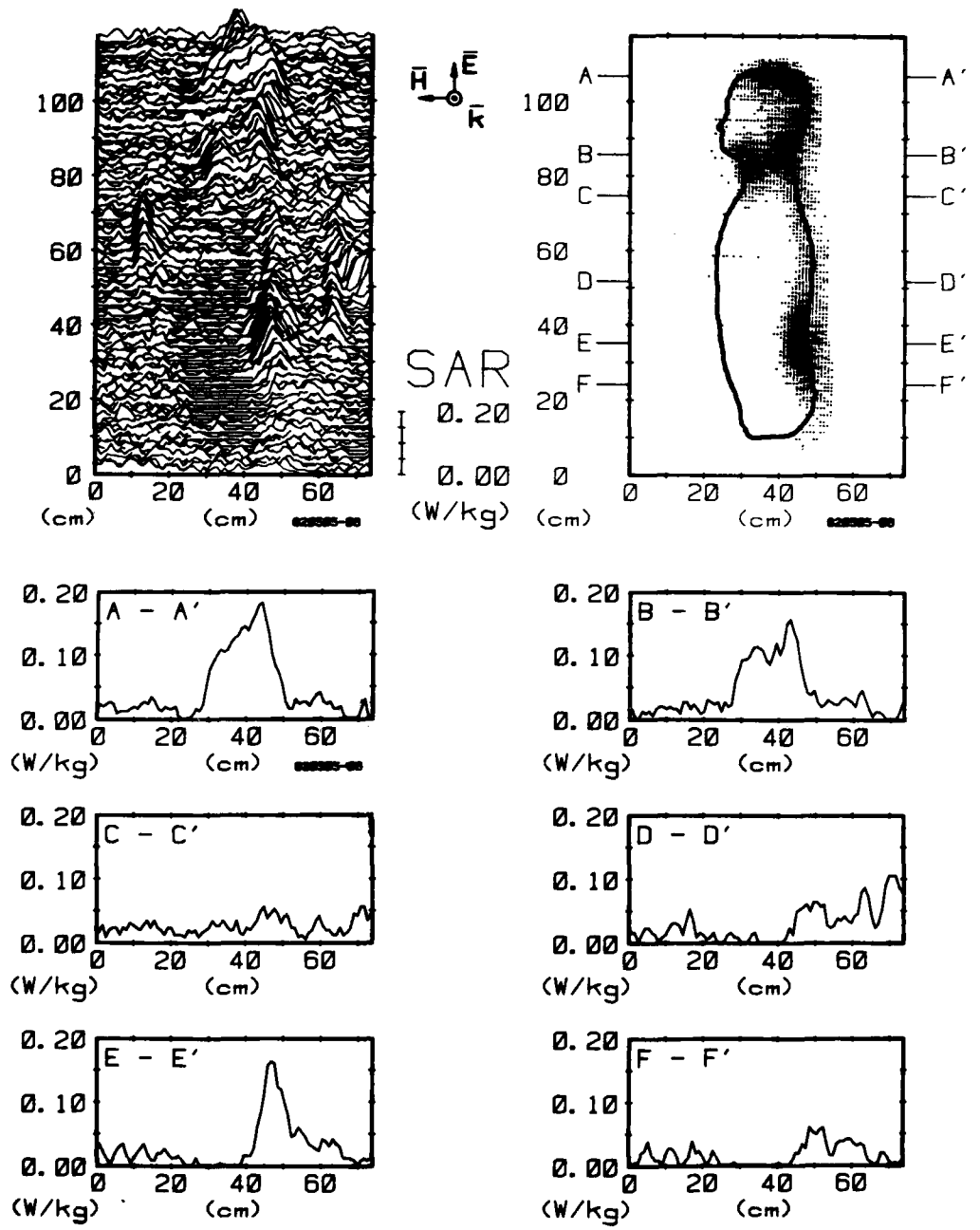

Figure 56. Computer-processed whole-body thermograms expressing SAR patterns for man sitting (sagittal plane) exposed to 1-mW/cm^2 450-MHz radiation with EKH polarization.

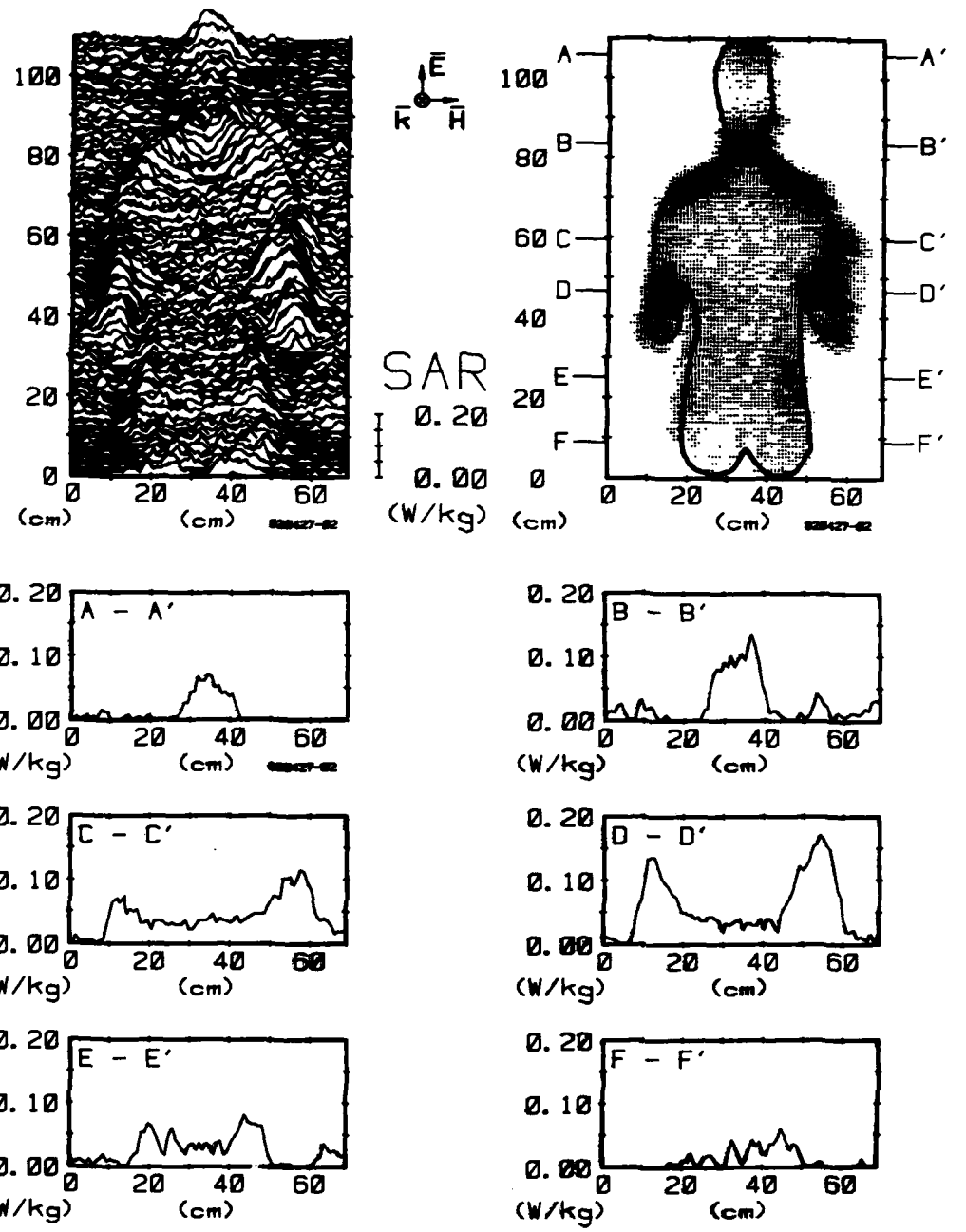

Figure 57. Computer-processed whole-body thermograms expressing SAR patterns for man sitting (frontal plane) exposed to 1-mW/cm^2 450-MHz radiation with EHK polarization.

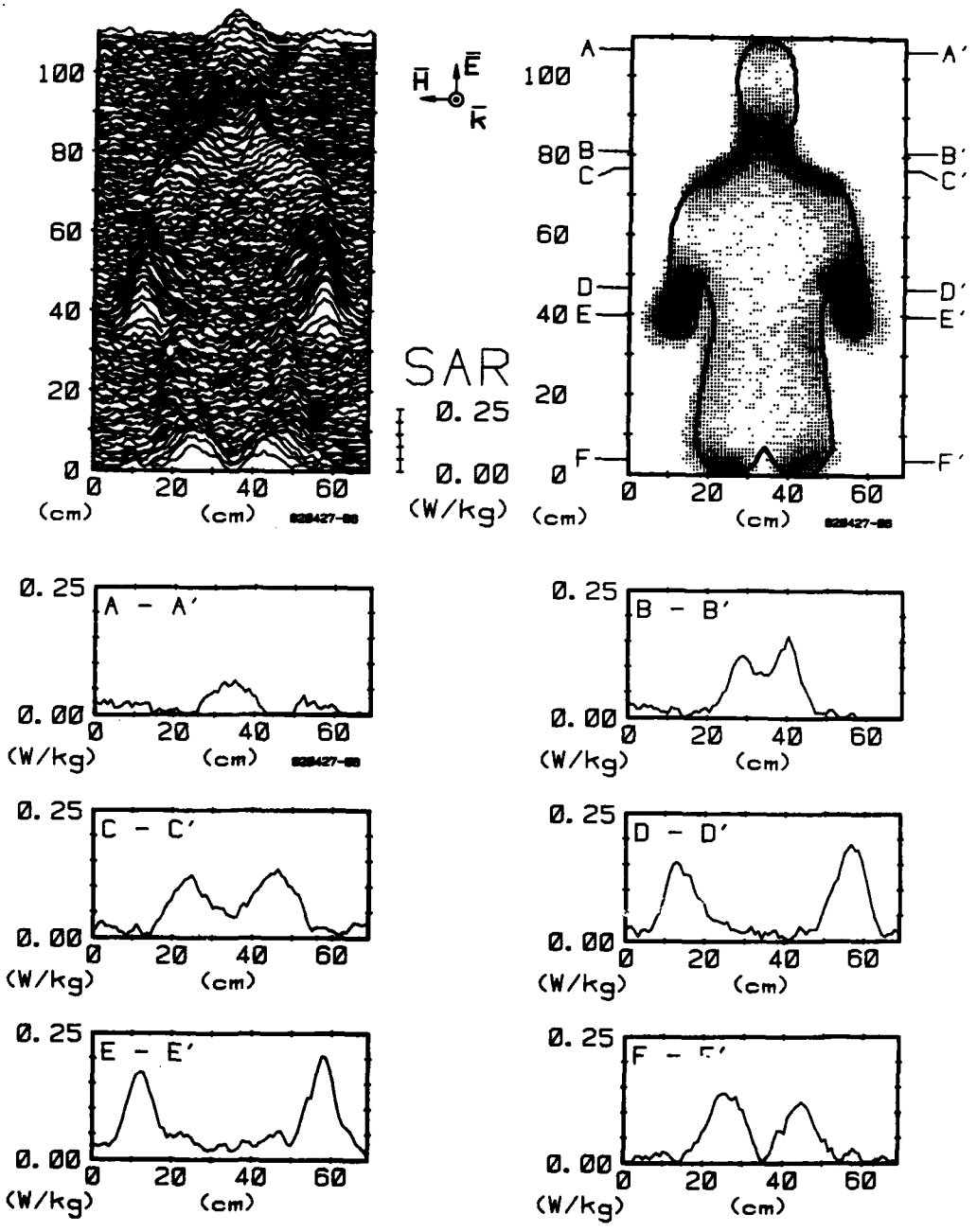

Figure 58. Computer-processed whole-body thermograms expressing SAR patterns for man sitting (frontal plane) exposed to 1-mW/cm^2 450-MHz radiation with -EHK polarization.

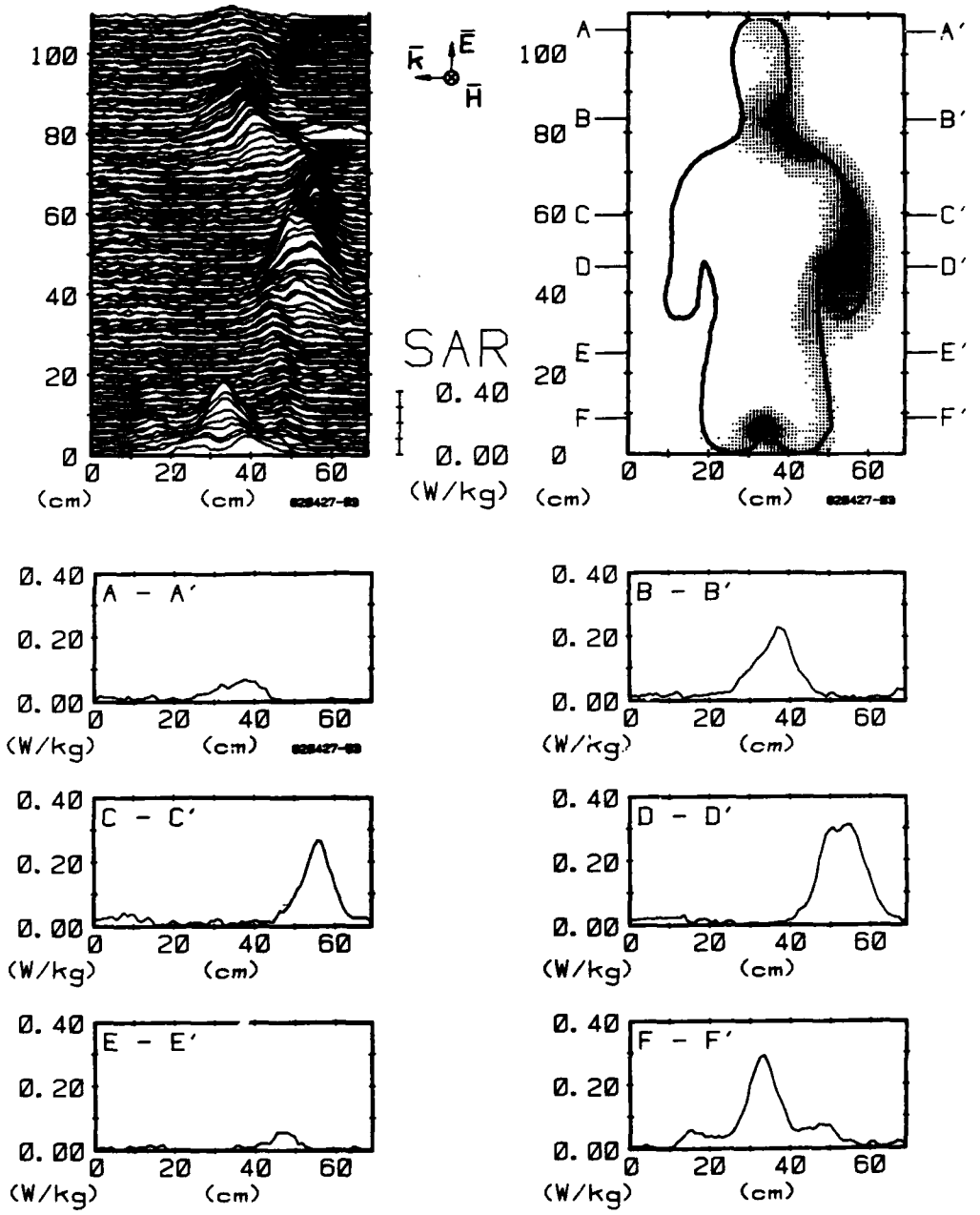

Figure 59. Computer-processed whole-body thermograms expressing SAR patterns for man sitting (frontal plane), exposed to 1-mW/cm^2 450-MHz radiation with EKH polarization.

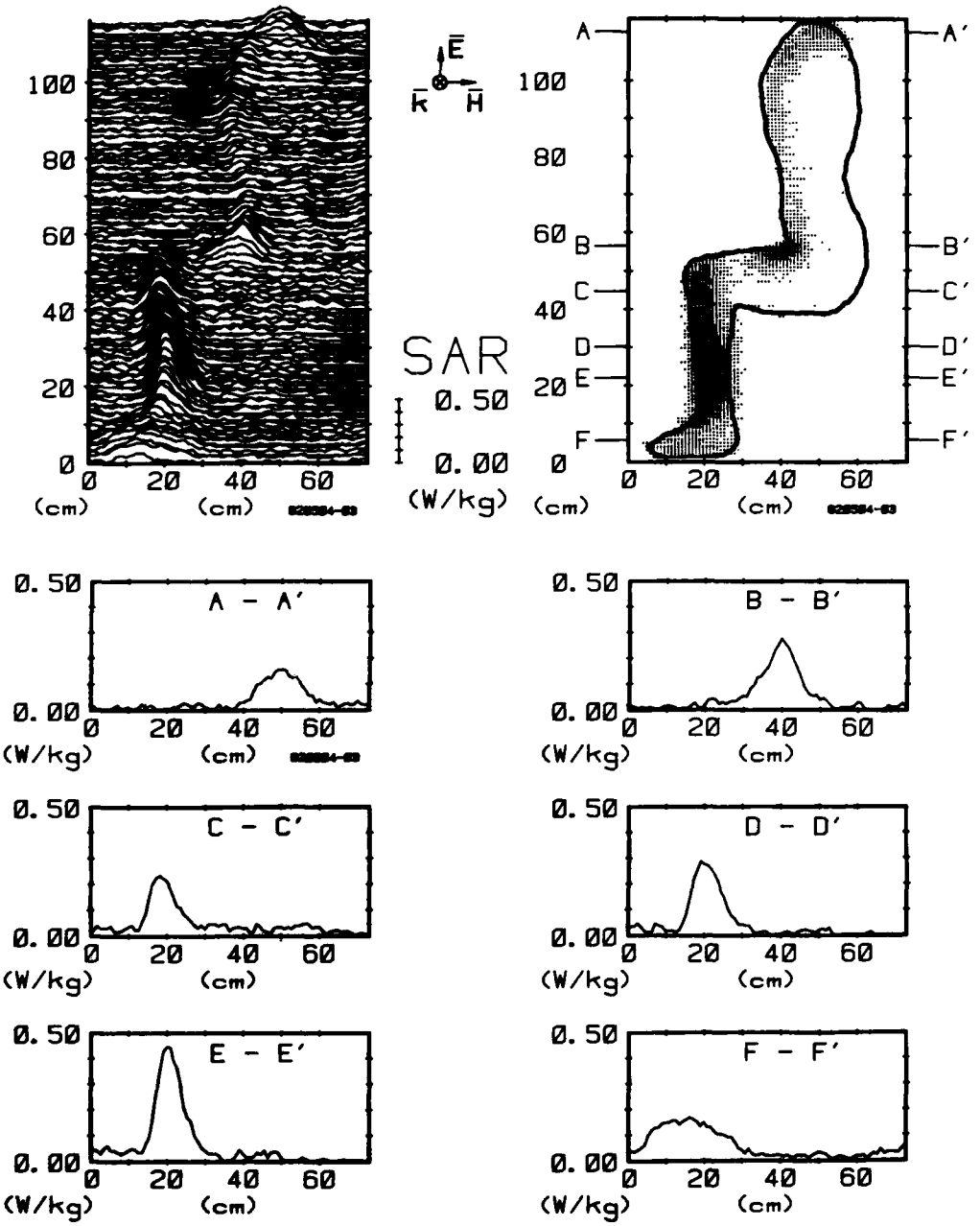

Figure 60. Computer-processed whole-body thermograms expressing SAR patterns for man sitting (sagittal plane through leg), exposed to 1-mW/cm^2 450-MHz radiation with EHK polarization.

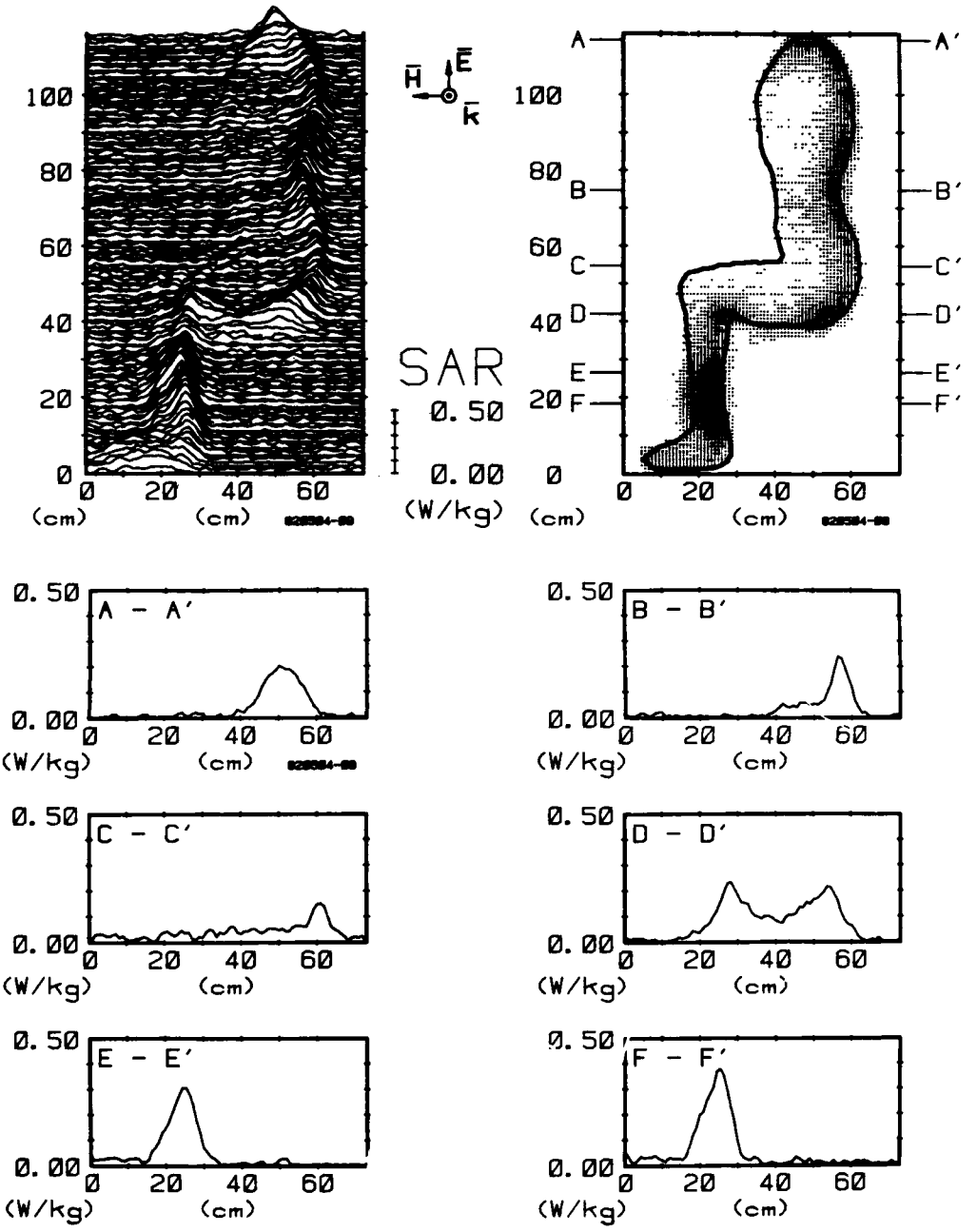

Figure 61. Computer-processed whole-body thermograms expressing SAR patterns for man sitting (sagittal plane through leg), exposed to 1-mW/cm^2 450-MHz radiation with -EHK polarization.

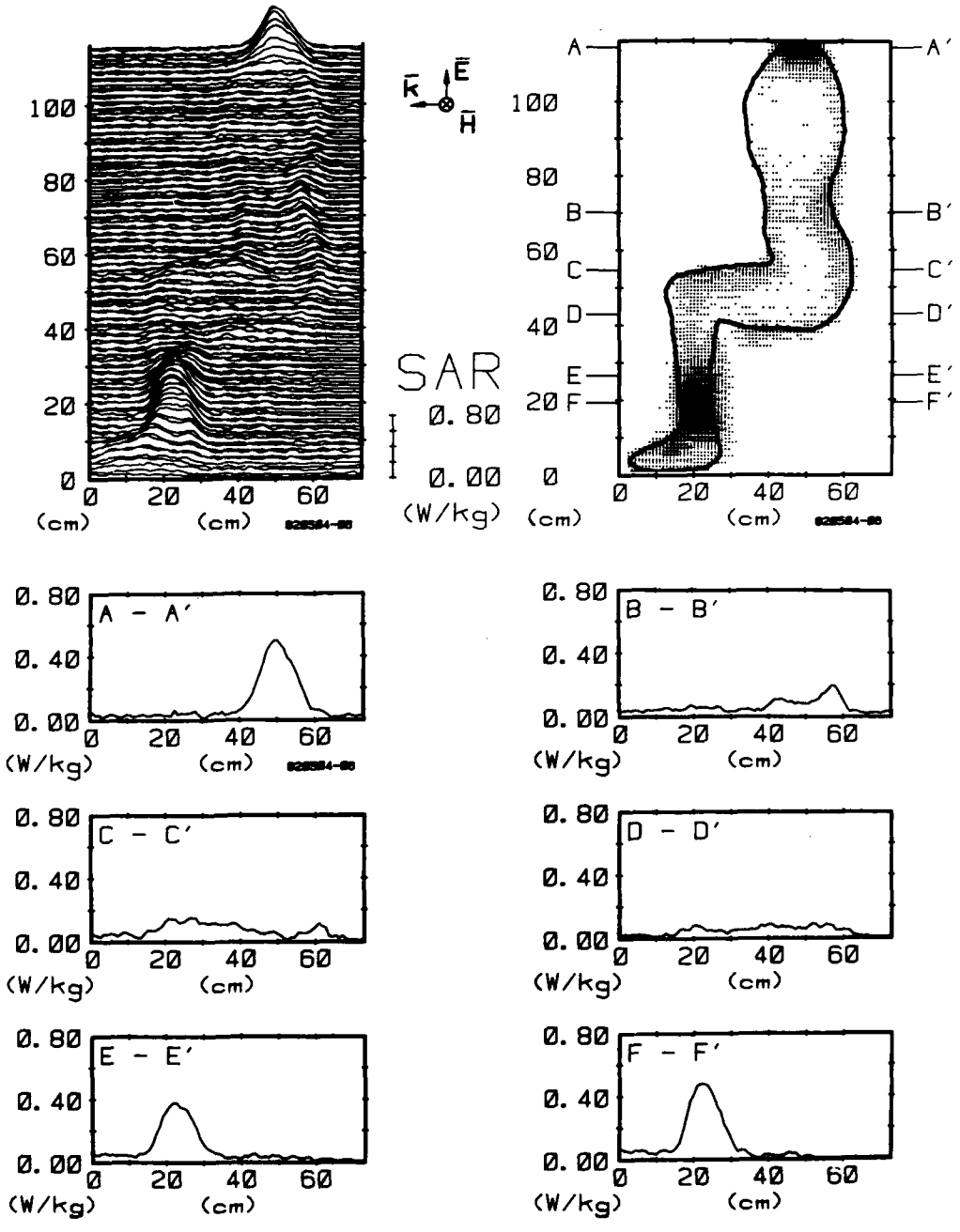

Figure 62. Computer-processed whole-body thermograms expressing SAR patterns for man sitting (sagittal plane through leg), exposed to 1-mW/cm^2 450-MHz radiation with EKH polarization.

AD-A135 455 EFFECTS OF LONG-TERM LOW-LEVEL RADIOFREQUENCY RADIATION EXPOSURE ON RATS..(U) WASHINGTON UNIV SEATTLE BIOELECTROMAGNETICS RESEARCH LAB A W GUY ET AL. SEP 83 2/2

UNCLASSIFIED SR-19 SAM-TR-83-18 F33615-80-C-0612 F/G 6/18 NL

END

DATE FILMED

1 84

DTIC

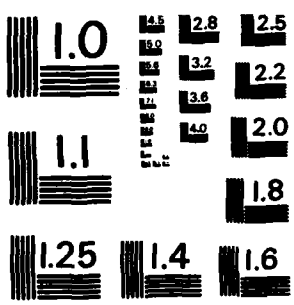

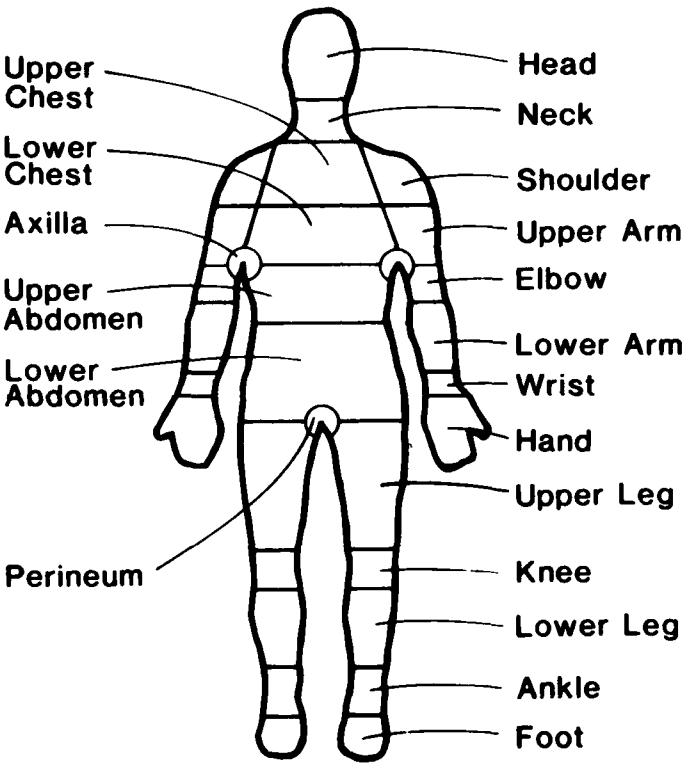

Figure 63. Regions of body where maximum SAR values were determined from closeup thermograms.

TABLE 5. MAXIMUM SAR_2 VALUES (W/kg) FOR MAN EXPOSED, ERECT WITH ARMS DOWN, TO 1-mW/cm^2 450-MHz RFR UNDER DIFFERENT EXPOSURE POLARIZATIONS

Body Part	Polarization									
	EHK	-EHK	EKH	HEK	-HEK	HKE	KEH	-KEH	HKE	-KHE
Head	.084	.100	.108	.061	.074	.150	.076	.164	.065	.249
Neck	.110	.150	.188	.032	.033	.032	.100	.164	.069	.024
Shoulder	.114	.100	.143	.066	.081	.056	.064	.279	.079	.048
Upper Chest	.099	.080	.055	.000	.000	.003	.028	.095	.049	.014
Upper Arm	.056	.056	.211	.140	.120	.048	.080	.115	.015	.010
Lower Chest	.021	.002	.128	.009	.000	.020	.032	.012	.060	.011
Axilla	.032	.020	.120	.154	.167	.057	.715	.111	.016	.020
Elbow	.266	.300	.300	.184	.119	.106	.214	.076	.013	.030
Upper Abdomen	.018	.006	.023	.000	.000	.816	.050	.006	.010	.016
Lower Arm	.403	.300	.270	.143	.101	.120	.484	.088	.045	.026
Wrist	.406	.250	.589	.109	.143	.10	.420	.140	.062	.029
Lower Abdomen	.020	.021	.014	.003	.000	.055	.171	.150	.000	.020
Perineum	.016	.027	.022	.219	.189	.084	.270	.030	.060	.169
Hand	.129	.084	.581	.258	.295	.135	.767	.724	.037	.244
Upper Leg	.081	.178	.207	.047	.114	.080	.150	.015	.052	.052
Knee	.187	.090	.144	.059	.076	.097	.157	.087	.049	.045
Lower Leg	.222	.108	.238	.061	.098	.050	.201	.195	.189	.053
Ankle	.230	.214	.264	.070	.101	.140	.275	.262	.090	.068
Foot	.077	.084	.113	.116	.158	.344	.138	.082	.295	.100

TABLE 6. MAXIMUM SAR VALUES (W/kg) FOR MAN EXPOSED, ERECT WITH ARMS RAISED, TO 1-mW/cm^2 450-MHz RFR UNDER DIFFERENT EXPOSURE POLARIZATIONS

Body Part	Polarization									
	EHK	-EHK	EKH	HEK	-HEK	HKE	KEH	-KEH	KHE	-KHE
Head	.076	.081	.006	.060	.095	.213	.173	.173	.085	.180
Neck	.054	.069	.045	.063	.032	.042	.031	.292	.024	.014
Shoulder	.090	.060	.178	.108	.072	.064	.501	.854	.035	.037
Upper Chest	.017	.008	.021	.032	.007	.007	.036	.005	.000	.016
Upper Arm	.142	.032	.148	.083	.120	.107	.251	.080	.052	.025
Lower Chest	.077	.051	.000	.075	.063	.005	.022	.000	.000	.032
Axilla	.240	.201	.332	.048	.079	.068	.264	.101	.024	.055
Elbow	.062	.093	.153	.076	.057	.060	.351	.300	.063	.071
Upper Abdomen	.020	.051	.220	.078	.060	.097	.161	.005	.026	.029
Lower Arm	.328	.398	.550	.085	.106	.070	.169	.201	.051	.198
Wrist	.425	.437	.547	.095	.115	.061	.819	.838	.128	.216
Lower Abdomen	.065	.105	.103	.055	.038	.066	.090	.106	.031	.012
Perineum	.008	.013	.052	.326	.133	.075	1.053	.130	.003	.015
Hand	.185	.255	.463	.192	.201	.074	.674	.674	.112	.148
Upper Leg	.054	.101	.191	.060	.078	.121	.172	.130	.033	.058
Knee	.070	.191	.145	.079	.058	.135	.203	.181	.062	.060
Lower Leg	.280	.158	.227	.090	.081	.120	.238	.170	.049	.060
Ankle	.353	.295	.348	.056	.084	.090	.418	.351	.161	.152
Foot	.063	.104	.139	.104	.173	.534	.185	.149	.518	.094

TABLE 7. MAXIMUM SAR_2 VALUES (W/kg) FOR MAN EXPOSED, ERECT WITH RIGHT ARM EXTENDED, TO 1-mW/cm^2 450-MHz RFR UNDER DIFFERENT EXPOSURE POLARIZATIONS

Body Part	Polarization											
	EHK	-EHK	EKH	-EKH	HEK	-HEK	HKE	-HKE	KEH	-KEH	KHE	-KHE
Head	.075	.123	.121	.051	.108	.062	.147	.188	.000	.204	.064	.304
Neck	.106	.123	.193	.030	.072	.046	.032	.028	.000	.146	.044	.038
Shoulder	.115	.109	.088	.029	.051	.056	.087	.038	.124	.565	.026	.069
Upper Chest	.000	.026	.000	.000	.018	.000	.004	.000	.000	.000	.000	.036
Upper Arm	.123	.105	.261	.246	.111	.070	.067	.073	.238	.174	.040	.093
Lower Chest	.000	.000	.000	.130	.043	.000	.006	.057	.024	.000	.000	.012
Axilla	.061	.074	.289	.356	.118	.167	.079	.043	.661	.116	.017	.036
Elbow	.245	.248	.402	.369	.100	.079	.077	.072	.136	.275	.035	.054
Upper Abdomen	.000	.000	.000	.173	.000	.000	.052	.036	.152	.080	.000	.000
Lower Arm	.373	.321	.448	.246	.364	.217	.111	.098	.306	.433	.054	.098
Wrist	.353	.345	.605	.624	.532	.456	.107	.134	.577	.778	.061	.073
Lower Abdomen	.000	.019	.013	.024	.025	.000	.081	.073	.029	.000	.000	.012
Perineum	.009	.008	.014	.048	.224	.129	.053	.024	.411	.042	.459	.009
Hand	.230	.162	.725	.526	.294	.162	.134	.089	.512	.573	.363	.085
Upper Leg	.049	.138	.188	.173	.076	.114	.086	.069	.147	.000	.165	.029
Knee	.094	.132	.185	.159	.113	.099	.062	.078	.162	.063	.136	.039
Lower Leg	.246	.126	.275	.144	.108	.125	.072	.090	.198	.105	.212	.055
Ankle	.272	.240	.290	.254	.123	.114	.149	.126	.375	.242	.199	.139
Foot	.079	.084	.105	.045	.153	.243	.386	.441	.176	.179	.300	.066

TABLE 8. MAXIMUM SAR VALUES (W/kg) FOR MAN EXPOSED, SITTING, TO 1-mW/cm^2 450-MHz RFR UNDER DIFFERENT EXPOSURE POLARIZATIONS

Body Part	Polarization		
	EHK	-EHK	EKH
Head	.198	.147	.138
Neck	.290	.227	.355
Shoulder	.253	.389	.469
Upper Chest	.087	.155	.072
Upper Arm	.219	.643	.476
Lower Chest	.096	.187	.077
Axilla	.245	.643	.694
Elbow	.657	.375	.635
Upper Abdomen	.116	.223	.216
Lower Arm	.242	.136	.258
Wrist	.121	.138	.290
Lower Abdomen	.076	.187	.080
Perineum	.198	.148	.466
Hand	.226	.142	.244
Upper Leg	.159	.121	.113
Knee	.154	.244	.222
Lower Leg	.545	.396	.545
Ankle	.353	.374	.249
Foot	.234	.161	.087

DISCUSSION

The average SARs for man exposed to 450 MHz in our current project are compared in Table 9 with data obtained previously by our group and other investigators. When phantom scale models of man (dolls or figurines) are used, measured values of average SAR for all polarizations are somewhat greater than values calculated theoretically with the prolate spheroid models or computer models consisting of a finite number of blocks. For the prolate spheroid model of man, average SAR values vary from .016 to .034 W/kg, depending upon polarization. These values are consistent with the average SARs reported for the computer block model (Gandhi et al., 1979). Our measurements of the average SARs for the 3- to 4-year-old child model (half the height of the man model) are also significantly (2-3 times) higher than those predicted by theory with the prolate spheroid model.

The differences between the theoretical and experimental results may be further explored by comparison of the values over a broad frequency range, as shown in Fig. 64. The theoretical curve in the figure, based on the work of Hagmann et al. (1979) with a human block model, is generally lower than the experimental curve derived from the work discussed in this report and our past work (Guy et al., 1978). The data for the human block model compare much better with the experimental values for above-the-body-resonance frequencies (maximum level) than with the values for the prolate spheroid model, given in Table 9. To gain a better understanding of these differences, we made additional measurements of average SAR for frequencies below resonance using the scale models (plotted as dots or circles in Fig. 64). These measurements required a different model-exposure technique, discussed in the Appendix.

TABLE 9. COMPILATION OF THEORETICAL AND EXPERIMENTAL DATA ON AVERAGE SAR FOR HUMAN EXPOSURE TO FREQUENCIES NEAR OR EQUAL TO 450 MHz AT 1 mW/cm^2

Investigator, frequency, and model	ε'	σ (S/m)	SAR (W/kg) Exposure Polarization EKH	EHK	HEK	HKE	KEH	KHE	-KEH	-KHE
Durney et al. (1978)										
450 MHz										
Theoretical:										
Prolate spheroid										
Avg man	36	0.82	.034	.034	.030	.030	.016	.016	.016	.016
Skinny man	36	0.82	.049	.049	.036	.036	.022	.022	.022	.022
5-yr-old child	36	0.82	.062	.062	.042	.042	.031	.031	.031	.031
1-yr-old child	36	0.82	.094	.094	.043	.043	.052	.052	.052	.052
Infant	36	0.82	.125	.125						
Gandhi (1977)										
462.3 MHz										
Measured:										
Human figurine	Unknown saline	Unknown saline	.045		.044		.063			
Gandhi (1979)										
462.3 MHz										
Theoretical:										
Computer avg man	36	0.82		.035						
Measured:	Unknown	Unknown							.056	.057
Human figurine	saline	saline								
Guy et al. (1978)										
442 MHz										
Measured:										
Human doll	58.9	1.68	.041	.046	.049	.049	.069	.043	.057	.039
(Current project)										
Human doll	50.2	1.18	.041	.050	.049	.041	.063	.050	.053	.049
Adult	33.1	0.89	.046	.059	.054	.042	.061	.048	.054	.050
450 MHz										
Measured:										
3-4-yr-old child	50.2	1.18	.187	.164	.108	.061	.165	.094	.158	.095

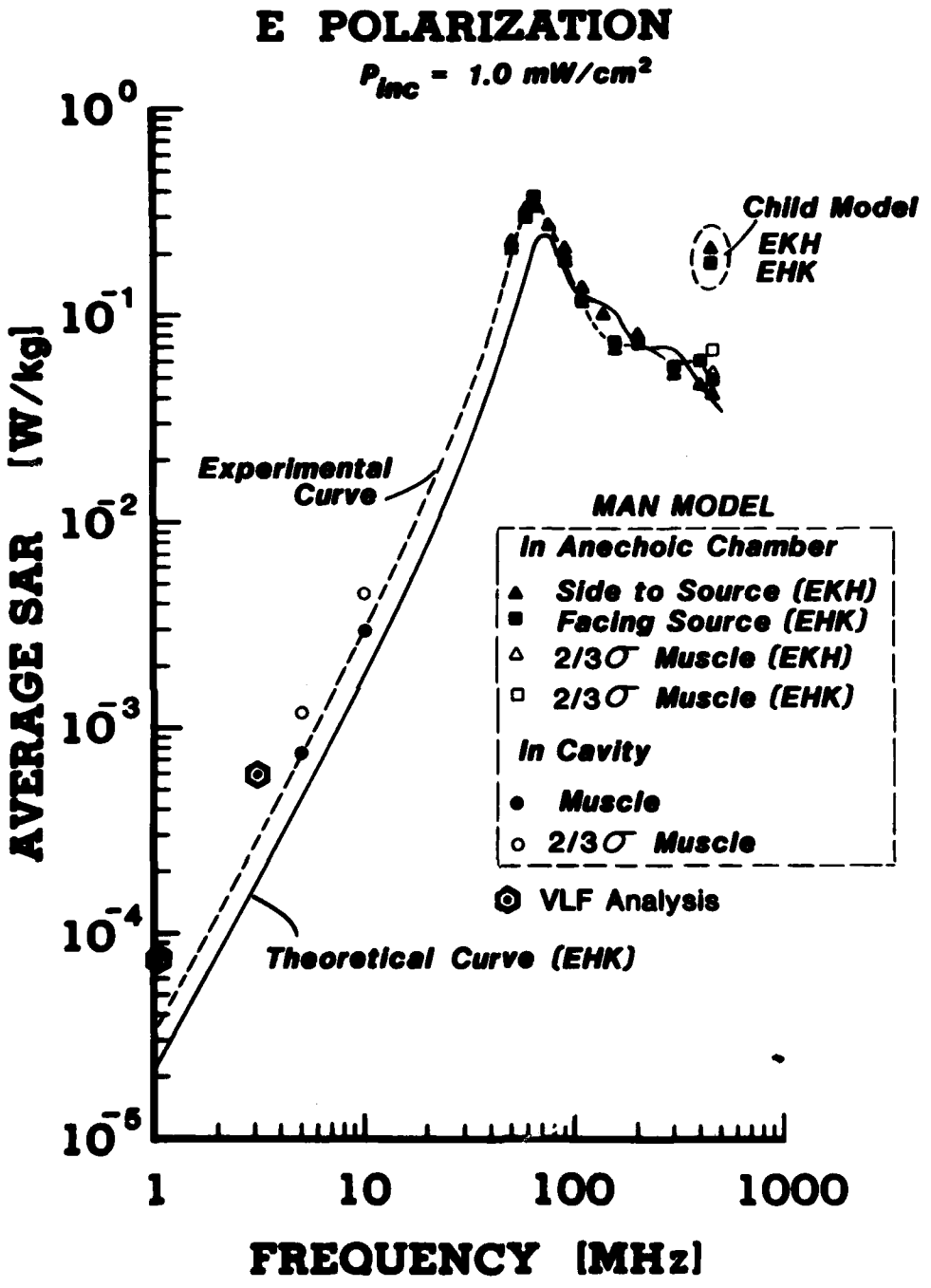

Figure 64. Comparison of theoretical and experimentally measured whole-body average SARs for realistic man models exposed at various frequencies.

Additional data, for frequencies ranging from very low to medium, were obtained for the below-resonance curve from Guy and Chou (1982), who used current distribution measurements from metalized full-scale models of man exposed to 60 Hz (Deno, 1977) and current, potential, and resistance measurements from a live human subject with 60-Hz to 300-kHz currents passing axially through the body. Their data, denoted on the curve by hexagons, seem to be consistent with our scale-model measurements.

As pointed out by Guy and Chou (1982), the shape of the model especially plays an important role in determining the average SAR during exposure. At frequencies significantly below body resonance, most energy absorption is in the lower legs; and the shape and size of the legs play an important part in the absorption mechanism.

Average SAR

In the Radiation Handbook (Durney et al., 1978) the variation of average SAR with polarization appears to be minimum at the frequency of 450 MHz. This phenomenon has been confirmed experimentally. Based on 41 values of measured average SAR, presented in Tables 3 and 4, for a homogeneous-muscle man model exposed under different posture and polarization conditions, the statistics for the SAR (W/kg) for an exposure level of 1 mW/cm^2 are as follows:

No. of values	Mean	Standard deviation	Minimum value	Maximum value
41	.0498	.0075	.0365	.0714

From these data we can assume that regardless of the exposure conditions for man--whether the polarization is vertical, horizontal, or circular; or the posture is erect, supine, or sitting; or the arms are extended or not--the average SAR remains relatively constant at a level of approximately .05 W/kg for a 1-mW/cm^2 exposure level. This SAR level is a factor of 8 below the level used as a basis for the ANSI C95.1-1982 RFR standard.

Maximum SAR and SAR Distribution

Figs. 22-62 and Tables 5-8 indicate that in the body of a man exposed at 450 MHz, the SAR is far from uniform and reaches values as high as 13 times the average.

In general, when the man is exposed with the electric-field vector parallel to the body, SAR is maximal in the narrow cross sections, such as the neck, wrists, and ankles, with the highest levels in the wrists. For frontal or back exposures under these conditions, the SAR patterns are symmetrical with respect to the sagittal plane; and typical maximal SAR values are 0.1, 0.4, and 0.3 W/kg for the neck, wrists, and ankles respectively. When the exposures are from the side, the patterns become asymmetrical with respect to the sagittal plane; maximal values for SAR are on the exposed side, with levels reaching 0.2, 0.6, and 0.3 W/kg in the neck, wrists, and ankles respectively.

When the man is exposed with the electric field perpendicular to the long axis of the body but parallel to the broad side, localized SAR can occur in the perineal and axillar areas of the body owing to sharp diversion of the RF currents around the wedge-shaped discontinuities of the body. In general, when the electric field is not tangent to the apex of such discontinuities, this localized SAR will not occur. The data on SAR distribution show that, even though the average SAR does not significantly vary with position or posture, the pattern of the localized SAR will change radically. Most of the maximal SAR levels, however, occur in the limbs and in the perineal and axillar areas, depending on exposure conditions.

Selection of Exposure Levels

On the basis of the interpretation of the data presented in Table 4, exposure conditions that would produce an average SAR of about 0.050 W/kg in the animal would be required for simulating exposure of an adult human to 450 MHz based on average SAR. In addition to the average SAR, we would need to compare SARs in hot spots in exposed humans and laboratory animals. Tables 5-8 show the measured maximum SARs at various locations of the body for simulated human exposure to 450-MHz 1-mW/cm^2 RFR. The thermographic measurements indicate that the maximum SAR values could be as high as 0.192 W/kg (or 4 times the average SAR) in the head and 1.020 W/kg (or 15 times the average) in the wrist or the perineum. During the planning stages of the experiment, two options (in addition to that proposed in the original protocol) were introduced for consideration, each based on a useful scientific consideration, in simulating chronic human exposure to RFR. These options are outlined in Table 10. The first option is consistent with the original intent to simulate exposure of man to 450-MHz 1-mW/cm^2 RFR. The second option is to simulate an exposure regime in which the worst-case conditions producing the maximum allowed average SAR (0.4 W/kg) specified in the 1982 ANSI C95.1 RFR standard would exist at some period in time, but would not be exceeded. The third option is to utilize an exposure level set for an average SAR over the lifetime of the animal, equal to the maximum 0.4 W/kg allowed by the ANSI standard. This exposure level is an average of the average SARs obtained over all ages for a given input power, as shown in Table 10. In option one, the decrease in average SAR from 0.270 W/kg for the 200-g young rat to 0.058 W/kg for the 800-g adult rat qualitatively spans a wide range similar to that for human exposures shown on Table 3. After careful consideration of all three options, the USAF School of Aerospace Medicine sponsors and the principal investigators mutually agreed that option two would provide the best scientific data, because it would best simulate human exposure at the maximum levels allowed by the ANSI C95.1-1982 standard. Thus, an input power level to each exposure alcove cluster was set so that the average input power averaged over time and all exposure waveguides for the entire group was 0.144 W.

TABLE 10. OPTIONS FOR CIRCULAR-WAVEGUIDE EXPOSURE PARAMETERS FOR SIMULATING CHRONIC EXPOSURE OF A HUMAN TO RFR

Option 1	Option 2	Option 3
450-MHz 1-mW/cm^2 RFR From child to adult (based on .068 W/kg for adult)	Equivalent to no more than allowed by ANSI C95.1 at any time during lifetime (max. 0.4 W/kg during childhood)	Equivalent to maximum allowed by ANSI C95.1 (0.4 W/kg averaged over entire lifetime)
Waveguide input = 0.097 W	Waveguide input = 0.144 W	Waveguide input = 0.390 W
Average power density = 0.324 mW/cm^2	Average power density = 0.480 mW/cm^2	Average power density = 1.30 mW/cm^2
Average SAR 200-g rat = 0.27 W/kg	Average SAR 200-g rat = 0.40 W/kg	Average SAR 200-g rat = 1.08 W/kg
Average SAR 800-g rat = .068 W/kg	Average SAR 800-g rat = 0.10 W/kg	Average SAR 800-g rat = 0.27 W/kg
Predicted range of hot-spot magnitude in 330-g rat 0.52-1.09 W/kg	Predicted range of hot-spot magnitude in 330-g rat 0.63-1.33 W/kg	Predicted range of hot-spot magnitude in 330-g rat 1.71-3.60 W/kg

REFERENCES

Deno, D.W. Current induced in human body by high-voltage transmission line electric field -- Measurement and calculation of distribution and dose. IEEE Trans PAS 96(5):1517-1527 (1977).

Durney, C.H., et al. Radiofrequency radiation dosimetry handbook, 2nd ed. SAM-TR-78-22, May 1978.

Gandhi, O.P., E.L. Hunt, and J.A. D'Andrea. Deposition of electromagnetic energy in animals and in models of man with and without grounding and reflector effects. Radio Sci 13(6S)39-47 (1977).

Gandhi, O.P., M.J. Hagmann, and J.A. D'Andrea. Part-body and multibody effects on absorption of radio-frequency electromagnetic energy by animals and by models of man. Radio Sci 14(6S):23-30 (1979).

Guy, A.W., M.D. Webb, and C.C. Sorensen. Determination of power absorption in man exposed to high frequency electromagnetic fields by thermographic measurements on scale models. IEEE Trans BME 23(5):361-371 (1976).

Guy, A.W., M.D. Webb, A.F. Emery, and C.K. Chou. Measurement of power distribution at resonant and nonresonant frequencies in experimental animals and models. Scientific Report No. 11, USAFSAM Contract F41609-76-C-0032 Final Report, Brooks AFB, TX 78235, 1978.

Guy, A.W., S. Davidow, G.Y. Yang, and C.K. Chou. Determination of electric current distributions in animals and humans exposed to a uniform 60-Hz high intensity electric field. Bioelectromagnetics 3(1):47 (1982).

Guy, A.W., and C.K. Chou. Hazard analysis: Very low frequency through medium frequency range. Final Report, Bioelectromagnetics Research Laboratory, Department of Rehabilitation Medicine, University of Washington, Seattle, WA 98195. USAFSAM Contract F33615-78-D-0617, Task 0065, 1982.

Hagmann, M.J., O.P. Gandhi, and C.H. Durney. Numerical calculation of electromagnetic energy deposition for a realistic model of man. IEEE Trans MTT 27(9):804-809 (1979).

Ho, H.S., and A.W. Guy. Development of dosimetry for RF and microwave radiation. II: Calculations of absorbed dose distributions in two sizes of muscle-equivalent spheres. Health Phys 29:317 (1975).

Stratton, J.A. Electromagnetic theory, pp. 488-489. New York and London: Mcgraw-Hill Book Company, Inc., 1941.

von Hippel, A.R. (Ed). Dielectric materials and applications. Cambridge, Mass.: The M.I.T. Press, 1954.

APPENDIX A

MEASUREMENT OF AVERAGE SAR VALUES BELOW BODY-RESONANCE FREQUENCIES

A special exposure system is needed for making average SAR measurements in models to simulate human exposure to frequencies below the body-resonance frequency. We used a 57.3-MHz resonant-cavity system to expose scale models of man to simulate exposures of man to HF electric fields, the greatest contributor to SAR at frequencies below body resonance. Though similar work had been done previously under another Air Force contract (Guy et al., 1978), the new cavity was much improved and provided greater accuracy and more flexibility in the choice of model sizes and shapes (Guy et al., 1982). Also, in the latest measurements we compared homogeneous muscle tissues and tissues with 2/3 conductivity of muscle (Durney et al., 1978). By adjusting the model conductivity in the appropriate manner, we exposed models to 57.3-MHz electric fields in the cavity to simulate the exposure of a full-scale man to 5-10 MHz. For example, the conductivity for the 10-MHz exposure for the 2/3 muscle mixture is given by

$$\sigma = (57.3 \text{ MHz}/10 \text{ MHz}) \times 2/3 \times 0.625 = 2.38 \text{ S/m}$$

After exposing the models, we measured the temperature change in each model and calculated the SAR. From the SAR, denoted by W (57.3 MHz), measured at the 57.3-MHz exposure frequency, we can calculate the SAR for exposure at the full-scale frequency, W (10 MHz), by the following equation:

$$W\ (10 \text{ MHz}) = W\ (57.3 \text{ MHz})/5.73$$

Theoretically the SAR, W (f MHz), at any other HF-band frequency (f MHz, significantly below the body resonance frequency) may be calculated in terms of the 10-MHz exposure by the following equation:

$$W\ (f \text{ MHz}) = W\ (10 \text{ MHz}) \times [\sigma\ (10 \text{ MHz})/\sigma\ (f \text{ MHz})] \times (10 \text{ MHz}/f \text{ MHz})^2$$

where σ (10 MHz) is the conductivity of the actual tissue of the full-scale man at 10 MHz, and σ (f MHz) is the conductivity at any other frequency in the HF band.

The SARs as measured for 5-10 MHz and the values as extrapolated to other frequencies are shown in text Fig. 64, represented by the dot and circle symbols respectively.

END

DATE
FILMED

L
84

DTIC